Flow Conditioning in Heat Treatment by Gas and Spray Quenching

Strömungsanpassung in der Wärmebehandlung mittels Gas- und Sprayabschreckung

Dem Fachbereich Produktionstechnik
der
Universität Bremen

zur Erlangung des Grades
Doktor-Ingenieur

vorgelegte Dissertation
von
M.Eng. Thibaud Bucquet

Gutachter: **Prof. Dr.-Ing. habil. Udo Fritsching**
Univ.-Prof. Dr.-Ing. habil. Olaf Keßler, Universität Rostock

Tag der mündlichen Prüfung: 12.05.2017

“Il semble que la perfection soit atteinte non quand il n'y a plus rien à ajouter, mais quand il n'y a plus rien à retrancher.”

- Antoine de Saint-Exupéry

Acknowledgments

First of all, I would like to express my profound gratitude to Prof. Udo Fritsching for believing in my capacity to complete this work and for the continuous support that truly embodied the definition of a *Doktorvater*. I am grateful for the trust and responsibility he invested in me, and for the more informal moments spent outside of work or during conferences.

I am also grateful to Prof. Olaf Keßler and Prof. Carsten Heinzel for supervising my work and defense, and for the editorial advices and the collaborative research works done together.

I have countless great memories from my time at IWT Bremen, and especially thank my colleagues from the VT department for the (working) days and (dancing) nights spent altogether.

I am very glad I could count anytime on my *Wohngemeinschaft* during its various occupancy, as a lively place to meet friends and colleagues. Same goes for *Lift*, which, besides being an Internet Café, is still like my second living room.

Finally, I am thankful I could continue developing my passion for music, along my colleagues, friends, and family, who have constantly been supporting my choices, with all the ups and downs.

Abstract

Gas quenching has been known for centuries as a convenient, affordable method to heat treat ferrous alloys. Heated parts are taken out of the furnace and quenched at ambient pressure, casually using a blower to increase the heat exchange.

Technical developments in the metal industry, over the last decades, have seen a constant improvement of the ratio of heat exchange, e.g. by using pressured chambers, specific blowers, and a variety of gases and gas mixtures. The current gas quenching technologies are adapted to heat treatable metals found in the automotive industry, requesting a minimum heat exchange ratio, also depending on the part geometry.

Little has been however investigated concerning the quenched batch, defined as the arrangement of the heated parts onto a single- or multiple-layer charge carrier. The present work, through a combination of experimental and numerical techniques, provides guidelines to adapt the batch to a specific gas flow pattern (spatial fitting), and to adapt the gas flow pattern to the batch structure (temporal fitting).

Measurement techniques have been developed to assess the flow patterns inside industrial quenching chambers. Evaluated flow structures have been converted to numerical boundary conditions for extended simulations tools. Simulations have helped implementing technical solutions for flow correction in industrial gas quenching chambers. Furthermore, simulations have served the design of batches of various geometries, to improve both quenching homogeneity and intensity.

Both experimental and numerical results confirmed the advantages of gas quenching for the homogeneous heat treatment of automotive steel grades, and demonstrated the potential of various flow correcting devices, such as perforated plates and cylindrical flow ducts. Heat treatment gas and spray quenching has also been integrated into the forging and the turning process chains of single components, successfully optimizing the *lean* process flow (automation, quality, and time), for various high-performance materials and part geometries.

Kurzfassung

Die Gasabschreckung ist seit vielen Jahrzehnten als eine bequeme und kostengünstige Methode in der Wärmebehandlung von Metallen bekannt. Erhitzte Teile werden bei Umgebungsdruck z.B. mit Luft abgeschreckt, gegebenenfalls mit einer Erhöhung des Wärmeaustauschs mittels eines Gebläses.

Technische Entwicklungen in den letzten Jahrzehnten legen Verbesserungen der Effizienz des Wärmeaustausches dar, z.B. durch Druckkammern unter Verwendung spezifischer Ventilatoren, oder einer Vielzahl von verwendeten Gasen und Gasgemischen. Die heutigen Technologien der Gasabschreckung werden z. B. in der Wärmebehandlung von Metallteilen aus der Automobilindustrie verwendet, wobei eine minimale Intensität des Wärmeaustauschs, in Abhängigkeit von der Teilegeometrie, erforderlich ist. Es wurde jedoch wenig im Bereich von abzuschreckenden Chargen, definiert als die Anordnung der erwärmten Teile auf einem ein- oder mehrlagigen Chargenträger, untersucht. Durch eine Kombination von experimentellen und numerischen Methoden werden in der vorliegenden Dissertation Richtlinien abgeleitet, um die Charge an eine bestimmte Gasströmungsverteilung (räumliche Anpassung) sowie die Gasströmungsverteilung zur Chargenanordnung (zeitliche Anpassung) anzupassen.

Geeignete Messmethoden wurden hierbei angewendet, um die Strömungsstruktur innerhalb von Gasabschreckkammern auswerten zu können. Die so abgeleiteten Strömungsstrukturen wurden in erweiterte Simulationstools als numerische Randbedingungen implementiert. Simulationen helfen bei der Umsetzung technischer Lösungen für die Strömungsanpassung in industriellen Gasabschreckkammern. Darüber hinaus unterstützen Simulationen bei der Gestaltung von Chargen aus verschiedenen Bauteil-Geometrien, was sowohl zur Verbesserung der Abschreck-Homogenität als auch -Intensität führt.

Die experimentellen und numerischen Ergebnisse in dieser Arbeit bestätigen den Vorteil der Gasabschreckung für eine homogene Wärmebehandlung von Automobilstahllegierungen und zeigen das Potential der verschiedenen Strömungskorrektureinrichtungen, wie Lochblechböden und zylindrischen Führungselementen. Methoden des Gas- und Spay-Abschreckens wurden in Schmiede- und Bearbeitungsprozesse einzelner Komponenten implementiert, durch eine erfolgreiche *Lean*-Prozessoptimierung (Automatisierung, Qualität und Zeit) für verschiedene Hochleistungswerkstoffe und Bauteil-Geometrien.

Selbstständigkeitserklärung

Hiermit erkläre ich, dass ich die vorliegende Dissertation selbstständig verfasst und keine anderen als die angegebenen Quellen und Hilfsmittel benutzt und die den benutzten Werken wörtlich oder inhaltlich entnommenen Stellen als solche kenntlich gemacht habe.

Diese Arbeit wurde nicht vorher an anderer Stelle eingereicht.

Bremen, den

_____

Thibaud Bucquet

1 Table of contents

Nomenclature

Latin letters

a	temperature conductivity	W/(m².K)
A	area	m²
Bi	Biot number	-
C_2	quenching unit empirical constant	-
C_p	volumetric heat capacity	J/(kg.K)
D, d	characteristic hydraulic diameter	m
e	thickness	m
$\dot{e}$	radiative heat flux of a real body	W/m²
$\dot{e}_r$	radiative heat flux of a black body	W/m²
Fa	tube arrangement factor	-
g	gravity	m/s²
G	nozzle array dimensional factor	-
h	heat transfer coefficient	W/(m².K)
H	nozzle-to-plate distance	m
k	turbulent kinetic energy	m²/s²
L, l	characteristic length	m
L_T	nozzle-to-nozzle spacing	m
m, n	empirical coefficients	-
$\dot{m}$	mass flux	kg/(m^2.s)
Nu	Nusselt number	-
p	operational gas pressure	bar
Pr	Prandtl number	-
$\dot{q}$	heat flux	W/m²
r	radius	m
R	resistance	Ohm
Re	Reynolds number	-
t	time	s
T	temperature	K
T_∞	flow temperature away from the wall	K
Tu	turbulence grade	-
T_w	wall temperature	K
u_∞	flow velocity away from the wall	m/s
$\bar{u}$	arithmetic mean of the velocity	m/s
u'	variable set of the velocity	m/s
u^+	non-dimensional near-wall velocity	-
U	voltage	V
V	volume	m³
$\dot{V}$	volumetric flow rate	L/min
x, y, z	distances	m
y^+	non-dimensional wall-distance	-

Greek letters

δ_t	thermal boundary layer	m
ΔT	temperature difference	K
ε	emissivity of a real surface	-
λ_g	thermal conductivity of the gas	W/(m.K)
λ_s	thermal conductivity of the solid	W/(m.K)
μ	dynamic viscosity	kg/(m.s)
ν	kinematic viscosity	m²/s
ρ	density	kg/m^3
σ_u	standard deviation of the velocity	m/s
τ	shear velocity	m/s

Constants

R	ideal gas constant = 8,3144621 J/(K.mol)
σ_{SB}	Stefan-Boltzmann constant = 5,67e-8 W/(m^2.K^4)

Abbreviations

avg	average
AFP	precipitation-hardening ferritic/pearlitic (steel)
AR	aspect ratio
ARN	array of round nozzles
ASN	array of slot nozzles
AT	alternately timed (quenching)
B	bainite
C	core
CAD	computer-aided design
CCT	continuous cooling transformation (diagram)
CFD	computational fluid dynamics
CHE	controllable heat extraction
CHS	case-hardening steel
CTA	constant temperature anemometry
DF	disc front
DNS	direct numerical simulation
DR	disc rear
Exp.	experimental
F	ferrite
FD	flow duct
FEM	finite element method
FVM	finite volume method
GAMG	geometric algebraic multi-grid
GQ	gas quenching
HB	Brinell hardness
HDB	high-strength ductile bainitic (steel)
HF	heat flux

HK	Knoop hardness
HPGQ	high-pressure gas quenching
HTC	heat transfer coefficient
HV	Vickers hardness
ITD	isothermal transformation diagram
lam	laminar
L	layer
LES	large-eddy simulation
LM	light microscopy
M/Ma	martensite
MS	martensite-start (temperature)
P	pearlite
PIMPLE	PISO + SIMPLE
PISO	pressure implicit with splitting of operators
rps	rotation per second
RANS	Reynolds-averaged Navier-Stokes
S	surface
Sim.	simulation
SEM	scanning-electron microscopy
SIMPLE	semi-implicit method for pressure-linked equations
SRN	single round nozzle
SSN	single slot nozzle
SST	shear stress transport (turbulence model)
stl	stereo-lithography
tkE	turbulent kinetic energy
turb	turbulent
TC	thermocouple
TF	tooth front
TR	tooth rear
TTP	time-temperature-properties (diagram)
TTT	time-temperature-transformation (diagram)
US	ultra-sound
v2f	turbulence model
VarCo	coefficient of variation
Vm	velocity magnitude
VI	virtual instrument

1 Introduction

Research and development, in the era of an *Industry 4.0*, focuses on greater process control and flexibility, cost reduction, low environmental impact, improved safety for the staff, and efficiency in the production cycle. For techniques in the domain of materials technology and heat treatment, process development may particularly take place in energy- and cost-saving technologies, such as gas and spray quenching. In this context, modeling gas quenching with computational fluid dynamics (CFD), and alternately timed (AT) quenching, have been identified as the major directions to investigate in the heat treatment engineering of the 21st century [Tot12]. In addition, continuous production processes, such as the so called *one-piece flow* process with integrated heat treatment, offer great potential for productions process improvements [Heu13a] [Her15].

In the past few years, gas quenching has become the green and safe alternative technique for several hardening processes. In comparison to conventional liquid quenching (using water or oil), gas quenching demonstrated an improved control of the quenching process. Parameters such as the cooling rate over the operating time, the local surface quality (surface hardness, roughness), and the distortion of the component are therefore more stable [Zoc09]. Gas quenching delivers an improved process safety (single-phase quenching, no phase transition) and a better environmental impact than its liquid counterparts (gas recycling and wide availability of nitrogen as a quenching medium).

The versatility and flexibility of gas and spray quenching for implementation into extended manufacturing processes, involving, for instance, machining, forging, or forming phases, makes it an attractive heat treatment process to complement a production line. The compatibility of gas quenching with electrical devices (gaseous environment) and human tasks (safety) are further advantages of the process implementation of gas quenching into manufacturing processes.

The major drawback of gas quenching is its lack of potential quenching intensity, characterized by lower heat transfer coefficients in comparison to oil or water quenching. Gas quenching only offers a profitable alternative to conventional liquid quenching for industrial applications requesting specific materials and component shapes (specific alloys, surface hardening for small specimens, and heat treatment such as vacuum carburizing).

A broader application of gas quenching as a profitable alternative for the industry requires an improvement of its quenching potential conditioned by a higher quenching intensity and homogeneity, obtained from a better spatial and temporal process control. Here, spray quenching (gas with liquid droplets) offers great potential to enhance heat transfer rates, and thus quenching process application field.

2 Motivation and Aims

Motivation

To broaden the industrial application of quenchant gases for heat treatment, hence improving the environmental impact, safety, and profitability of quenching processes, gas and spray quenching intensity has to be controlled and significantly increased, without reducing the existing potential of homogenous quenching solutions. The major application field for gas and spray quenching is found in the automotive industry, e.g., in the lean manufacturing of gear components.

Hypothesis

The main hypothesis of this thesis is that, based on detailed scientific investigations of gas and spray quenching processes, significant contributions can be done on technical development and impact in manufacturing processes for ecological and economic benefits.

Aims

In the present work, various gas and spray quenching process configurations are evaluated over the process dimension and scale using a combination of simulation and experimental techniques.

The research work focuses on determining the technical parameters impacting the flow structure and patterns during gas quenching and how to spatially and temporally control them to improve both quenching intensity and homogeneity in the relevant process scales.

The suggested technical improvements provide guidelines to implement gas and spray quenching into lean production lines to manufacture high-performance components and complex geometries, as well as potential cost-reduction in comparison to conventional liquid and existing gas-based, heat treatment processes.

Structure

The introducing chapter of the thesis (Chapter 3) details the state of the art for gas quenching technology (materials sciences, heat treatment techniques, and gas and spray quenching), the experimental methods of investigation (flow characterization and evaluation, and heat transfer measurement to assess the effectivity of the improvements), as well as numerical modeling and simulation (for computational fluid dynamics and transient heat transfer).

Chapter 4 introduces the applied measurement and simulation techniques used in the present investigation (flow and heat transfer), and their validations in the context of heat treatment gas quenching processes.

Chapter 5 exposes the main results of both experimental and numerical investigations over the various process scales and dimensions according to the following development, pictured in **Fig. 2-1**:

- the gas flow in top-to-bottom quenching units (single and multi-layer) is investigated with respect to observations at **macro scale** in gas quenching processes, whereas flow conditioning techniques are applied to improve gas flow homogeneity and intensity;
- the structure of the batch (**meso scale**) is investigated, from conventional, multi-layered batch arrangements to lean-oriented, single-layered batch arrangements, as well as one- or single-piece flow arrangements. The arrangement of various gear specimen batches is optimized to provide ideal quenching gas flow conditions;
- the flow control for single specimen (**micro scale**) is investigated over spatial (heat treatment homogenization around single gears), and temporal (process-integrated stepped quenching) aspects to reduce the time duration and steps conventionally needed in heat treatment processes.

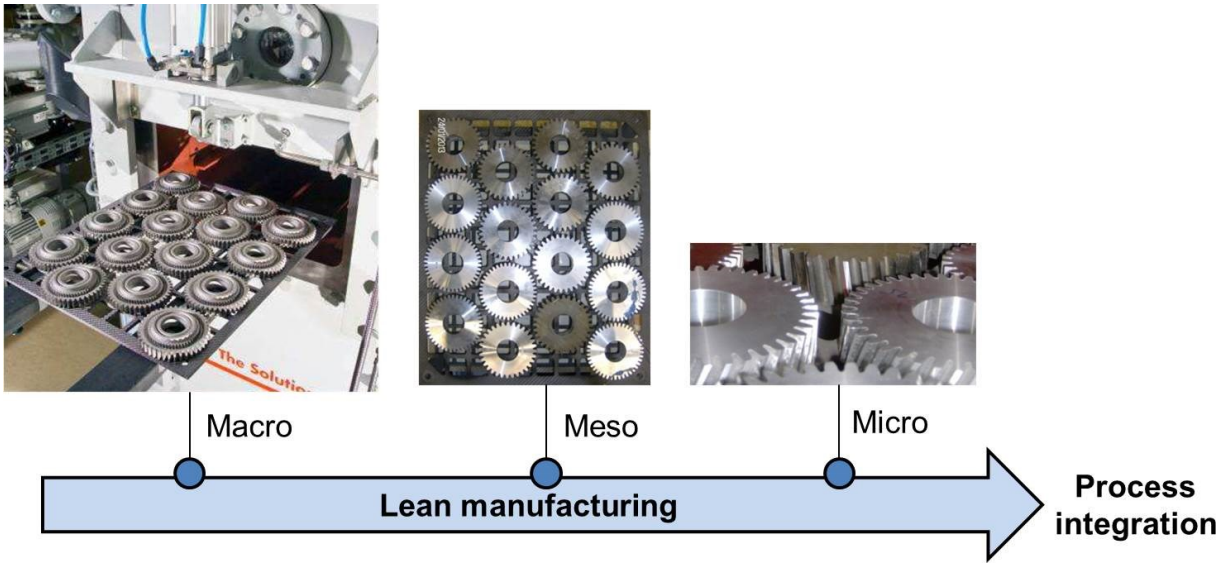

***Fig. 2-1**: Process scales (macro, meso, and micro) in the lean manufacturing of a 1-layer batch of helical gears (left part adapted from [Heu1b])*

3 State of the art

3.1 Heat treatment of metal alloys

Heat treatment is an essential step in metal manufacturing processes, providing workpieces with superficial material properties. The International Federation for Heat Treating and Surface Engineering (IFHTSE) defines it as *"a process in which the entire object, or a portion thereof, is intentionally submitted to thermal cycles and, if required, to chemical and additional physical actions, in order to achieve desired structures and properties"* [Sin89].

Löser et al. [Lös95] define the following criteria for the profitability of heat treatment processes:

- **non-personal/material costs:** building, amortization, interests
- **working costs:** personnel, energy, gas, maintenance
- **process:** integration, storage, transport
- **quality:** process capability, distortion
- **ecology:** pollution, safety

Steel and aluminum, the two major branches of metal alloys in the car industry, concentrate the financial means and production capacity, thus attracting research and innovation focus.

3.1.1 Steel

As of today, steel is the world most produced metal. The modern era of steel can be dated to the 19th century with the industrial application of the Bessemer process, dramatically decreasing the cost of steel production, and allowing the mass production of steel-made goods and constructions which led to the second industrial revolution shaping the industrial world of the 20th century.

3.1.1.1 Physical metallurgy

A steel thermal cycle is the successive steps undergone by a workpiece of specific steel alloy to increase the strength and toughness by locally controlling the microstructure. Heat treatment steps usually include heating, temperature-holding (austenizing), and quenching phases, with eventually relieving, normalizing, annealing, or tempering, as additional steps that might be performed to improve the mechanical properties of the part.

Common transformation products during heat treatment are described below, and are partially pictured in **Fig. 3-1**:

- **austenite** provides the initial conditions before hardening through non-magnetic, face-centered-cubic iron crystal structure;
- **ferrite** is the state of body-centered-cubic iron crystal structure;
- **pearlite** is a blend in lamellar structure (whose space increases with the transformation temperature) of ferrite and cementite formed after slow quenching;
- **cementite**, taking either lamellar or spheroid form, is a hard and brittle compound also known as iron carbide;
- **ledeburite** is a mixture of austenite and cementite;
- **bainite** may be produced during continuous cooling or isothermally at temperatures ranging from those to obtain pearlite and martensite. Mechanical properties diverge between upper bainite (feathery appearance, plates of cementite in a ferrite matrix), and lower bainite (acicular, close to tempered martensite, ferrite needles containing carbide platelets), depending on the temperature during transformation;
- **martensite** is the product of a diffusionless transformation due to rapid quenching. Pearlite and bainitic transformations do not take place if the temperature reaches the martensite-start (MS) temperature before one of the other transformations occurs. Martensite quality depends on the initial carbon content of the austenite state.

3.1.1.2 Heat treatment

Traditional heat treatment process for steels involves the production of martensitic microstructure using a 2-to-3-phase heat treatment [Cal07]:

- **austenizing** or heating the batch/part up to a specific temperature and holding it so that the complete steel part will reach an austenized state (gamma-phase iron);
- **quenching** from the austenite state to the desired microstructure if the process is controlled (bainitizing for instance), or as fast as possible to ensure the formation of martensite in the part. Quenchants can take the form of water, polymer solutions, oils, or gases;

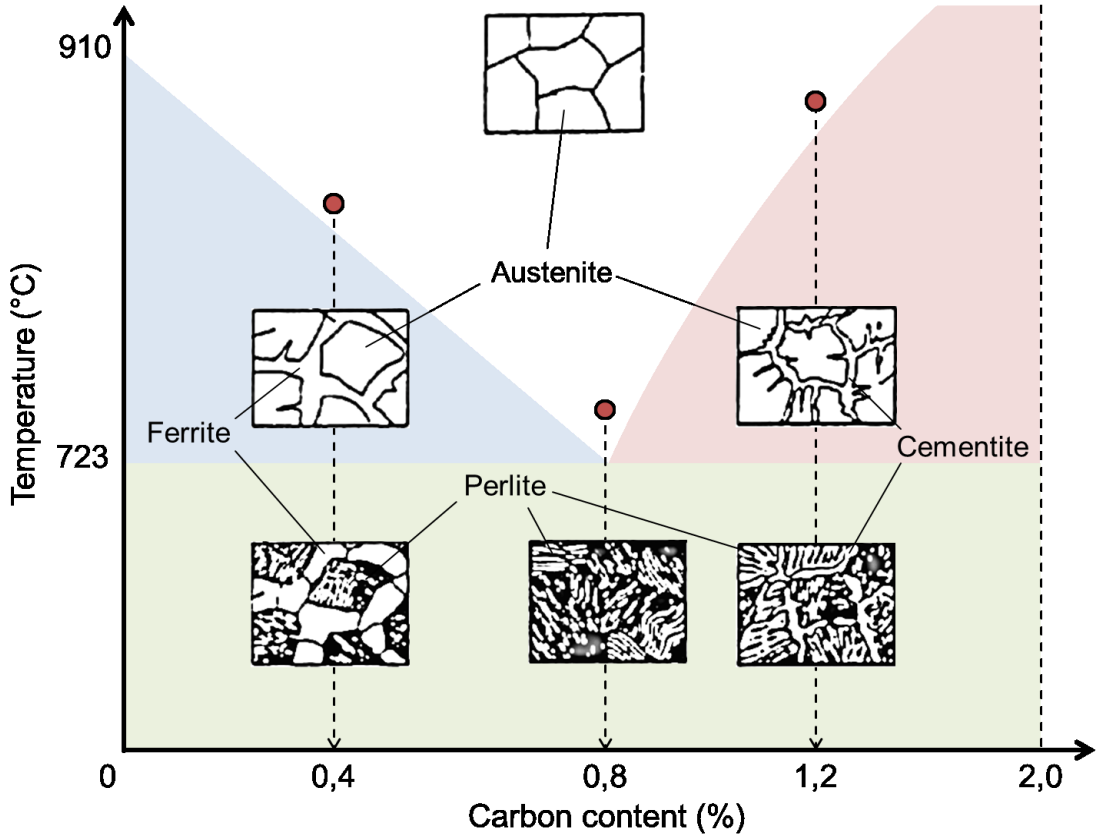

***Fig. 3-1**: Simplified Fe–C phase diagram, adapted from [Can10]*

- **annealing**, or in re-heating the part to a lower temperature than its austenizing temperature to produce a succession of micro-phenomena improving the mechanical properties. It takes the form of **tempering** if the so-obtained martensite requires an increase in toughness and ductility, thus reducing the generated excess of hardness in the part.

Additional heat treatment methods can take place in order to improve the hardenability potential or distribution of steel alloys, as well as to operate superficial heat treatment on the part, with for instance:

- **surface hardening**, taking the form of hardening or tempering, allowing local heat treatment, and the possibility of providing strong property gradients into the part based on the quenching/tempering process and resulting microstructures. It often takes the form of **induction hardening** in the case of automotive industry, usually followed by a strong (water) or controlled quenching (air or spray);

- **case hardening**, as the inclusion of elements through diffusion process into the superficial area of the part, maintaining the initial properties in the core of the part. It takes often the form of **carburizing**, using a furnace with carbon-rich atmosphere.

Time-temperature-transformation diagrams (TTT), such as ITD- (for isothermal transformation), or CCT- (for continuous cooling transformation) diagrams, are derived from the heat treatment of steel samples according to various parameters to allow a map of the phases and transformations starting from the austenizing temperature. The diagrams are utilized in the industry to monitor the transformations of the workpiece by measuring the temperature. The borders of the phase regions are plotted depending on the temperature and the logarithmic time, as reactions take place from very fast (martensite, bainite) to very slow time scales (pearlite).

3.1.1.3 Bainitizing

The attractive properties of lower bainite, combining high-strength and ductility, have been investigated in connection to numerous applications in the automotive industry [Beh14]. New steel alloys follow a large microstructure transformation in heat treated specimen, depending on the heat treatment conditions, to ensure the production of given mechanical properties at lower process requirements [Hu13] [Ele14] [Wir14].

Precise spatial and temporal quenching operations are however requested to succeed in bainitizing such specimens. In **Fig. 3-2**, for instance, the process optimization of hot-forging for a new high-strength ductile bainitic (HDB) steel alloy [Keu12] [Fis14], including process-integrated gas and spray-quenching field, has been designed to perform quenching and bainitizing [Hin12a] from the remaining forging heat.

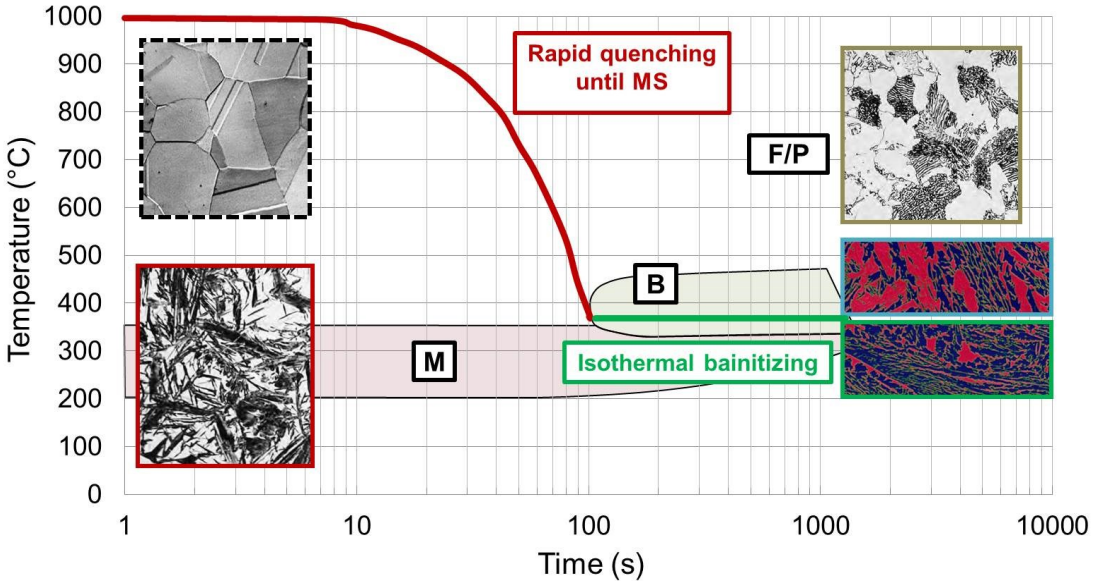

***Fig. 3-2**: Ideal time-temperature-transformation curve of an austenized HDB steel after rapid quenching, then isothermal bainitizing (micrographs from [Cal07])*

3.1.2 Quenchants

Quenching, defined as *"cooling of an object at a rate faster than in still air"* [Tyr86], is a crucial step in most heat treatment processes. Strength, ductility, toughness, and hardness of the part are direct products of the microstructure handling during quenching. Thus, the uniformity and intensity of a quenching process, influencing the distribution and intensity of heat transfer at the surface of the part during quenching, requires a strong control to obtain specific mechanical properties.

The quenching process depends on the nature of the quenchant employed; in fact, the medium selected to extract the heat contained in the hot part or batch. The ability of a quenchant to extract the heat from a surface corresponding to a certain temperature interval is defined by the heat transfer coefficient *h* as

$$h = \frac{\dot{q}}{\Delta T} \tag{3-1}$$

Quenching takes place after heating the part and maintaining it to a certain temperature (austenizing, in the case of steel), and takes the form of many processes using various '*quenchants*'. Quenchants exist under three phases:

- **solid** as e.g., fluidized beds,
- **liquid** as water, oils, emulsions, solutions (e.g. salt), and polymers in water,
- **gaseous** as air, nitrogen, argon, helium, hydrogen, and gas/liquid mixtures,

whose impact on the manufacturing process goes beyond the lone quenching role (environmental issues, safety).

3.1.2.1 Quenchants selection

Luty [Lut10] mentions several criteria to pick up a viable quenchant for heat treatment of metal alloys, such as the abilities to

- extract heat from a considerable portion of the quenched workpiece at a rate at least equal to the critical cooling rate,
- demonstrate acceptable cooling kinetics (small cooling rates for temperatures below MS-temperature to avoid deformation),
- keep stable through their service life (resistant to thermal decomposition and oxidation),
- not interact with the quenched surfaces and quench tank nor with the heat treatment atmosphere,
- conform to safety and environmental standards,
- preserve the quenched surfaces from non-cleanable residues,
- not generate a high investment per unit production.

Depending on the heat treated alloy, quenchants take the form of various solutions described below.

3.1.2.2 Steel quenchants

Quenchants, ranging from liquid to gaseous solutions for the heat treatment of steels, include [Lut10]:

- **water**,

  advantages: high specific heat of vaporization and heat capacity, possibility to dissolve inorganic compounds, as well, non-flammability, low cost, no health hazard, environmentally friendly;

  disadvantages: low boiling temperature and corrosive effects, high HTC variations at T°-range belonging to martensitic transformations;
- **water solution of nonorganic salts and alkali** (brines),

  advantages: heat transfer coefficients more independent towards temperature, less cracks, lower distortion, less variation due to agitation, elimination of the vapor film stage;

  disadvantages: requires protection from corrosion, brine vapors are harmful (safety), higher cost than water (material, personnel) and can generate toxic wastes;

- **water-oil emulsions** (replaced by aqueous-polymer solutions),
  advantages: heat transfer coefficients HTC between oil and water;
  disadvantages: high unstability, generates cracks and distortion;
- **aqueous-polymer solutions**,
  developed because of the disadvantages of water/oil: insufficiently high cooling rates in the range of pearlitic transformation, oils require safety procedures (environment, personnel protection), quenched parts must be washed (and washing product must be disposed);
- **mineral quenching oils** (most commonly used quenchants),
  advantages: best compromise between high resulting hardness and low distortion;
  disadvantages: safety, environment, byproducts disposal, cleaning, cost;
- **saltbaths** (used in martempering and austempering),
  advantages: stability of the heat treatment;
  disadvantages: safety, environment, byproducts disposal, cleaning, cost;
- **fluidized beds**,
  advantages: good replacement for hot oil and saltbaths, no toxic vapors, easy temperature adjustment, almost unlimited service life;
  disadvantages: low HTCs, shield effect of particles on quenched surfaces, difficulty in mechanizing the process;
- **gas quenching**,
- and **spray quenching**, both extensively described below.

3.1.2.3 Quenchants intensity

Heat transfer coefficient values for common quenchants in heat treatment process are listed in **Tab. 3-1**, and pictured in **Fig. 3-3**. The heat exchange highly depends on the physical state of the quenchant. Gaseous quenchants have the lowest heat exchange potential, whereas liquid quenchants have the largest. Solid quenchants (e.g., saltbaths) provide heat transfer coefficients ranging between the two other states.

Whereas liquid quenchants provide higher heat transfer coefficient under convective mechanisms, the boiling phenomenon for water, for instance, increases the heat transfer coefficient by a two-fold factor due to the change in physical state (vapor film).

***Table 3-1**: Heat transfer coefficient range for conventional quenchants, ranked by type and increasing intensity (gas < liquid) [Bau85] [Con93]*

Quenchant and conditions	**Heat transfer coefficient h (W/(m²K))**
Air, free convection	0-50
Nitrogen, forced, 1 bar	100-150
Nitrogen, forced, 6 bar	300-400
Nitrogen, forced, 10 bar	400-500
Helium, forced, 6 bar	400-500
Helium, forced, 10 bar	550-650
Helium, forced, 20 bar	900-1000
Hydrogen, forced, 6 bar	450-600
Hydrogen, forced, 10 bar	750 (extrapolated)
Hydrogen, forced, 20 bar	1300 (extrapolated)
Saltbath	350-800
Oil, quiet, 20-80 °C	1000-1500
Oil, agitated, 20-80°C (at surface temperature > Leidenfrost)	1800-2200
Spray, 15-25 °C (at surface temperature > Leidenfrost)	1500
Water, agitated, 15-25 °C (at surface temperature > Leidenfrost)	3000-3500

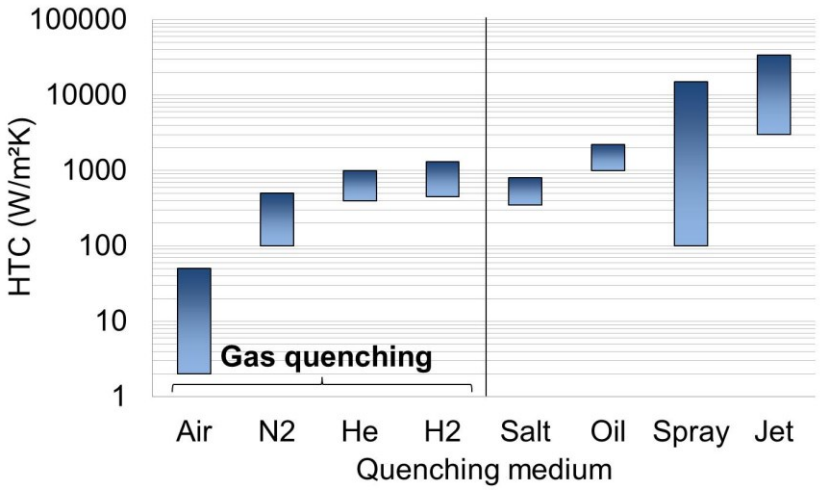

***Fig. 3-3**: Heat transfer coefficient range for common quenchants utilized in metal heat treatment processes*

3.2 Heat treatment gas quenching

Heat-treatment gas quenching was introduced into industrial processes in the mid-70s [Lös05], growing since then exponentially until the new millennium, as pictured in **Fig. 3-5**. Whereas the interest of researchers on this industrial topic grew almost equally in this period, the 2010-2014 periods exhibited a less intense interest from researchers in the topic of heat treatment gas quenching. Figure 3-5 demonstrates the balance between industrial and academic research on heat treatment gas quenching, progressively intensifying, and the recent decrease in publications, indicating the technology acceptance as today's investigation topics primarily consist in fine-tuning the technology optimization methods.

3.2.1 Parameter analysis

Several parameters influencing and influenced by gas quenching have been identified in both academic and industrial research projects, as transcribed in **Fig. 3-6**. The main parameters influencing gas quenching are [Lho92] [Lös95] [Loh96a] [Loh96b] [Dou08] [Sch13]:

- the treated **workpiece**, consisting of a certain metal (chemical compounds), geometry (dimension, form), mass and pre-treatment (surface), where physical parameters such as thermal diffusivity, heat capacity, and density play the most important roles;

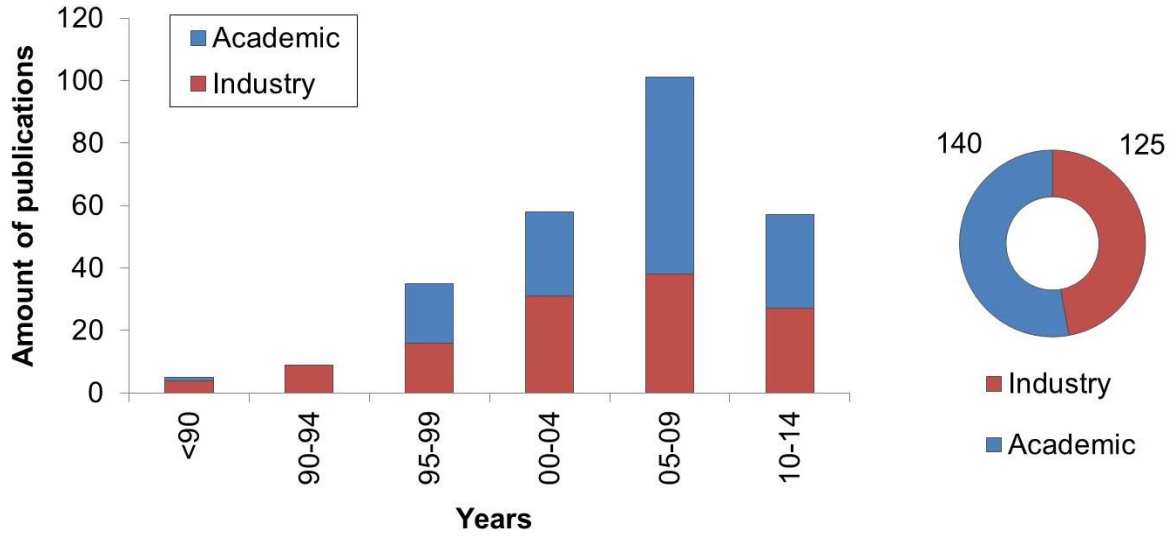

***Figure 3-5**: Amount of publications (divided between industrial and academic research) covering heat treatment gas quenching*

- the treating **quenching medium**, in this case the gas type, velocity, pressure, temperature, and flow type, with parameters such as heat conductivity, dynamic viscosity, density, and heat capacity for the gas itself;
- the **quenching unit**, gathering the constructive solutions to ensure the pressure level and motion of the gas through flow conditioners (for incoming flow and around the batch) and the recirculation system (flow ducts and heat exchanger);
- the **batch**, onto which the workpieces are distributed, or hanging to charge carriers from various metal compounds. Batch parameters are its mass, complexity (arrangement in layers with/without offset), density, and nature of the carriers.

The main target of heat treatment gas quenching processes is the improvement of the workpiece mechanical properties, categorized in [Lös95]:

- its **microstructure**; grain size, boundaries, and regions of various material properties affecting the mechanical properties;
- its **hardness**; the mechanical ability of a material to resist to a punctual/superficial plastic deformation;
- its **distortion**; or form variation from a specified ideal form;

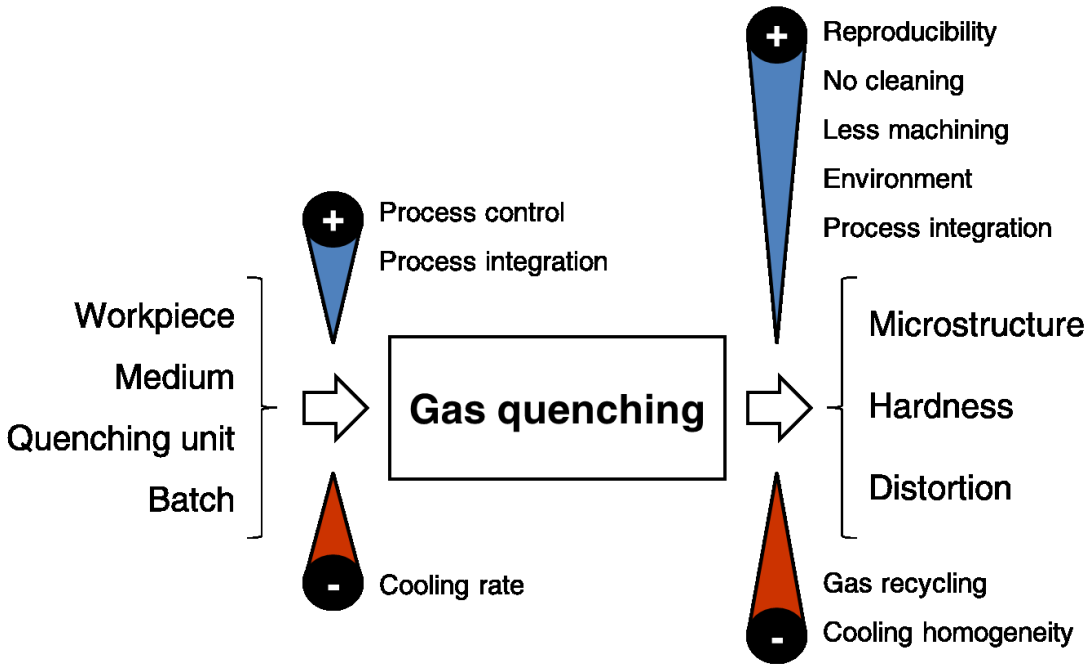

***Figure 3-6**: Parameters influencing and influenced by heat treatment gas quenching*

Common advantages of gas quenching cited are belonging to process-connected, financial, environmental, and safety aspects [Lho92] [Lös95] [Hof98] [Alt98] [Lös05] [Liš07] [Lös07] [Dou08] [Qin08] [Bel10] [Heu13a] [Sch13]:

- the intensity of quenching is mostly based on the sole gas pressure and velocity, providing a **high process control** thus **high reproducibility** with low standard deviation of the results;
- **distortion** can be reduced using the process control, varying the intensity of the quenching to homogenize the temperature profile inside the part.
- strictly **one phase** exists during the process (gaseous), avoiding the strong instability of latent heat delivered during phase changes as with water quenching for instance (Leidenfrost phenomenon), gas quenching is thus a pure convective heat treatment. Compared to liquid quenchants, heat transfers are more stable above MS-temperatures (thus limiting distortion effects) while their values are often higher than those of oil quenchants below MS-temperatures;
- **post-machining** is largely reduced, and can even be eliminated (such as grinding, for instance) in the manufacturing process integrating heat treatment gas quenching;
- **cleaning** the part is not necessary, making gas quenching a '*clean*' heat treatment process that does not require investing in part post-washing;
- as nitrogen is often the quenchant utilized during gas quenching, this process remains **affordable** and **environmentally friendly** in comparison to those requiring oils (added recycling cost, fire hazard, personal safety risks, part cleaning required).

Usual drawbacks of gas quenching include [Lho92] [Liš07] [Lös07] [Dou08] [Qin08] [Sch13]:

- **lower cooling rates** than conventional liquid quenchants, as previously quantified;
- **low cooling homogeneity** when increasing batch size and density due to the high local variations of the flow velocity from the gas streaming through the batch, as well as the workpiece geometry complexity influencing the surrounding gas flow;

- **larger initial investment** and **process costs** (gas), especially for quenching chambers requiring flexibility (if integrated into a production line or covering large workpiece specifications), high pressures (if above standard furnace pressure tolerances), or expensive gases (argon, helium for low recovery rate, or high purity requirements).

3.2.2 Workpieces

The selection of a quenchant depends on various factors related to the nature of the material to be quenched and the quenching process itself, as also stated in [Alt04] [Can10]:

- the **nature of the metal/alloy** with which the quenchant might react, with undesired consequences for the end quality of the product (e.g., oxidation);
- the **carbon content** of a steel has a direct influence on the cracking propensity, thus influencing the choice of a less severe quenchant for steel with high carbon content;
- the **geometry of the part** has to be correlated to the quenching technique (bath or field of nozzles) to reduce potential cooling rate gradients, inducing temperature gradients, and thus distortion risks. Both intensity and homogeneity of the selected quenching technique play an important role over the distortion risk and the desired case and core hardness;
- **charge carriers** have to primarily fit the batch or single part, but also allow the quenchant to reach the surface of the part. Liquids or solid quenchant might suffer from the structure of the carrier while gas quenchants can easily stream around the carrier, suffering from minor decreases in intensity;
- the **stage of the heat treatment process**, if the part needs for instance additional machining steps.

Decades of industrial use of heat treatment gas quenching covered various workpiece geometries, as stated in **Fig. 3-7**. Whereas large, complex geometries, extruded profiles or plates, and steel tools remain less investigated in research fields, automotive components, specifically rings and flat gears, as well as cylinders, shafts, or bevel gears, are thoroughly investigated. Initially, investigation on gas quenching mostly focused on steel tools due to the high hardening potential [Alt91] [Kul91] [Pet92].

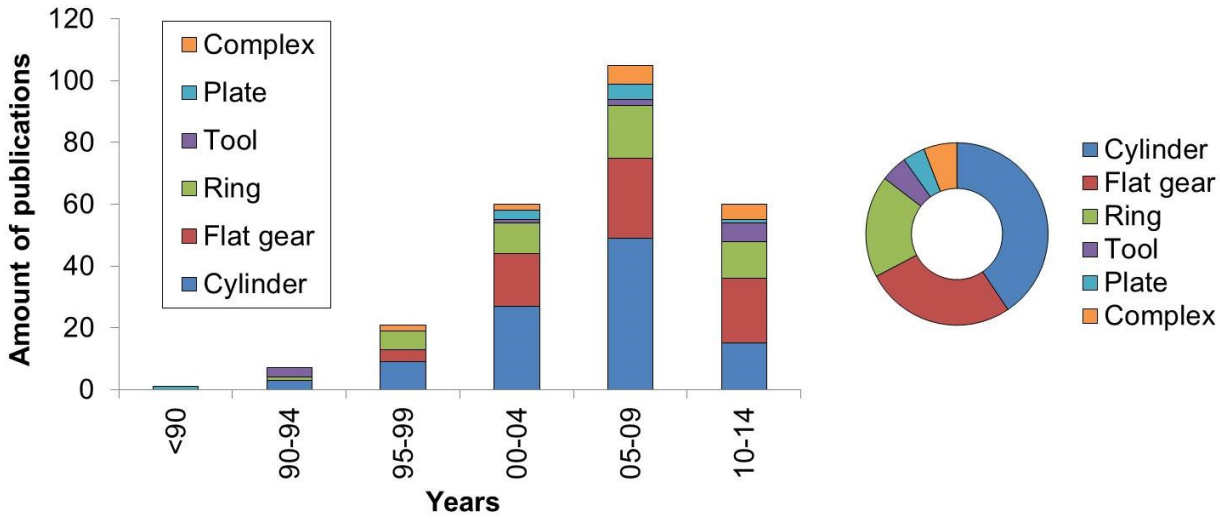

***Figure 3-7**: Amount of publications on heat treatment gas quenching ranked by type of quenched workpiece geometries*

Since the 2000s, intensive work has been done on single [Lio04] [Sch04] and batch [Lho92] [Sch08] [Cor13] of cylinders, in order to determine the optimal flow parameters during gas quenching.

3.2.2.1 Cylinders

Single cylinders

The heat treatment of single shafts or cylinders is performed either in small quenching units [Lio04], if a high process-control is needed, or in gas-nozzle fields [Sch04], to ensure the even distribution of the heat transfer coefficient on the surface of the specimen.

Batch of cylinders

Larger quenching units are needed to perform the heat treatment of batch of cylinders. The length of the specimens, combined with the relative large dimension and density of such batches, makes this process usually challenging, justifying the numerous investigations on this topic, as seen in Fig. 3-7, either experimentally [Lho92] or numerically [Fod07] [Xia11] [Sch13].

More complex specimen geometries (e.g., bevel gears) are also investigated [Alt05] [Lös07] [Jur08]. The complex flow patterns occurring in the batch, due to batch-cylinder and cylinder-cylinder interactions, are causing unstable heat transfer coefficient distributions, thus often negatively affecting the quenching performance.

3.2.2.2 Gears

Type

Depending on the direction of the shafts, gears are divided into different types:

- parallel shafts are set in motion using **spur gears**. **Helical gears** allow smoother action but with axial thrust, thus reducing the power transmitted radially. **Internal gears** often take the form of spur or helical gears using teeth pointing inward toward the center of the gear;
- intersecting shafts use **bevel gears** (straight or spiral) to allow the motion of the shafts usually placed 90° one from another. Face gears are combined with conical shafts to carry out the movement transmission.

Material

Gear materials range from low-strength polymers to ultra-high strength steels [Dav05a] [Dav05b]. The high strength-to-weight ratio of steel makes it particularly suitable for the various applications found in the automotive industry. Lightweight, but high-resistant materials are utilized for aerospace applications requiring safe compromises between weight and mechanical properties.

The choosing criterion for steel materials is the hardening ability, either through-hardening (core of the gear, also surface-hardened via induction heating), or case-hardening (surface of the gear). High-performance gears are usually carburized, with special cases involving heat treatment such as carbonitriding or nitriding instead. Sanitary standards (food or chemical equipment) can require the use of stainless or nickel-based steels (anti-corrosion) [Dav05c].

Single gears

Little is reported about gas quenching of single gears. Most research works focus on the numerical flow investigation (coupled heat transfer and turbulence models, optimal grid numbers) to test the validity of numerical models on reduced dimensions [Pel05] [Str07].

Batch of gears

Batches of gears have been mostly investigated since the technique of gas quenching in gears heat treatment progressively took over conventional liquid-based quenching during the 1990s. Gas quenching efficiently tackles the negative effects of oil quenching [Lös95], consisting of a poor process control and a high distortion risk in the teeth area.

The second industrial revolution has put gears and their manufacturing on the foreground of metal process and methods. Effort transmissions require safe elements combining high surface hardness and structural strength, thus precise combinations of heat treatment processes.

3.2.2.3 Rings

Single rings

Due to their high-sensibility to distortion, caused by quenchants intensity and homogeneity, high process-control used to be needed during the quenching of rings and ring gears. As for single shafts, gas-nozzle fields [Sch04] and small quenching units [Wün93] [Fer03] have been investigated and utilized in the industry to perform heat treatment. The rotation of the ring specimen led to improving the resulting distortion and hardness quality [Vol01].

Batch of rings

The investigation of batches of rings is widely found for industrial applications [Tro98] [Alt00], numerically [Sug06] and even recently [Heu13], in order to optimize the ring batch so that the distortion risk can be minimized. Whereas a larger batch usually fails to provide satisfying distortion results, a smaller batch, consisting of one layer of workpieces, is more suitable to heat treatment processes [Tro98] [Heu13].

3.2.2.4 Distortion

Distortion is a phenomenon taking the global form of body distortion (out of roundness, out of flatness, run-out dimensions), or the local form of tooth distortion [Rak00], being directly influenced by the first form of distortion. Part manufacturing requires acknowledging the potential risks of distortion to minimize its effect and avoid additional corrective manufacturing steps. Numerically [Hun04] [Fre05] and experimentally [Jur08] [Heu09] investigated, stress-induced distortions take their origin in two forms of stress:

- **thermal stress**, due to the conductivity in the body, leading to temperature gradient from the severely quenched surface to the core undergoing lower quenching rates. Thermal gradients affect the local stress through local thermal shrinkage or expansion;

- **transformation stress**, consisting in the latent heat released and in the change of crystal structure for steel, from austenite (cubic face-centered) to ferrite (cubic centered), thus changing the volume of the solid;

The engineering measures to control and minimize the distortion of specimens throughout the entire manufacturing chain (process chain) has been termed *Distortion Engineering*, and has been extensively investigated during the past decade [Hun04] [Fre05] [Kes06] [Zoc09]. Considering gas quenching, uniform and homogeneous flows induce lower residual stress, thus decrease the distortion risks [Thu99].

3.2.3 Medium

Heat treatment gas quenching features a variety of gases whose application depends on the status of the quenching unit and the quality of the quenched workpieces. Besides requiring inert gases to avoid interaction with the furnace, its atmosphere, and the workpieces, several criteria influence the choice of a gaseous quenchant [Dou08]:

- **high thermal conductivity** (for fast diffusive heat dispersion),
- **high density** to maximize the convective heat dispersion,
- **high heat capacity** to increase the heat sensitivity of the gas,
- **low viscosity** to limit energy viscous dissipation,

Figure 3-8 shows the gases commonly used in gas quenching: nitrogen and helium, considering air as close to nitrogen.

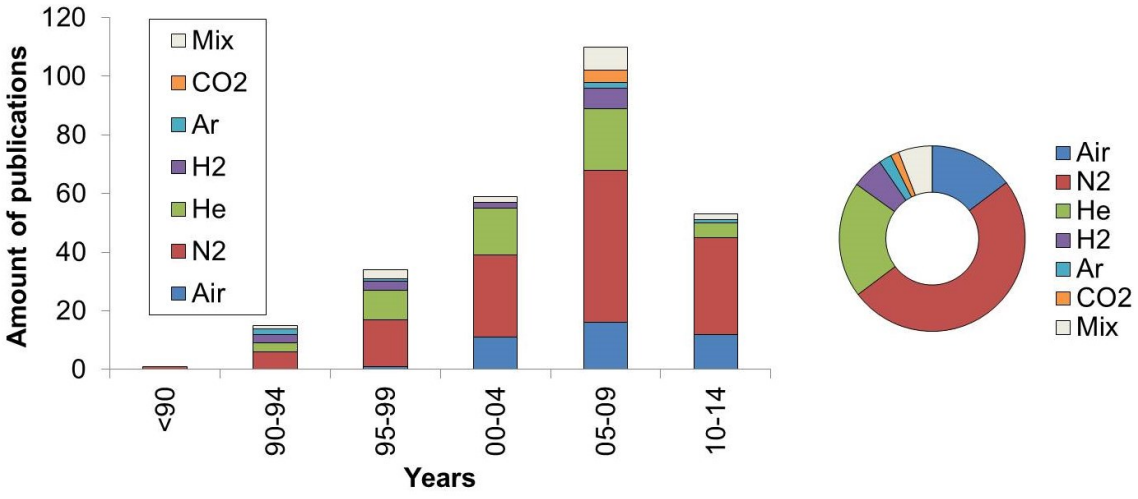

***Figure 3-8**: Amount of publications on heat treatment gas quenching ranked by type of gas operated*

CO_2, argon, and hydrogen represent a small fraction of the gases utilized during gas quenching because of their performance-to-cost low ratio (argon) or their highly hazardous properties (hydrogen), even though they often exhibit high cooling rates (hydrogen), or are inert (argon). Whereas researchers focused early on the use of various gas quenchants, today's trends are largely going towards nitrogen and air quenching techniques, as observed since the technology acceptance of heat treatment gas quenching in the 2000s.

3.2.3.1 Helium

In comparison to hydrogen, helium exhibits less safety issues for slightly lower cooling rates (seen in Tab. 3-1). Helium is the chosen quenchant for numerous works investigating high-pressure gas quenching [Alt02] [Heu03] (up to 40 bar [Mid96]) at high velocities [Wün93], in order to reach the cooling rates of oil. Helium has however the significant drawback of high product and processing/recycling costs, in order to maintain its purity [Mid96] [Bea04] [Stra06].

3.2.3.2 Nitrogen

Argon and nitrogen are more affordable than helium due to their lower processing costs. These byproducts of air are therefore found in relatively larger quantity. Air separation units can provide the gas quenching process in gaseous quenchant directly on-site [Mid96]. Liquid nitrogen also found an application as gaseous and phase-change quenchant (*CHE* for Controllable Heat Extraction method [Liš07]).

3.2.3.3 Gas mixture

Mixing between gases provides a positive influence on the thermal and kinetic parameters of the resulting quenchant [Lho92] [Bea04]. Hydrogen and helium exhibit a high thermal conductivity but a low density, thus better utilized for conductive dissipation than convective. Therefore, a mixing with a denser gas leads to positive effects in industrial gas quenching applications [Fau98] [Dou08].

Mixtures of helium and argon [Fau98], hydrogen and nitrogen [Lüb98], or helium and CO2 [Bea04] demonstrate higher cooling rates than pure hydrogen, helium, or nitrogen for low investment and cycle costs.

3.2.3.4 Operating pressure and velocity

The operating pressure of the cooling gas has a major influence on the heat transfer coefficient and, by extension, the cooling during the quenching process [Mid96] [Lin07] [Nar09]. Their values are depending on the nature of the gas, as low-density gas (helium) allows higher operating velocities and pressures. The advantage of a higher pressure is a more homogeneous cooling rate for the batch [Sto01]. Correlations relating the increase in heat transfer coefficient due to an increase in operating pressure or velocity are described below.

3.2.4 Quenching unit

Until the 1990s, gas quenching applications were exclusively operated in single-chamber, vacuum furnaces due to the combination of pressure-based furnaces and quenching processes. **Figure 3-9** summarizes the basic components of a high-pressure gas-quenching (HPGQ) single-chamber, as described in [Lho92] [Cha08]. After the batch is heated up to the heat treatment temperature for a given time, gas quenching starts by filling the chamber with gas from the buffer tank up to the operating pressure. The blower is activated before the chamber is filled up, and progressively reaches the given rate to provide the recirculating gas its nominal velocity.

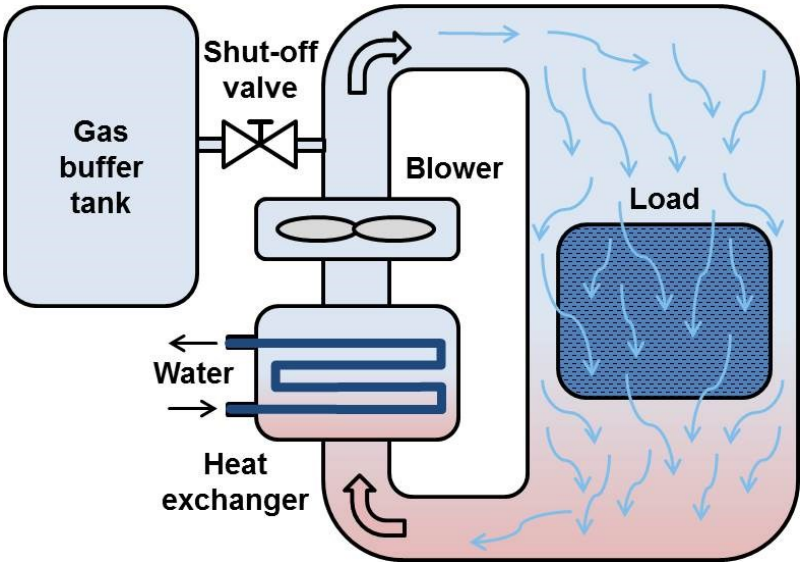

***Figure 3-9**: High-pressure gas-quenching (HPGQ) single-chamber featuring the basic components and functionalities*

Later on, 2-chamber vacuum furnaces proved higher quenching potentials for steel due to their second *cold chamber* offering lower temperature levels to comply with the need for more intensive cooling rates. Indeed, single-chamber gas quenching unit had the disadvantages of a high quantity of heat remaining in the hot chamber through isolation and heating elements, the high free stream area, the high furnace volume, and the limited place for the batch in the furnace [Pet92] [Ede97] [Rit03].
The early 2000s showed high interest in gas quenching applications in the development of heat treatment processes such as *low-pressure carburizing* (LPC) combined with 2-chamber vacuum furnaces [Grä01] [Alt02] [Kle02] [Alt06].
A move towards high-integrated quenching chambers in manufacturing processes has been observed in the recent years with, for instance, multiple cold chambers for a mobile furnace [Lös03] [Lös07], or smaller furnace/quenching unit for the lean manufacturing of gears [Heu13b] [Kor16].

3.2.4.1 Classification

Quenching units are usually classified according to the employed gas-stream technique, consisting in [Kay92] [Ede98] [Tro98] [Lös03] [Win05]:

- **peripheral cooling system**, or horizontal furnace, mostly consisting of a field of nozzles whose impinging jets perform a local, intensive cooling on complex, massive geometries;
- **through-cooling system**, or vertical furnace, whose recirculated gas, flowing through an aperture larger than a nozzle, aims at quenching batch of small workpieces, taking the form of rigid nozzles/perforated plates, large, rotative nozzles or diffusor. The gas flow can take the form of one- or bi-directional (or reverse) flow;
- **multiflow cooling system**, as the recent combination of horizontal and vertical cooling techniques to provide more flexible quenching options for various geometries.

Figure 3-10 shows the evolution of gas quenching apparatus [Win05], in terms of flow structure, from the 1960s up to today. The shift towards better controlled multiflow technologies aims at improving both cooling speed and uniformity of quenching in the batch.

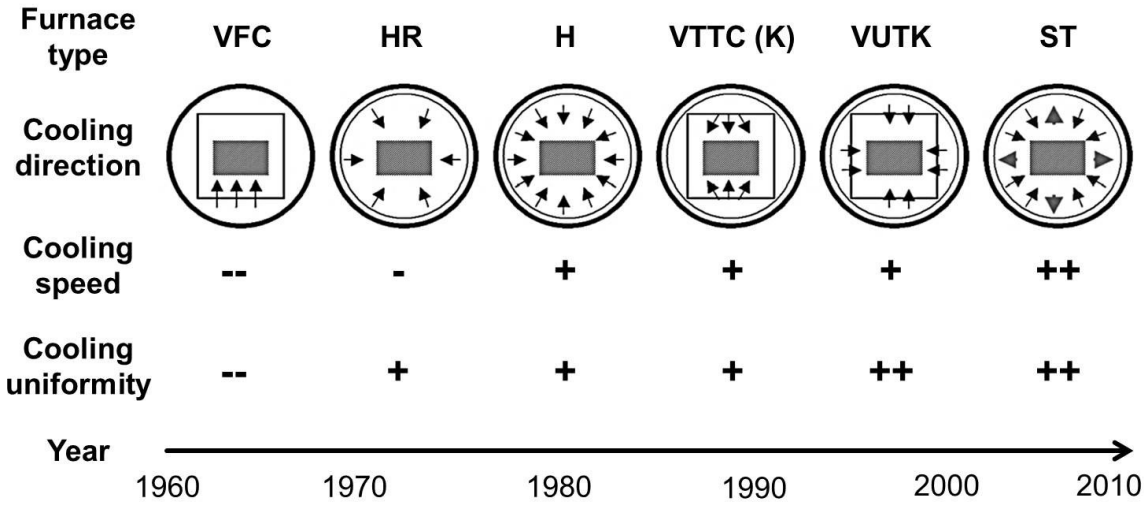

***Figure 3-10**: Examples of gas-quenching apparatus developments since the 1960s, adapted from [Win05]*

3.2.4.2 Peripheral flow using nozzle fields

Quenching chambers using single or field of nozzles mostly focus on batches of reduced dimensions, aiming at intensively and precisely quenching geometries with high distortion potential. Numerous experimental [Irr04] [Sch04] and simulative [Hec01] [Str07] [Rei09] works cover this topic. Applications are also found for larger batch dimensions with quenching systems using round hot zones consisting in a larger nozzle field, also investigated both numerically [Elk03] [Wan12] and experimentally [Kow08] [Zie13].

The application of nozzle-field gas quenching is largely operated using air [Kes06] or nitrogen [Sch05], and can be categorized based on the stream nature of the gaseous quenchant.

Steady-state gas stream

Gas quenching using steady-state nozzle gas stream is a common method to perform local, medium-intensified gas quenching in ambient pressure. Air cleaner pistols are examples of affordable quench solutions in forming applications for non-controlled quenching.

Controlled quenching applications however request a fine tuning of several parameters of the quench field, as shown in **Fig. 3-11**, for the case of cylindrical geometries [Wün93] [Şim09] [Sch12]:

- the **gas properties**, chemical, mass flow, and pressure, directly affect the intensity of the heat exchange happening at the surface of the quenched object. When using air as quenchant, the cleanliness needs to be verified in order to avoid small particles and dust that perturb the nozzle internal air flow;
- the **nozzle shape**, conditioning the gas flow impinging onto the quenched object. Technical features can provide additional motion to the flow, for instance swirl motion if providing an angle to multiple gas outlets;
- the **arrangement of the nozzle field**, specifically for parts requesting intense and/or located quenching. The combination between nozzles should not decrease the benefits of one single nozzle (e.g., due to shear jet interaction);
- the **relative motion** of the workpiece towards the quenching field, in order to lessen the heterogeneity of the cooling rates distributed over the quenched surface.

Figure 3-11 [Sch12] presents a specific quenching setup for aluminum alloy of cylindrical shape, featuring the use of 48 nozzles and air under ambient atmosphere. The arrangement of 4 arrays of nozzles every 90° ensures the even distribution of the heat transfer coefficient on the surface of the part. The nozzle shape provides a focused jet cone that leads to low jet-jet interaction and high heat transfer coefficient on the cylindrical quenched surface.

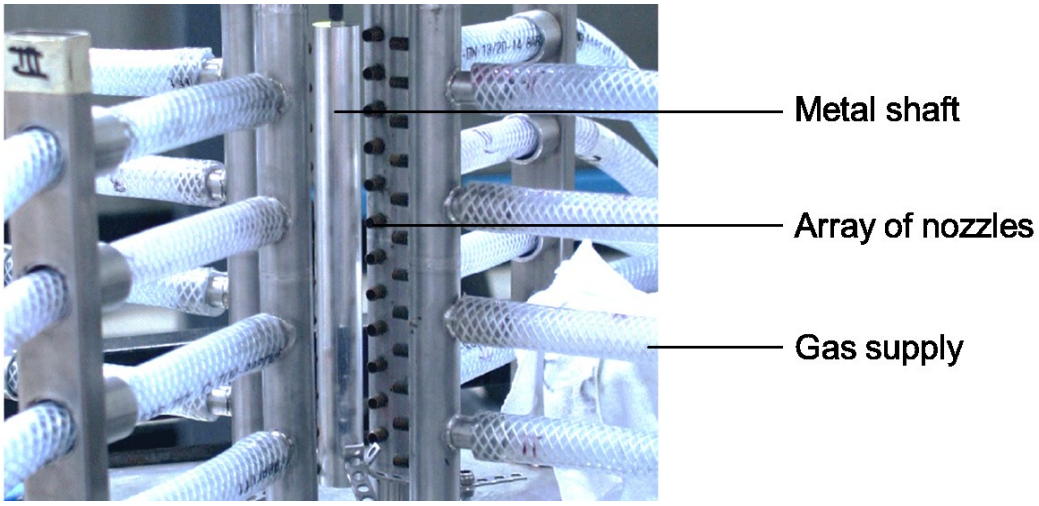

***Figure 3-11**: Gas nozzle field quenching system used in experimental verification of simulations for the quenching of aluminum specimen, adapted from [Sch12]*

Pulsating gas stream

Confined areas suffer from the poor ability to evacuate the heat that is exchanged between the object surface and the fluid. In impinging techniques, a transverse flow usually improves the circulation of the hot quenchant, thus its cooling rate.

Alternative solutions have been recently investigated with the example of acoustic streaming [McG08], aiming at carrying out the heat extraction within one quenching method. Acoustic streaming is mostly used in micro-electronics applications requiring low quenching intensity yet rapid heat evacuation in small dimensions [Pav06] [Lea13].

The use of high oscillating flows (e.g., ultrasound) as industrially viable improvement in heat treatment process, in combination with conventional nozzle quenching processes, has not been reported yet. This technique is however employed to tackle water quenching issues, notably in aluminum heat treatment, to control the boiling phenomenon (Leidenfrost effect), and intensify the effect of the quenchant [Red11]. The ultrasound offers the ability to break the vapor film formed on the surface of the quenched object earlier, thus increasing the heat transfer coefficient via a shift of the bubble boiling phenomenon to higher temperatures.

In **Fig. 3-12**, Legay et al. [Leg11] reports the use of several periodic streaming techniques to improve the heat exchange, underlining an increase in heat transfer *h* concentrated in the range h_{US} = *1-5*h*, however by far without specific relation to metal heat treatment.

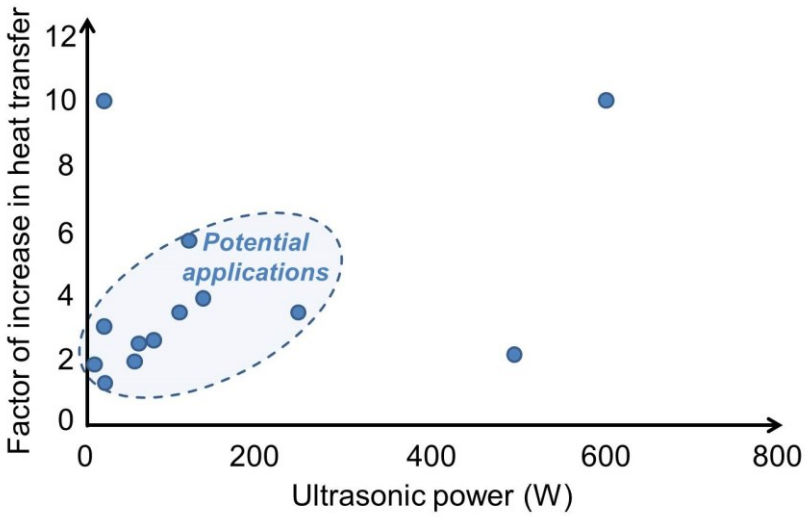

***Figure 3-12**: Increase in convective heat transfer due to ultrasound power; the numbers relate to specific literature sources from [Leg11]*

3.2.4.3 Uni-directional, through-cooling flow

Axial flow quenching chambers have been the first and so far the most common type of gas quenching chambers found in industrial applications, thus being largely investigated experimentally [Ede98] [Bea04] [Ros06] [Sin10] [Heu11a] [Heu13a] [Zie13], and numerically [Sug06] [Fod07] [Sch09] [Cos12]. They cover a large range of part geometries and dimensions (mostly gears for steel hardening applications), as well as a large range of process parameters (gas type, velocity and pressure, flow conditioners), and offer a great flexibility in adapting to different batches, or process conditions due to the dimension of the quenching chamber [Ede97].

Figure 3-13 (first and second positions) [Tro98] presents the principles of a 1-chamber, experimental hardening unit operated in uni-directional (respectively from the top and from the right side) gas flow configuration. Heat exchangers are situated below the batch to ensure proper temperature difference between the quenchant and the batch, improving the heat flux in the various operative directions of the process during gas recirculation.

3.2.4.4 Bi-directional, through-cooling flow

Horizontal and vertical flow quenching chambers aim at quenching batches of more complex part geometries than with chambers using 1-directional quenching flow. They require larger dimensions to provide a second recirculating gas unit. The batch also requires to be optimally arranged, so that the two flow directions are the most profitable, avoiding unnecessary energy dissipation. Bi-directional, through-cooling flow quenching units have remained so far only experimental [Zie13] [Zie14].

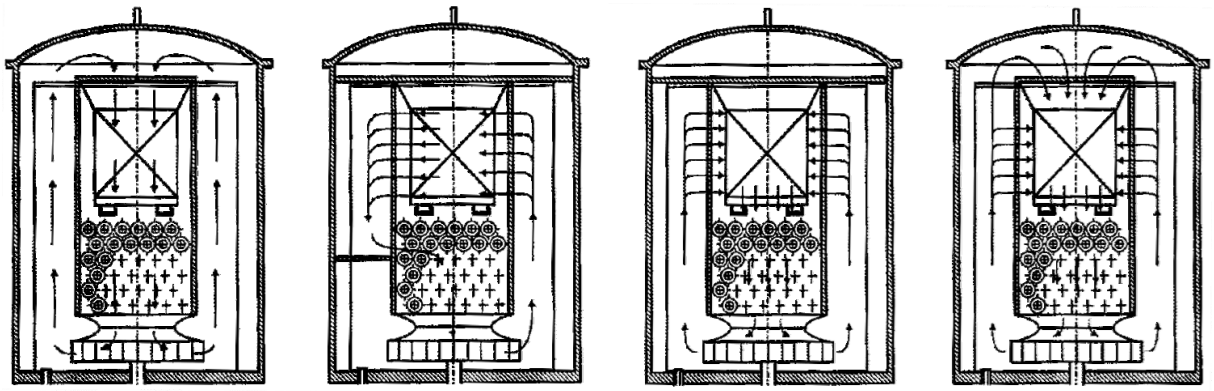

***Figure 3-13**: Gas flow directions available in a flexible experimental high-pressure gas quenching unit, adapted from [Tro98]*

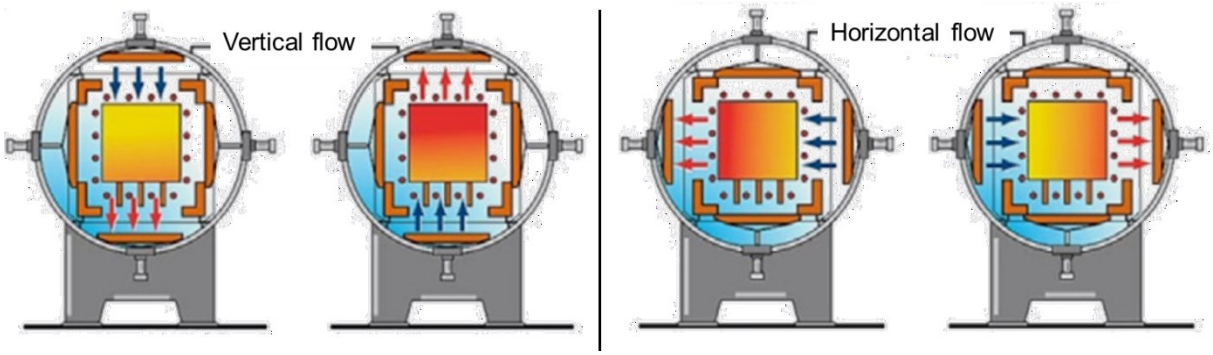

***Figure 3-14**: Quenching unit for large batch with horizontal and vertical cooling gas stream with reversing function and rectangular hot zone design, adapted from [Zie13]*

Figure 3-14 [Zie13] presents the process of bi-directional quenching with reversing flow of a large batch. The process flexibility offered by the gas impingement on four sides of the batch provides a more even quenching inside the batch and reduces the effect of recirculating zones in the quenching chamber. For both cases of pure axial flow and additional transversal flow quenching chambers, the hot zone consists of a rectangular design.

3.2.4.5 Multi-directional quenching chambers

Very complex batch arrangements, containing smaller parts or a very large, single part requiring an even quenching on all sides in the same time interval, are challenging features for conventional, 1-directional gas quenching techniques. Little can be found about experiments of multiflow quenching units [Kay92] [Tro98] [Zie13]. Due to obvious technical reasons, the implementation of three flow directions in uni-directional quenching units has not been performed yet. Nozzle field and peripheral-flow quenching units can be modified as seen in Fig. 3-13 (fourth position) to allow an additional flow axis in the quenching chamber in order to improve the cooling homogeneity of the batch.

3.2.4.6 Reverse flow

Reverse flow [Lös03] [Alt04] [Heu13a] [Zie13] has been introduced for the quenching of automotive components, essentially bevel gears, due to their high dimension variation along the shaft, and gear wheels for an evenly distributed quenching rate in the teeth area.

Top-to-bottom, uni-directional flows have the drawback of producing large recirculation zones or shadowing effects in the successive layers of a large batch [Kay92]. Reversing flows partially solve both local and global drawbacks of a flow impacting the batch only to one side [Lös03].

Figure 3-15 shows the effects of the reverse flow and the contribution of a second blower on the quenching intensity and homogeneity of a large batch [Lös03]. During the quenching process, better results are found for a batch of gear wheels if the uni-directional flow starts with top-to-bottom, then bottom-to-top flow configuration. Single top-to-bottom flow offers more satisfying results than single bottom-to-top gas flow [Alt04].

3.2.5 Batch

In order to decrease the costs of production cycles, workpieces are heat treated in batches. A larger batch density means a decrease in energy and process costs whereas the homogeneity and intensity of quenching are less controllable [Sch10a], due to the increase in flow complexity. The batch distribution of the quenched workpieces has a strong effect on the local cooling rates of the single workpieces due to the *workpiece-workpiece* and *batch-workpiece* interactions, as well as on the global cooling rate, due to the impinging gas flow and the density of the batch [Tro98].

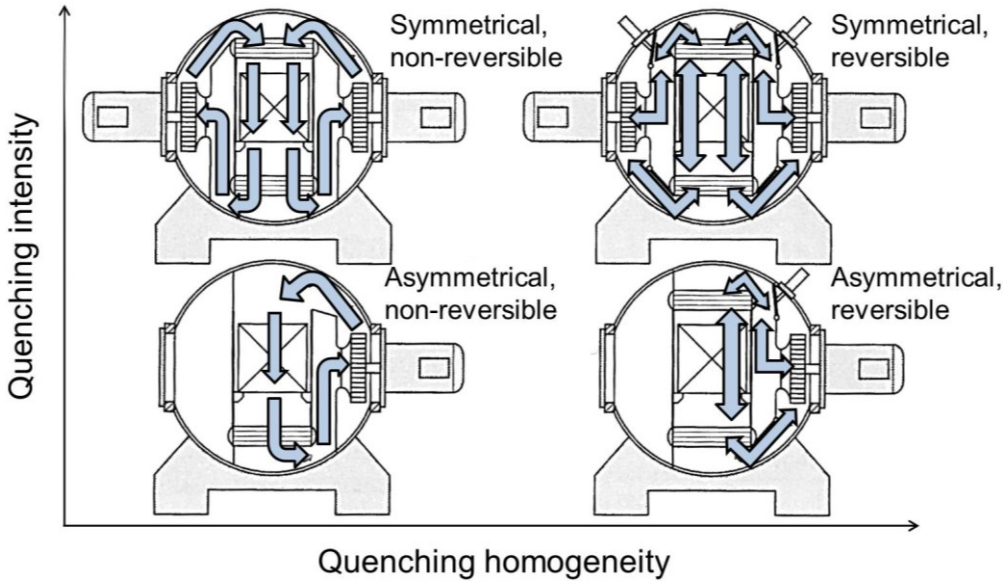

***Figure 3-15**: Effects of the reverse flow and the contribution of a second blower on the quenching intensity and homogeneity, adapted from [Lös03]*

3.2.5.1 Batch of cylinders

Whereas literature widely covers batch arrangements of cylinders parallel to the main flow direction [Lüb98] [Alt06] [Sch10a], little has been published about transverse or staggered batch arrangements in the case of uni-directional gas quenching [Lho92].

Batches of cylinders usually comprise two [Kat05] [Alt06] [Sch10a] to three [Lüb98] layers of cylinders, even though longer shafts might be arranged according to a one-layer batch [Lös07]. The space between cylinders plays a major role in homogenizing and intensifying the heat transfer between quenchant and workpiece.

Simulations [Sch01] mention the increase in heat transfer when the space between workpieces decreases, as the small eddies develop and the recirculating flow occurring along the cylinder reduces in size. The reduction of the gap between layers also lessens the effect of bottom recirculation by forming a continuous cylindrical geometry [Sch10a]. The arrangement of the layers (possibility to create an offset between two successive layers [Sch01]) presents the advantage of distributing the flow more equally towards the cylinder, and to avoid a large difference in cooling rates between the first layer impacted by the flow and the successive layer(s).

For more complex geometries such as bevel gears, consisting in a long shaft and a larger geared head, denser batch [Alt06] and reverse flow [Lös07] are seen as successful quenching strategies to homogenize the cooling rates of the different sections, and tackle the large recirculating areas produced by the large gear head.

3.2.5.2 Batch of gears

In comparison to batches of cylinders, mostly experimentally and numerically covered, batches of gears are usually more complex to model, thus often modelled as thick discs [Fri08] [Lio09]. The heat treatment industry however provides an important source of results concerning batch of gears [Tro98] [Alt04] [Qin08] [Ast12].

For economic reasons, gears have been quenched using two to three [Fri08], or more [Heu04] [Heu13a], layers in the batch. Only recently, one-layer batches are targeting the lean manufacturing market [Heu11a], adopting the *one-piece-flow* [Heu11b] [Kor16] strategy. In-line arrangements are also numerically investigated with the same perspective of reducing process cycle time [Lio09]. Gears are also hung to the batch structure to ensure a complete carburizing process [Her04] [Bri11], thus avoiding the shadowing effect on the surface of the charge carrier.

The major drawback of such techniques is the high distortion (out-of-roundness) potential of the batch distribution, higher than the distortion found using oil quenchants [Tro98] [Cla09].

3.2.5.3 Batch of rings

Whereas batches of gears strongly influence the pressure drop due to the large blocking grade of the single workpieces [Fri08], rings offer a large free stream area being less problematic to a dense arrangement of the batch. The thinner material however increases the distortion risks during quenching, so that this geometry is critically depending on the batch distribution. Large, multiple-layer batches of rings are usually found in the literature to have a low impact on the flow, and the flat dimension do not limit the amount of successive layers in comparison to gears or shafts [Lös08] [Heu13a]. However, a single layer of rings produces a better result than two layers, whereas hanging the rings does not provide acceptable results due to high distortion [Tro98]. Larger rings requiring higher quenching rates also need better control of the local heat transfer from the gaseous quenchant, thus single-quenched in a nozzle field [Vol01] [Fer03].

3.2.6 Process classification

Current manufacturing processes require a high level of flexibility to quickly adapt to batch sizes or various geometries. Heat treatment gas quenching, directly integrated into the manufacturing process, requires the same flexibility. The technological trend, at present, clearly shows an evolution from larger to smaller-sized batches, and even one-piece-flow, with rapid and high-efficient productivity. In this scope, specific flow conditioners aim at adapting the process to the batch size and the specimen geometry. Depending on the dimension of the charge, gas flow techniques in quenching may vary from individual jets to bigger inlets. The main purpose of flow conditioning is to improve the intensity and homogeneity of the gas quenching process, for targeted mechanical properties. The frontiers between macro, meso, and micro levels have been defined in situations where the effect of the gas quenching system on the heat exchange is similar to these between part themselves: firstly, when the scale is set to groups of parts (macro - meso), and secondly, when the system has almost no impact on the heat transfer anymore, thus remaining locally into effects between single parts, the level of the problem is set to micro-scale.

As also found in [Cos12], gas quenching processes are split in this work between **three process levels** as pictured in **Tab. 3-2**:

- **micro**, consisting of the surrounding elements of a part (single or located in a batch), where the quenching action focuses on the surface properties (geometry, temperature) of the part. The gas flow needs to be optimized in order to satisfy the quenching requirements, depending on the material properties of the part, and the geometry influencing the impinging or streaming gas flow;
- **meso**, including a system of parts with its carrier. The interaction between neighboring parts is investigated over the impact on the gas flow, and the influence over the local heat exchange (intensity and homogeneity). The blocking grade of the ensemble of parts and of the charge carrier is also investigated at this level;
- **macro**, considering the flow of the gas into the whole quenching chamber, thus investigating the effect of the macro geometry of the batch (as a whole system) on flow structures taking form from the gas;

For the three process levels, various part types are quenched according to specific batch organization represented in Tab. 3-2. Excluding the micro-level, where the single part is observed, gas quenching processes can be split into 4+ dimensions (0 to 3-D, with a possible integration of dynamic quenching process).

***Table 3-2**: Scaling in gas quenching processes*

Part type (Micro)	**Cylindrical, long** 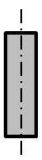	**Cylindrical, flat with high block grade** 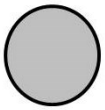	**Cylindrical, flat with low block grade** 	**Complex (e.g. motor block, teeth)** 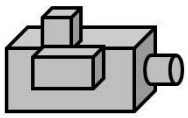
Batch type (Meso)	**0D** 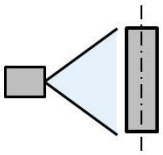	**1D** 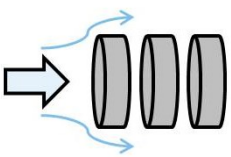	**2D** 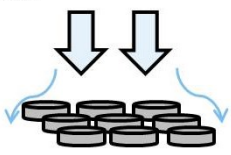	**3D** 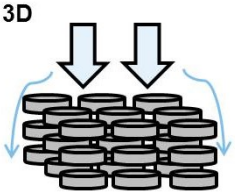
Chamber type (Macro)	**Peripheral/nozzle** 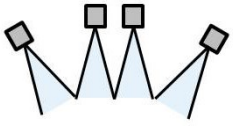	**Uni-directional, through-cooling flow** 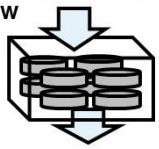	**Bi-directional, through-cooling flow** 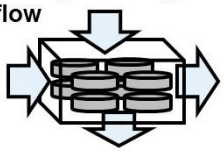	**Multi-directional** 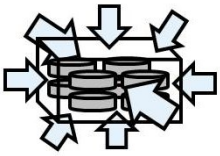

The notion of dimensionality in gas quenching has been extended from the development of "*2-D*" quenching chambers, as in [Heu11b] [Heu13a] [Heu13b]. In order to improve the efficiency of the production cycle, and expand the gas quenching applications field to larger and more complex geometries, the *one-piece-flow* [Heu11b] or *single-piece-flow* [Kor16] strategies have been investigated, as seen in **Fig. 3-16**, as part of lean manufacturing processes of gears.

The present work defines flow conditioning under the **dimensionality of gas quenching** as follow:

- **0-D**, focusing on quenching a single specimen, flow conditioning requires a complete dependence of the quenching setup on the specimen geometry and material, initial or targeted properties;
- **1-D**, focusing on quenching an in-line arrangements of specimen, where flow conditioning ensures that the flow around each part is almost similar, with particular attention to the flow impacting the first part, whose intensity strongly decreases, a posteriori;
- **2-D**, focusing on quenching a 2-dimensional, flat batch of specimens, where the distribution of the impacting flow onto the surface requires to be uniform;
- **3-D**, focusing on quenching a 3-dimensional, full batch of specimens with requirements integrating the 1-D and 2-D aspects, including the impacted surface of the batch, and the neighboring effect between parts.

The *4-D quenching* systems mentioned in [Her15] [Kor16] and seen in Fig. 3-16 are in fact dynamic 0-D systems: the static nozzle field specially fits the specimen geometry which is rotating inside the field.

This integrated heat treatment line illustrates the concept of lean manufacturing with its in-line arrangement of helical gears successively carried through the different phases of the process, from the initial heating phase, to low-pressure carburizing, a diffusion phase, and finally gas quenching of single specimens.

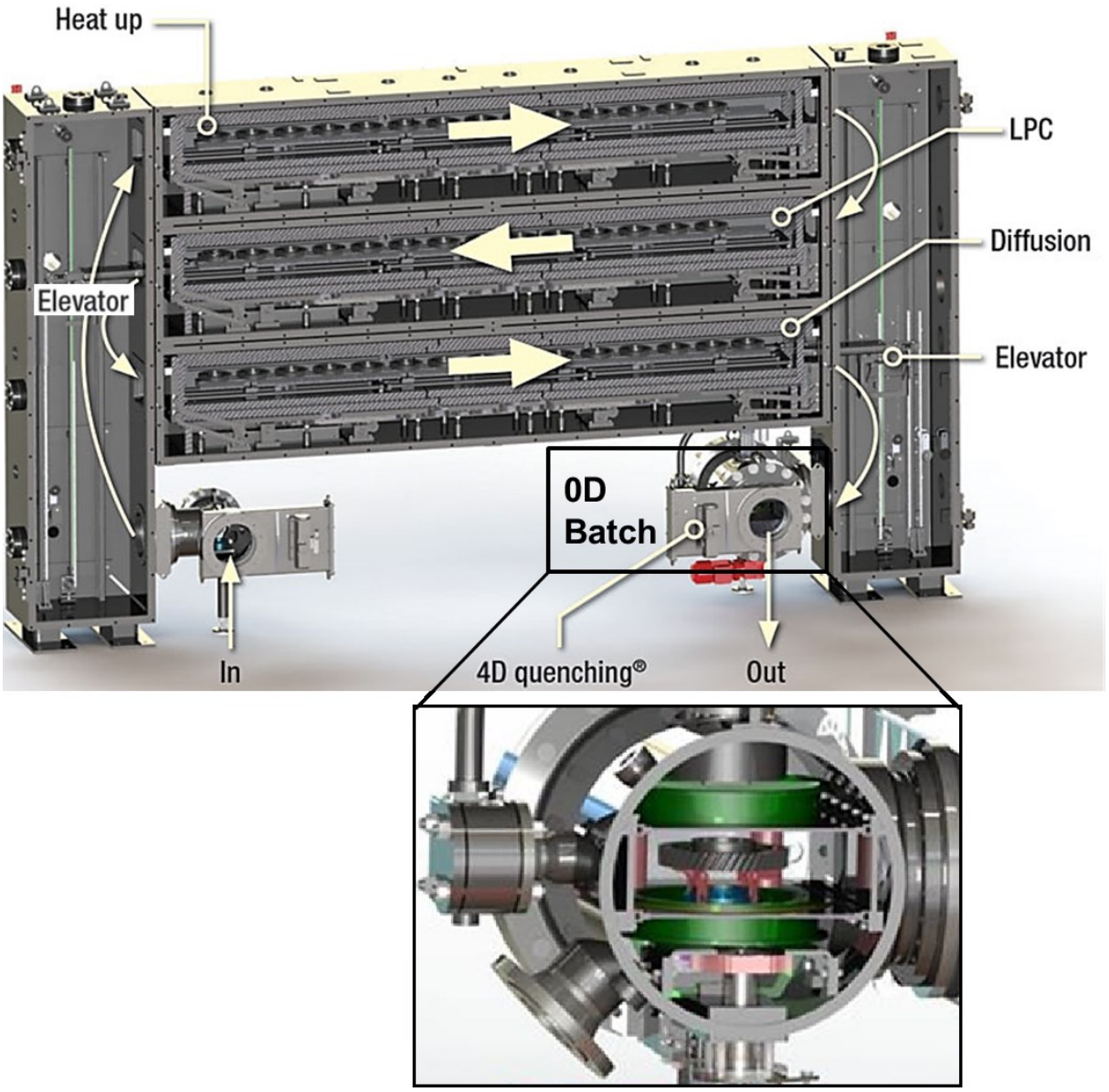

***Figure 3-16**: Load transport in a low-pressure carburizing and high-pressure gas quenching furnace (top), and a closer view of the 15 bar nitrogen gas quenching unit with a rotating helical gear at the center of the chamber (bottom), adapted from [Her15] and [Kor16]*

Trends are summarized for the various dimensions connected to time and specimen geometries in **Fig. 3-17**, demonstrating the recent growing interest for smaller batches, still mostly focusing on cylindrical or flat gear geometries.

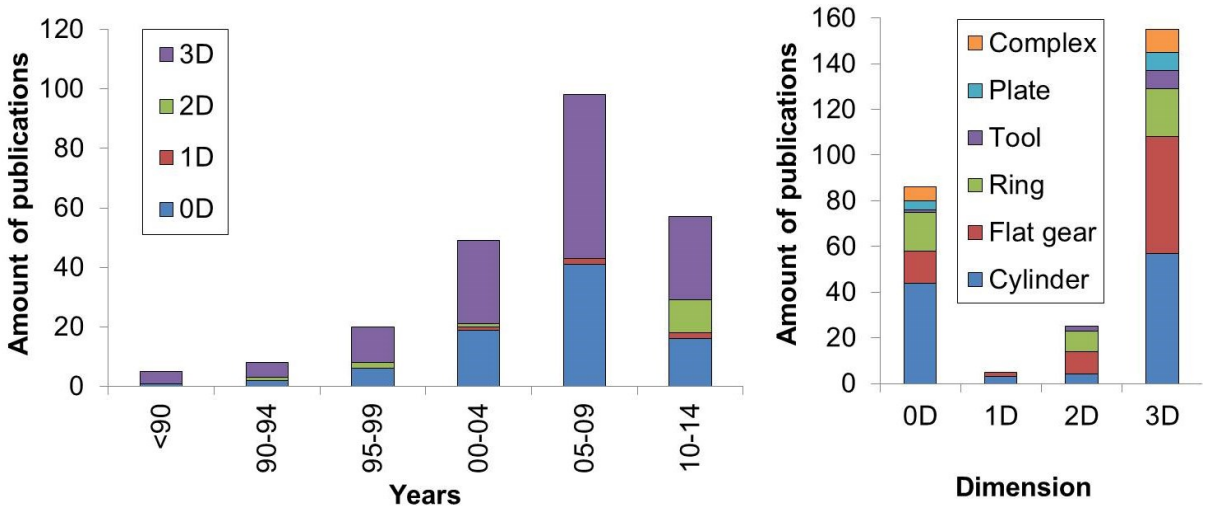

***Figure 3-17**: Amount of publications regarding the dimension of the batch in gas quenching through the years (left) and distribution of the geometries according to their batch dimension (right)*

Gas quenching chamber types can be split, according to Tab. 3-2, in:

- a **peripheral cooling system**, or *horizontal cooling system*, mostly consisting in a field of nozzles whose impinging jets perform a local, intensive cooling on complex, massive geometries;
- a **through-cooling system**, or *vertical cooling system*, whose recirculated gas flow, consisting of an aperture larger than a nozzle, aims at quenching a batch of small workpieces, taking the form of rigid nozzles/perforated plates, large, rotative nozzles, or diffusor. The gas flow can take the form of one- or bi-directional (or reverse) flow;
- a **multiflow** cooling system, such as the combination of horizontal and vertical cooling techniques to provide more flexible quenching options for various geometries.

The selection of the process dimension depends primarily on the part or batch geometry, and secondly on (also strongly related to) cost aspects, as presented in **Tab. 3-3**.

With increasing process dimension, the cost per part and the process time decrease, whereas the advantages brought by a smaller batch size or from single parts will reduce, such as the quenching intensity and homogeneity, as well as the ability to integrate the quenching process into a production cycle (process integration).

***Table 3-3**: Evaluation of the impact of batch size and dimensionality on conventional process parameters (cost, time, integration capability and quenching effectivity)*

	0D	1D	2D	3D
Cost per part	--	-	+	++
Process time	--	-	+	++
Process integration	++	+/-	+/-	--
Quenching intensity	++	+	-	-
Quenching homogeneity	++	+	-	--

3.3 Heat treatment spray quenching

Spray quenching, as reported in [Dei89] [Sch12] [Pol13], offers a greater range of heat transfer coefficients in comparison to gas quenching, and a greater flexibility and control over the process in comparison to conventional oil-based quenching media. Spray quenching enhances the temporal (the specimen is not *dropped* in a bath, sprays can be rapidly switched on and off), and spatial (quenching medium distribution over the specimen) heat treatment possibilities. The main drawback of quenching in liquids compared to gas quenching is the problem of facing uncontrolled changes in its temporal heat transfer distribution: from film boiling to nucleate boiling, and finally, pure convection and different heat transfer mechanisms prevail [Sta14]. Spray quenching aims also at reducing workpiece distortion caused by the variations in the heat transfer coefficient values, due to the phase transformation happening during conventional liquid-based quenching.

As seen in **Fig. 3-18** [Sch12], a spray is obtained through the atomization of a liquid by a pressured gas in a specifically shaped nozzle. Critical parameters, such as the droplet size and the spray distributions, influence the heat transfer induced by the spray at the surface of the specimen, as detailed below.

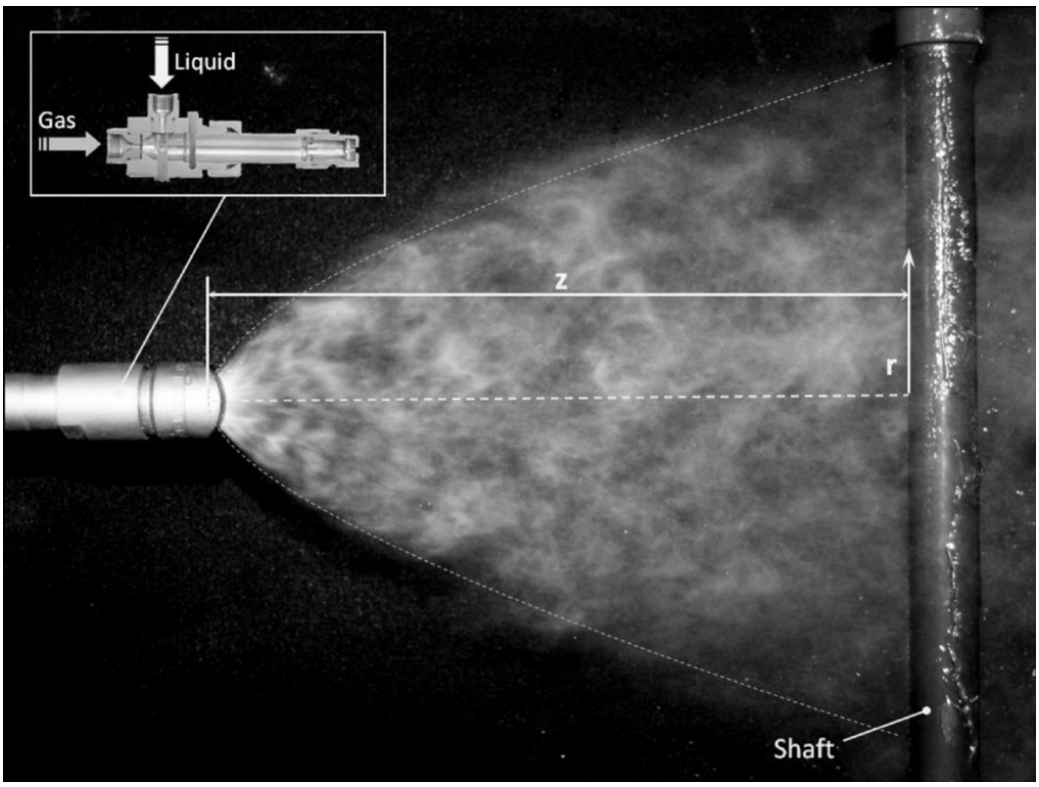

***Figure 3-18**: Atomization and spraying of water onto a metal shaft specimen using pressured air by a twin-fluid, flat-spray nozzle [Sch12]*

3.3.1 Parameters

3.3.1.1 Impingement density

The impingement density, as defined by [Jes10], is the quantity of liquid reaching the solid per unit of time and area (mass flow rate). An increase in the impingement density produces an increase in heat transfer and a shift of the Leidenfrost temperature to higher values.

For a given spray nozzle geometry, the impingement density can be evaluated by the means of a patternator, which consists of one (or more) linear arrangement of equidistantly-spaced tubular containers capturing the water droplet along the sprayed surface.

3.3.1.2 Spray shape

Nozzle geometries offer the possibility to vary the spray shape, depending on the positions of the liquid and gas outlets, as well as their respective pressures. The spray shape allows a focus of the heat transfer activity towards specific solid shapes, as thin, long shafts (Fig. 3-18), for instance.

Figure 3-18 shows the expansion of a spray cone characteristic of a flat-spray, twin-fluid nozzle (with water and air in Fig. 3-18). The combination of multiple sprays, as in **Fig. 3-19**, improves the spatial quenching control by fitting the quenching conditions (nozzles distribution) directly to the quenched part geometry, furthermore saving quenching medium.

3.3.2 Range of applications

Recent forming processes of metal components (aluminum, steel), e.g. in the automotive or aerospace industries, require a precise definition of the cooling parameters during the quenching phase of the metallic specimen. Spray quenching offers the spatial (control of the droplet distribution at the specimen surface), and temporal (control of the gas and liquid mass flow rates, or pressure) flexibility to heat treat various specimen alloys and geometries.

The two main applications of heat treatment spray quenching are (Fig. 3-19):

- the **sheet-metal** industry (left) [Dei89] [Hal97], consisting in the forming of thin metal parts (usually aluminum), of complex shapes;
- the **forging** industry (right and bottom) [Hin12] [Pol13], mostly consisting of massive parts requesting homogeneous cooling higher intensity than gas quenching.

Spray quenching is a reasonable method to control heat transfer across a specimen shape, as seen in Fig. 3-19 (right), where an array of eight nozzles covers the surface of a stepped shaft (controlled steel bainitizing). The multiplication of application points (amount of nozzles), and its management over the time (stepped quenching), ensure the smooth quenching of larger specimens (Fig. 3-19, bottom).

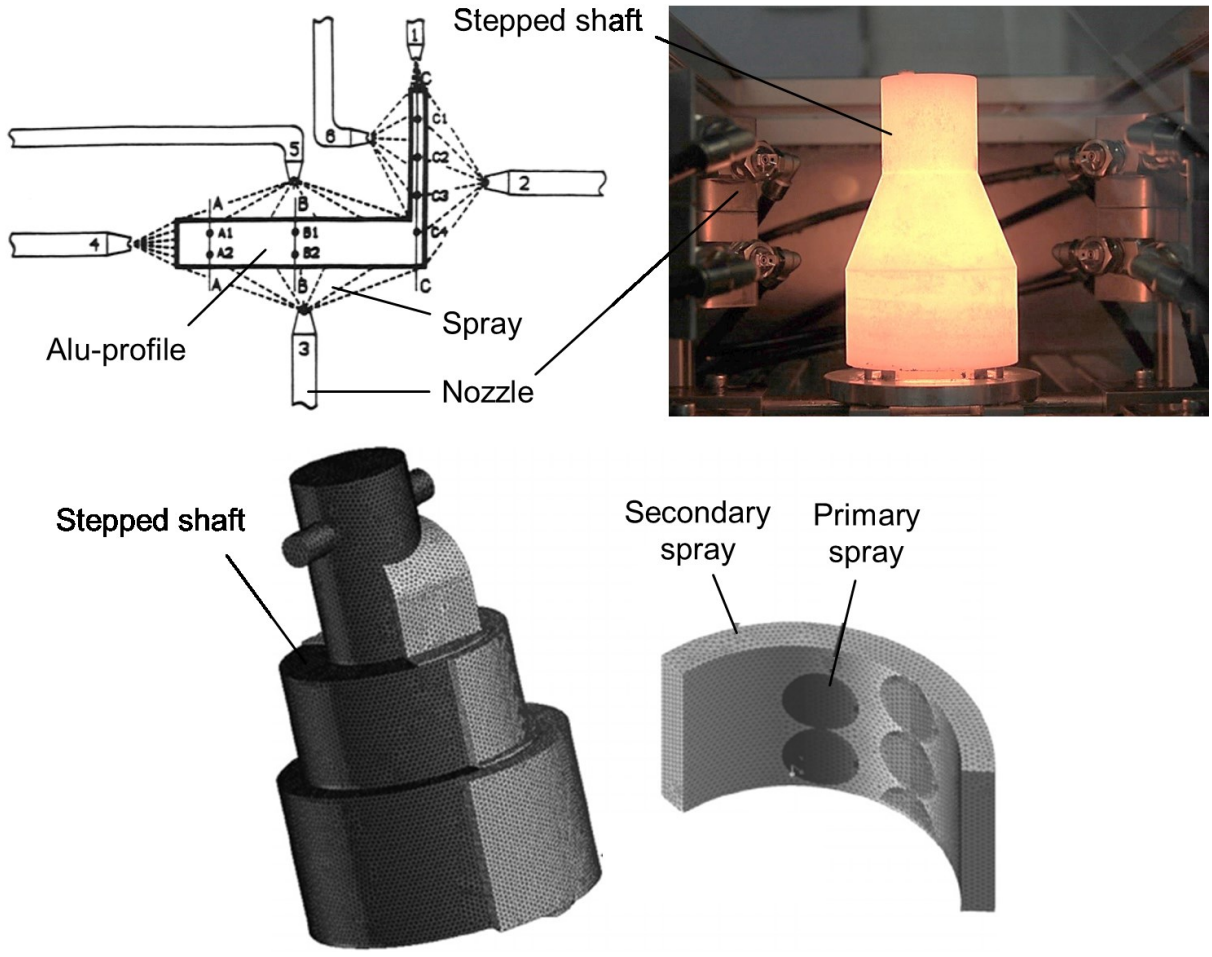

***Figure 3-19**: Arrangement of spray nozzles to quench an aluminum part (left), adapted from [Dei89], two levels of four spray units surrounding a heated stepped shaft specimen (right), and spray distribution over a quenched stepped shaft (bottom), adapted from [Pol13]*

3.4 Gas flow and heat transfer in quenching processes

The heat treatment quality is correlated to the intensity and homogeneity of the heat transfer coefficient, distributed at the surface of the parts to be quenched in the batch. The heat transfer coefficient relies directly on the gas flow around the batch of parts. As a consequence, the main physical values involved in the analysis of flow dynamics for heat transfer are being introduced below.

3.4.1 Characteristic physical values and numbers

3.4.1.1 Fluid dynamics numbers

The Reynolds number defines the flow structure as

$$Re = \frac{u_\infty L}{\nu} \tag{3-2}$$

with u_∞ defining the velocity of the streaming flow, ν representing the kinematic viscosity of the gas, and *L* as a characteristic length (along the workpiece). In gas quenching process, gas flows commonly reach $Re > 3.10^6$ [Lio04], thus belonging to the range of highly turbulent flows, based on the inlet velocity.

The Prandtl number provides the information about the behavior of the momentum-transport to the heat transport as

$$Pr = \frac{\nu}{a} = \frac{C_p \eta}{\lambda_g} \tag{3-3}$$

with *a* the temperature conductivity, and η the dynamic viscosity.

The turbulence intensity *Tu* is an indicator of the level of turbulence transported inside a flow. The production and dissolution of eddies [Bös07] directly influence the production of turbulences in the three dimensions when the flow is non-laminar. The turbulence intensity is quantified using the fluctuating part of the velocity, defined as the difference between the velocity in one direction and its temporal mean [Rat92],

$$(u_{x,y,z})_t = \overline{u_{x,y,z}} + (u_{x,y,z}{}')_t \tag{3-4}$$

The turbulence intensity of a flow is defined as the ratio of the root-mean-square of the turbulent velocity fluctuations (proportional to the turbulent kinetic energy, *k*) to the root-mean-square of the three mean velocity components as

$$Tu = \frac{\sqrt{1/3\left(\overline{u_x'^2} + \overline{u_y'^2} + \overline{u_z'^2}\right)}}{\sqrt{\left(\overline{u_x{}^2} + \overline{u_y{}^2} + \overline{u_z{}^2}\right)}} \tag{3-5}$$

which takes the following form in an isotropic flow [Sig08],

$$Tu = \frac{\sqrt{\overline{u'^2}}}{\bar{u}} = \frac{\sqrt{\frac{1}{n}\sum_1^n((u)_n - \bar{u})^2}}{\bar{u}} \tag{3-6}$$

When expressing the standard deviation of the velocity under the form

$$\sigma_u = \sqrt{\frac{1}{n-1}\sum_1^n((u)_n - \bar{u})^2} \tag{3-7}$$

the approximation of n-1 ≈ n for a large amount of samples lead to reformulating the turbulence intensity of a flow as the ratio of the standard deviation to the mean of its velocity,

$$Tu = \frac{\sigma_u}{\bar{u}}\,. \tag{3-8}$$

The turbulence intensity has a direct influence on the flow-velocity uniformity/homogeneity and intensity, thus on the heat transfer taking place during gas quenching processes.

The pressure loss generated by a quenching apparatus is the sum of the successive pressure losses created by the chosen technologies through which the gas flows, such as the varyating pipe geometries, the heat exchanger arrangement, or the quenched charge itself. For all types of flow patterns, the pressure loss can be expressed as

$$\Delta p = \zeta a \frac{\rho u^2}{2},$$

where ζ is the drag coefficient (depending on the Reynolds number), and a a factor depending on the nature of the flow [Kas10].

3.4.1.2 Heat transfer numbers

In heat treatment mechanisms, the process effectivity and efficiency are quantified using the heat transfer coefficient, represented by the non-dimensional Nusselt number:

$$Nu = \frac{hL}{\lambda_g} \tag{3-9}$$

which is the ratio of the convective to the conductive heat transfer in the fluid, where h, L, and λ_g respectively define the heat transfer coefficient, a characteristic length depending on the geometry of the system, and the heat conductivity of the gas.

The Biot number, in analogy to the Nusselt number when considering solid materials, is defined by

$$Bi = \frac{hL}{\lambda_s} \tag{3-10}$$

where λ_s is the heat conductivity of the solid material, and serves as a reference to use the lumped-capacitance method for specimen heat transfer evaluation. Knowing the cooling rate of a quenchant for a given geometry, the Biot number determines the ability of the part to reach certain core hardness due to the effect of the heat conductivity.

3.4.1.3 Heat transfer mechanisms

Optimizing a quenching process requires a full understanding of gas flow dynamics and heat exchange properties for applications in metal heat treatment. Heat transfer mechanisms in heat treatment gas and spray quenching are governed by four types of mechanisms:

- **conduction**, a diffusive process for heat exchange based on the molecular motion or vibration. The ability of a material to conduct heat is given by its thermal conductivity (0.0246 W/(K.m) for air). Those of solids, improved by the motion of free electrons, are far larger than those of gases, making the conductivity effect in gaseous heat exchange neglectible [VDI10]. For gases, the thermal conductivity ranges from 0.015 for carbon dioxide to 0.15 W/(K.m) for hydrogen whereas liquids and solids range from 0.1 to 0.65, and from 1 to 450 W/(K.m), respectively. The thermal conduction is carried out via molecular motion, thus improved when the temperature increases in the system. The Fourier's law relates the thermal conductivity of the material, the temperature temporal evolution, and the heat flux by

  $$\dot{q} = -\lambda \frac{\partial T}{\partial x} \tag{3-11}$$

  as the positive heat transfer is directed towards the decreasing temperature.

- **radiation**, is the conversion of thermal energy (charged particles) from all matter into electromagnetic waves diffused in its surroundings, based on the emissivity property of the material and the temperature of the surface of the matter, as defined by the heat flux of a real body $\dot{e}$ compared to the one of a black body $\dot{e_r}$,

$$\dot{e} = \varepsilon \, \dot{e_r} = \varepsilon \, \sigma \, T^4 \tag{3-12}$$

with ε the emissivity of the real surface ($0 < \varepsilon < 1$, with metal grey surfaces tending to 0), and σ the Stefan-Boltzmann constant ($5.67.10^{-8}$ W/(m²K⁴)).

- **convection**, is the heat transfer resulting from the macroscopic motion of matters, involving the dynamics of fluids. Difference has to be made between *free* (or *natural*) convection, which is produced by buoyant forces (fluid motion produced by itself, due to e.g., thermal expansion), and *forced* convection, where the heat transfer is resulting from an external fluid motion (e.g., through artificial convective current from a fan or a pump).

  The convective heat transport is given by the relation

$$\dot{q} = h(T_W - T_\infty) \tag{3-13}$$

  with *h* the heat transfer coefficient, and stating $T_W > T_\infty$, thus cooling the wall using the convective fluid at the surface.

- **evaporation**, where vapor bubbles are formed from nucleus located at the surface of a liquid film, depending on the local temperature or surface roughness. The vapor in the bubble requires a higher pressure than the liquid layer around in order to grow from the superheated film.

Considering a non-slip condition and a fluid at rest at wall-level in the configuration of the boundary layer, and a heat balance at wall level comparing Eq. (3-11) and Eq. (3-13), the heat transfer coefficient can be expressed as

$$h = -\lambda \frac{\left.\frac{\partial T}{\partial y}\right|_{y=0}}{T_W - T_\infty} \tag{3-14}$$

with the thermal boundary layer defined as $\delta_t \sim {}^{\lambda}/_{h}$.

During heat treatment gas quenching, the heat extracted during the process can be described as the sum of the convective and radiative heat loss undergone by the batch. The potential heat exchange undergone by the quenched batch expressed as heat flux is then

$$\dot{q_b} = \dot{q_r} + \dot{q_c} \tag{3-15a}$$

$$\Leftrightarrow \dot{q_b} = \varepsilon\, \sigma({T^4}_W - {T^4}_\infty) + h(T_W - T_\infty) \tag{3-15b}$$

Considering a batch temperature of around 1000 K and free convection at room temperature (*h ~ 25 W/(K.m²), T ~ 300 K*), Eq. (3-15a) can be approximated to

$$\dot{q_b} \sim 16872 + 17500 \tag{3-15c}$$

thus demonstrating comparable influence of both radiation and convection on the thermal exchange in the quenching chamber. The use of a gaseous quenchant improves the heat transfer coefficient by a factor 10 to 100, thus reducing the influence of thermal radiation. The decrease in batch temperature also reduces the effect of thermal radiation. Thermal radiation can therefore be neglected during heat treatment gas quenching involving forced convection as also stated in [Loh96] [Sch13].

3.4.1.4 Correlations

The integral heat transfer coefficients are compared with the standard correlation for the streamwise flows over a surface from [Gni10a],

$$Nu_{L,0} = 3 + \sqrt{Nu_{lam}^2 + Nu_{turb}^2} \tag{3-16a}$$

with

$$Nu_{lam} = 0.664 Re^{1/2} Pr^{1/3} \tag{3-16b}$$

$$Nu_{turb} = \frac{0.037 Re^{4/5} Pr}{1 + 2.443 Re^{-1/10}(Pr^{2/3} - 1)} \tag{3-16c}$$

Pr and *Re* are dimensionless numbers, and respectively define the Prandtl number and the Reynolds number.

In gas quenching processes, Belinato et al. [Bel10] state that the heat transfer coefficient is proportional to the flow rate and the pressure of the gas in similar ways, so that

$$h \sim (u_\infty p)^m \tag{3-17}$$

where *m* takes a non-dimensional, empirical value from 0.6 to 0.8. In fact, the heat exchange increases due to the molecular impacts produced by an increase in pressure (molecular density), or velocity (molecular motion), as also demonstrated experimentally [Mid96] [Nar09].

Heuer and Löser [Heu04] [Lös05] mention a formulation of the heat transfer coefficient in industrial gas quenching in terms of the basic physical parameters:

$$h = C_2 {u_\infty}^{0,7} p^{0,7} l^{-0,3} \eta^{-0,39} {C_p}^{0,31} {\lambda_g}^{0,69} \tag{3-18}$$

based on the conventional Nusselt-based correlation involving the flow characteristics by the Reynolds number (*Re*), and the gas characteristics by the Prandtl number (*Pr*). This practical-oriented correlation directly identifies the influence of the velocity and the pressure of the streaming gas on the batch on the heat transfer. The constant C_2 is a chamber constant depicting the influence of the quenching chamber geometry to the gas flow, and the final heat transfer coefficient value resulting.

3.4.2 Flow structures

Various constructive parameters in quenching and batch processes play a role on the flow structure developing during heat treatment gas quenching [Sch01] [Lös03]:

- the charge produces a blocking grade leading to two effects on the surrounding gas flow: the mean flow velocity is directly proportional to the free surface offered by the batch (e.g., the room between the parts). Higher batch density implies a higher average velocity, hence a more effective heat exchange, but also a higher pressure loss due to the higher blocking grade. Moreover, the blocking grade from the charge leads the flow to escape to the side of the batch as the batch cannot exactly fit the complete space of the quenching chamber. Higher flow velocity is thus expected on the sides of the batch;

- the gas mass flow circulating inside the quenching compliance undergoes various fluid dynamics phenomena during its circulation, such as turbulence generation and pressure drops, due to the technical solutions (flow conditioners, heat exchangers), and geometry of the facility. The ventilator has a specific response, also relating the pressure drop to the available mass flow;
- most of the heat transfer between the batch and the gas is produced by impinging gas onto the surface of the part. With low velocity, recirculating flows fail to reach the intensity of impinging flows, so that the optimal condition for intensifying gas quenching processes resides in improving impinging flows.

It is however possible to classify gas flows in gas quenching process according to flow configurations found in the literature, as introduced below.

3.4.2.1 Flow patterns in gas quenching chambers

Laminar versus turbulent flow

The gas flow in a quenching chamber is characterized by its Reynolds number, defining the level of turbulence contained in the flow. High turbulent flows are mostly found in gas quenching process, which leads to the increase in convective heat transfer [Hof92] [Wib03], but also to high heterogeneity of the heat transfer coefficient, as described in the configurations below.

Pipe flows

Pipe flows [Gni10b] are among the most studied flow structures in fluid dynamics as they are part of several technical processes (e.g., process engineering, oil). In the context of gas quenching, pipe flows take place inside the gas supply system, in the gas quenching compliances, and condition the gas flow before entering the quenching chamber, through the heat exchanger or flow conditioner situated before the charge to be quenched, in the case of multi-dimensional gas quenching processes.

The drag coefficient ζ related to pressure losses in pipe flows can be obtained in the case of flows inside smooth pipes in the range $2.10^4 < Re < 2.10^6$ (usual in gas quenching) from the Hermann equation [Kas10],

$$\zeta = 0.00540 + \frac{0.3964}{Re^{0.3}}. \tag{3-19}$$

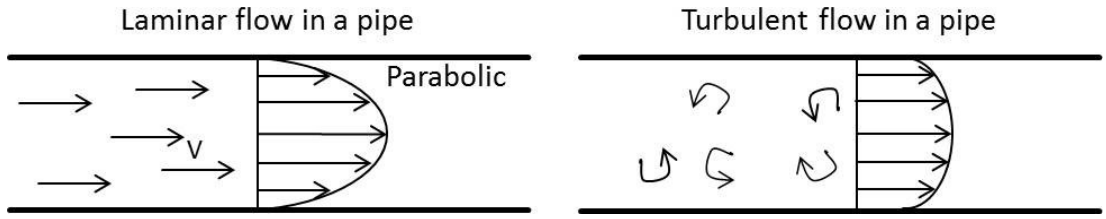

***Figure 3-20**: Effect of the turbulence in pipe flow with corresponding velocity profiles*

Depending on the intensity of the turbulence, pipe flows are split between turbulent and laminar flows, as described in **Fig. 3-20**, using the velocity profiles in the two various configurations.

Considering the Reynolds number, laminar flows (in pipes) occur at *Re < 2300*, transitional flows at *2300 < Re < 10000* and turbulent flows at *Re > 10000* [Gni10b]. For gas quenching applications, the complexity of the chamber with gas supply, heat exchanger, and additional flow conditioners leads the gas flow to be highly turbulent (with a Reynolds number ranging from about 10000 up to 1000000), thus belonging to turbulent gaseous flows.

Gnielinski [Gni10b] suggested a correlation for the heat exchange in fully developed pipe flows,

$$Nu_m = \frac{\left(\frac{m}{8}\right) RePr}{1 + 12{,}7\left(\frac{m}{8}\right)^{0{,}5}\left(Pr^{0{,}66} - 1\right)}\left[1 + \left(\frac{D}{L}\right)^{0{,}66}\right] \tag{3-20}$$

with

$$m = (1{,}8 log_{10} Re - 1{,}5)^{-2}$$

and a validity range defined as *0.1 < Pr < 1000*; *10000 < Re < 1000000*; *D/L < 1*.

A rather simplified expression for approximate calculations exists for transitional flows (*Re < 10000*) in the range *0.5 < Pr < 1.5*, thus valid for the flow in gas quenching processes, as

$$Nu_m = 0{,}0214(Re^{0.8} - 100)Pr^{0.4}\left[1 + \left(\frac{D}{L}\right)^{0.66}\right]. \tag{3-21}$$

Flow over/past a plate

Considering higher process dimensions, when the size of the chamber is far larger than the size of the boundary layer at the surface of the part to be quenched, the gas flow can be approximated to a 1-D flow streaming onto the surface of the plate (excluding the case of impinging quenching techniques).

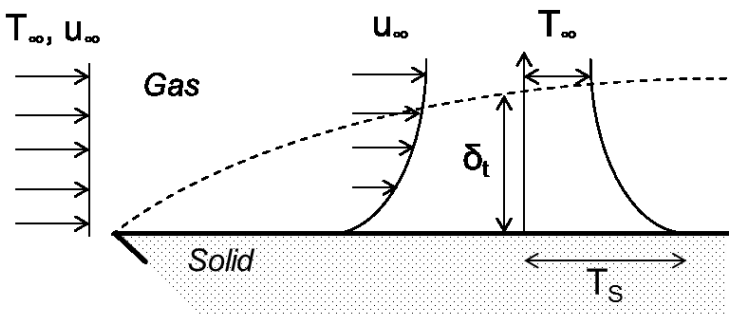

***Figure 3-21**: Scheme of the boundary layer from a flow stream onto a plate with velocity and temperature profiles near the wall*

The boundary layer can be seen in **Fig. 3-21** as the area between the quenching gas and the solid to be quenched where the heat exchange takes place.

After the streaming gas flow reaches the edge of the quenched surface, the boundary layer logarithmically increases with the streamed length on the surface as profiled in Fig. 3-21.

Recirculating flows

Recirculating flow is a particular case of flow separation. It occurs when the boundary layer leaves the area to where it was previously connected, and when the effect of adverse pressure gradient causes the reverse of the flow at this location. Separation induces the formation of eddies and vortices, as well as recirculating zones.

Recirculating zones are presented in this work divided into two groups, depending on the size (micro and macro), and influence of the zones on the gas quenching process:

- **micro-recirculation**, is the recirculation happening around single parts and characterized with smaller turbulence scales, as observed in simulative [Pel05], and experimental [Kay92] [Lio04] [Wib05] works (**Fig. 3-22**). The separation occurs at high turbulence in the front side of the impinged part, and features lower velocities at the rear side of the part, as depicted by the streamlines.
- **macro-recirculation**, is the recirculation happening in the quenching chamber due to the blocking grade of the batch and other flow conditioning elements. While micro-recirculation does not harm the global stability of the gas flow as the scale of turbulence stays small, macro-recirculation often leads to unbalance in the heat treatment process, and requires technical improvements in order to lessen their influence [Lös03].

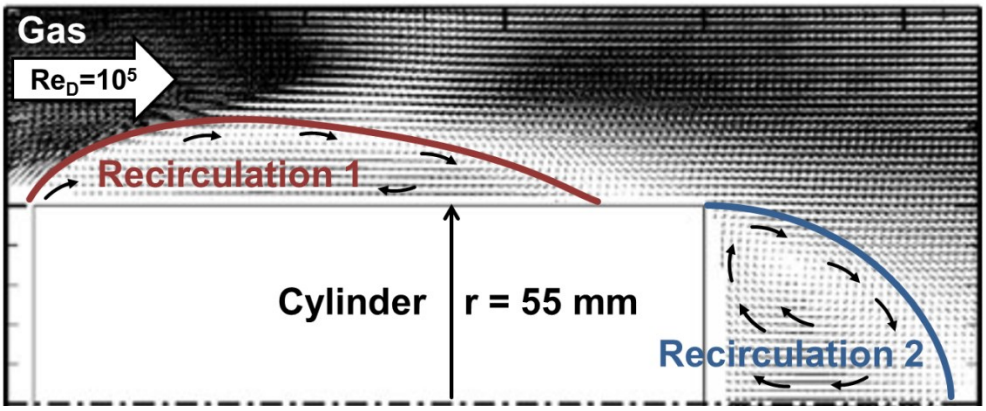

***Figure 3-22**: Velocity distribution around a magnetically supported right circular cylinder aligned with the free stream, adapted from [Hig08]*

Impacting flow on cylinders

Gas flow affecting heat transfer on cylinder has been widely investigated concerning the two main available configurations [Lho92]: transverse flow (characteristic for heat exchangers [Gni10c]), and axial flow (conventional gas quenching process [Lio04]), so that

- a **transverse flow** occurs when the gas flow is transverse to the cylinder. For group of cylinders, correlations are given depending on the arrangement of the cylinders (through a varying tube arrangement factor F_a), in-line,

$$Nu_D = 0{,}34 F_a {Re_D}^{0{,}61} Pr^{0{,}31} \quad \text{(3-22a)}$$

  or staggered,

$$Nu_D = 0{,}35 F_a {Re_D}^{0{,}57} Pr^{0{,}31} \quad \text{(3-22b)}$$

  based on the Grimison approach [Kha06].
- an **axial flow** occurs when the gas flow is parallel or in a narrow angle of incidence to the cylinder. For group of cylinders, heat transfer is quantified as an analogy to a duct configuration, with the following Colburn correlations, similar to the Dittus-Boelter correlation [Lho92]:

$$Nu_D = 0{,}023 {Re_D}^{0{,}8} Pr^{0{,}33} \quad \text{(3-23)}$$

Due to the large recirculation occurring along the cylinder in axial mode (Fig. 3-22), heat transfer coefficients are usually lower in this configuration in comparison to transverse configurations [Hof92].

Impinging/Jet flows

Impinging flows are the product of single ducts/pipes, or array of nozzles, transporting a gas stream into a larger area where the stream expands and impinge onto a plate. The present application of impinging flow is limited to one fluid (the surrounding fluid is of the same nature as the impinging fluid) for heat treatment (supposing the plate having a higher temperature than the impinging fluid). A turbulent impingement jet flow occurs at *Re > 100* [Sch10b].

As represented in **Fig. 3-23**, three characteristic regions are found when the flow impinges the plate:

- the **free jet**, expanding and decelerating while mixing into the surrounding flow with dominating vertical velocity component until the free jet flow reaches the plate to convert into
- the **stagnation flow**, characterized by increasing horizontal velocity component, and a stagnation point in the middle of the jet axis on the plate with high turbulences and low velocity. The stagnation flow horizontally expands in the form of a free jet decelerating along the wall;
- the **wall jet** is quickly decelerating as it expands radially onto a broad surface;

additionally, the surrounding fluid will undergo recirculation/entrainment due to the motion of the jet stream from the outlet of higher velocity.

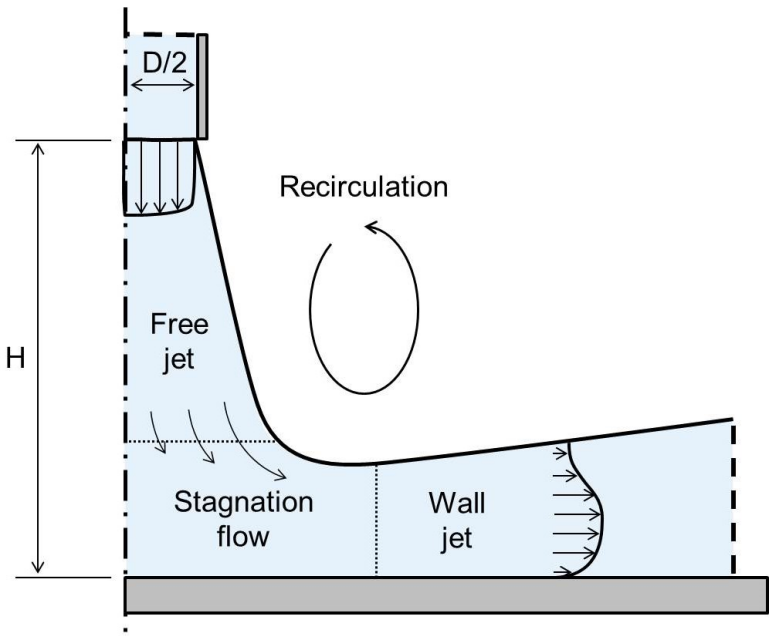

***Figure 3-23**: Development of a jet impinging flow normal to a plate with corresponding velocity profiles and characteristic dimensions, adapted from [Sch10b]*

Correlations are found in the literature covering two categories of jet flows: single round nozzle (SRN), and single slot nozzle (SSN), as represented in **Fig. 3-24** [Sch10b]. In a delimited area *r* around the stagnation point *2.5 < r/D < 7.5*; considering a ratio *2 < H/D < 12* and a turbulence range *2000 < Re < 400000*, the Nusselt-number can be expressed in both cases as [Sch10b]

$$Nu_{SRN} = \frac{1 - \frac{1.1D}{r}}{\frac{r}{D} + 0.1\left(\frac{H}{D} - 6\right)} \cdot F(Re) \cdot Pr^{0.42} \tag{3-24a}$$

with

$$F(Re) = 2[Re(1 + 0.005Re^{0.55})]^{0.5} \tag{3-24b}$$

for a SRN, and

$$Nu_{SSN} = \frac{1.53Re^{m}}{\frac{r}{D} + \frac{H}{D} + 1.39} \cdot Pr^{0.42} \tag{3-24c}$$

with

$$m = 0.695 - \frac{1}{\frac{r}{D} + \frac{H}{D}^{1.33} + 3.06} \tag{3-24d}$$

for a SSN in the range *2 < r/D < 25*, *2 < H/D < 10* and *3000 < Re < 90000*.

A correlation is proposed by Krötzsch et al. [Sch10b] for arrays of round nozzles (ARN) in the form of

$$Nu_{ARN} = G \cdot Re^{0.66} \cdot Pr^{0.42} \tag{3-25}$$

where *G* relies on the dimension of the perforated plate (hole diameter and distance between holes), valid in the range *0.004 < f < 0.04, 2 < H/D < 12,* and *2000 < Re < 100000*.

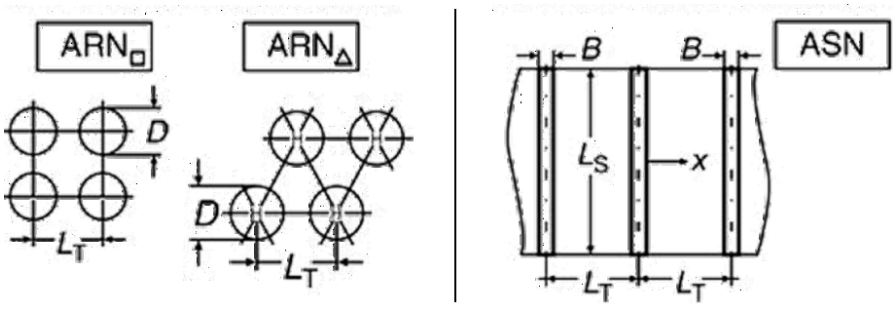

***Figure 3-24**: Two configurations for an array of round nozzles (ARN), left; and representation of an array of slot nozzles (ASN), right, adapted from [Sch10b]*

3.4.2.2 Flow conditioners

Flow conditioners aim at correcting the flow structure and patterns generated by the geometry of the batch and the quenching chamber. Flow inhomogeneity is the main reason of unbalanced cooling rates distributed in a batch, leading to hardness heterogeneities [Tro98] [Fri08]. Two types of flow conditioners are found in the literature: local ones, focusing on correcting the flow of single or few parts, and global ones, in the form of heat exchangers or perforated plates, for instance.

Local flow conditioning

Local flow conditioning implies to treat the workpiece almost individually, and can be in some cases assimilated to a nozzle-field heat treatment, as already described above [Sch04] [Ros06] [Kor16]. Solutions have been tested and simulated covering the technical implementation of flow conditioner in conventional, large batch of cylinders in a nozzle field arrangement [Fri08]. Individual constructive solutions for complex geometries demonstrate an enhancement of the quenching homogeneity and intensity due to the reduction of recirculative flows and increase in focusing flow on the surface of long gear shafts [Mac05] [Sch09].

Various simulative works are found dealing with individual flow conditioners in batch gas quenching whereas no literature is found about such techniques in experimental, industrial heat treatment, due to the high pressure drop and relative increase in investment per part issues.

Global flow conditioning

Heat exchangers are fundamental devices in gas quenching processes as they maintain the temperature difference between quenched surface temperature and quenchant temperature which, combined to high heat transfer coefficients, ensures a high heat transfer between quenched workpiece and quenching medium. Several examples and correlations [Gni10a-c] covering heat exchanger technologies (geometry, fluid, and arrangement) are found to enhance the re-cooling of the fluid. Heat exchangers, however, strongly influence the flow structure, depending on their position before or after the quenching chamber [Tro98] [Ros06] [Fod07] [Cha08]. Situated before or above (in top-to-bottom flow configuration) the quenching chamber, pipe heat exchangers reduce the size of the large eddies developed during the recirculation while producing smaller eddies, which might be source of flow uniformity, corrected using perforated plates [Tro98].

Literature about the influence of a perforated plate on the gas flow homogeneity is largely found in the field of electrostatic precipitators [Sah87] [Haq07] [Hou09] [Swa10] [Guo13], whereas the use of perforated plates in heat treatment gas quenching applications is less investigated [Lau98] [Tro98] [Lio04].

The integration of single to multiple [Sah87] [Hon07] perforated plates in the circulating gas facility aims at [DeB57] [Lio04] [Swa10]

- **regulating the low-frequency velocity fluctuations** by eliminating the recirculation eddies;
- **improving the flow uniformity**, independent of the type of gas, caused by the reversed gas direction and mixing before the entrance;

whereas their integration should avoid

- **too high pressure drops;**
- **slowing down the gaseous flow.**

Perforated plates are characterized by their hole geometries, mostly defined by the diameter and shape (round, chamfer), and their holes distribution (use of various hole dimensions, distance between holes).

The porosity (ratio of free to covered area) and the surface-to-plate distance are constructive parameters describing the application range of perforated plates [Sha01].

Positive results are mostly reported in the literature quoted above about the integration of perforated plates to uniformize gaseous flow velocity. Guidelines are described in order to select operative parameters for single to multiple perforated plates:

- a better flow uniformity is reached by **arranging the plates** (inclination, distance from inlet/outlet), the proximity of the inlet increases flow non-uniformity [Swa10];
- **varying the dimension and distribution of the holes** over a single plate brings better flow uniformity, compared to uniform distribution of same-size holes [DeB57] [Haq07];
- in heat treatment gas quenching, **larger holes** produce a slightly better HTC but a higher standard deviation [Lau98];

- whereas perforated plates mostly influence low-frequency velocity fluctuations, uniform perforated plates demonstrate low uniformization effectivity at the peripheral region: **perforating only the central region** (25% in the center, peripheral is free) is highly effective [DeB57];
- for uniform perforated plates, a **minimal porosity of 40%** is advised [DeB57];
- for two plates arranged normal to the flow, **medium porosity** provides better flow uniformity [Sah87];
- low porosity tends to diverge the flow to the peripheral area whereas high porosity produces a poor flow distribution, and high velocity in the center [Swa10];

Martin et al. [Sch10b] suggest three parameters to perform the optimization of perforated plates, as shown in Fig. 3-24:

- the **hydraulic diameter D** of the nozzle, directly influencing the blocking grade of the perforated plate, thus the pressure loss caused by the plate to the system;
- the **nozzle-to-plate distance H**, which is in most applications (not only heat treatment) the critical factor, as it relies on the vertical dimension of the process;
- the **nozzle-to-nozzle spacing L_T**, indirectly conditioning the blocking grade of the perforated plate in combination with the hydraulic diameter.

Determining H from experimental and constructive considerations, the two other parameters offer the best heat transfer configuration, according to Martin et al. [Sch10b], when

$$D \sim \frac{1}{5} H \tag{3-26a}$$

and

$$L_T \sim \frac{7}{5} H \tag{3-26b}$$

Besides the hydraulic diameter, the shape of the orifices distributed on a perforated plate is also underlined when optimizing the heat exchange potential of it, as stated by Polat et al. [Sch10b].

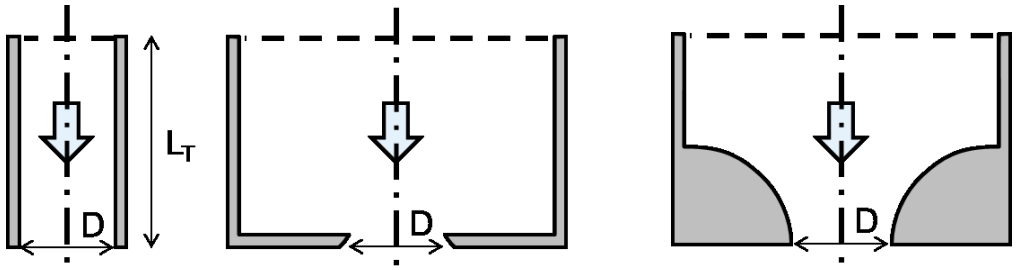

***Figure 3-25**: Nozzle outlet shapes: pipe nozzle (left), -sharp- orifice nozzle (middle) and quadrant nozzle (also contoured contraction) (right), adapted from [Sha12]*

Figure 3-25 presents the categories of shapes for orifice of jet nozzles [Sha12]. For constant exit diameter *D*, the influence onto the flow structure if different as detailed in **Tab. 3-4**. The full dimension of the orifice mostly depends on the perforated plate shape (pipe nozzle occurs from $H_{plate} \sim 10D$, in case of a fully developed pipe flow).

Zuckerman and Lior [Zuc06] summarize the effect of nozzle orifice shapes into Tab. 3-4, transposed below.

For small *H, nozzle-to-surface* distance, interactions between single jets are strong. Jet-jet interaction covers the combination of the jet entrainment effect onto the neighboring jet in a *fountain* characteristic pattern as represented in **Fig. 3-26**.

The interaction is set to significantly happen for $L_T < 4D$, while the highest heat exchanges are found for $L_T \sim 8D$, for confined array arrangement of nozzles ($H/D = 2$) [Zuc06] [Zuc08].

For higher *H, nozzle-to-surface* distance $H > 6D$, and small *nozzle-to-nozzle* distance $L_T < 2D$, which is often the configuration found for perforated plates, the jet-jet interaction is characterized by strong shear-layer interaction.

***Table 3-4**: Effect of the nozzle outlet shape onto the flow, adapted from [Zuc06]*

Nozzle type	Initial turbulence	Free jet shearing force	Pressure drop	Nozzle exit velocity profile
Pipe	High	Low	High	Close to parabolic
Sharp orifice	Low	High	High	Close to uniform (contracting)
Contoured contraction	Low	Moderate to high	Low	Uniform (flat)

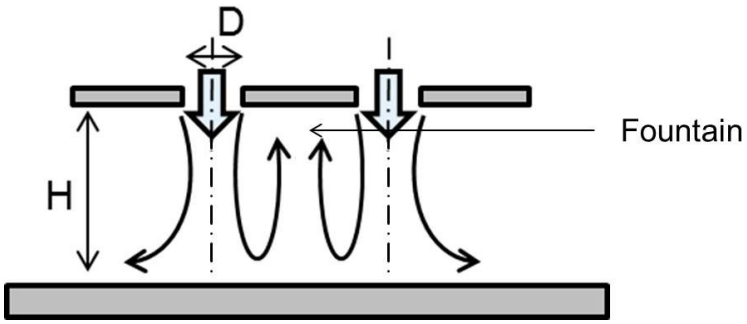

***Figure 3-26**: Jet-jet interaction producing a fountain flow in low H/D ranges, adapted from [Sch10b]*

Zuckerman and Lior [Zuc06] state that the combination of neighboring growing shear layers reduces the velocity gradient at the edge of the jet, reducing the turbulence generation furthermore. The effect of jet height and spacing of an array of nozzle is summarized in **Tab. 3-5**.

***Table 3-5**: Jet height and spacing effect of an array of nozzles, adapted from [Zuc06]*

H/D	Effect
< 0.25	Highly constrained flow, may have strong crossflow and high additional back pressure
0.25 - 1.0	Fountain flow may greatly affect heat transfer in confined arrays
1 - 2	Mild fountain effects may occur. Minor turbulence generation. Flow will be affected by confinement wall, need to ensure a clear exit pathway
2 - 8	Shear layers may interact, need to maintain sufficient L_T Best performance tends to lie in this range
8 - 12	Minimal confinement effect is overshadowed by nozzle type Need to ensure that neighboring jets remain separate
> 12	Confining wall does not influence flow, instead nozzle type and jet spacing dominate the flow field

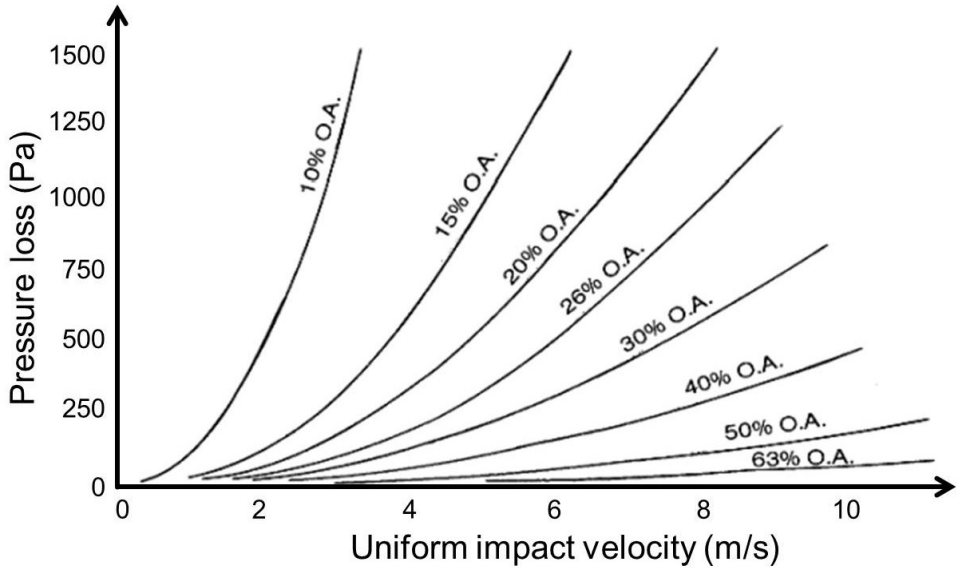

***Figure 3-27**: Pressure loss vs. impact velocity for various perforated plate porosity (in percentage of "Open Area"), adapted from [IPA93]*

The benefits on the heat transfer provided by perforated plates in uniformizing and intensifying the flow velocity [Lio04], and generating turbulences [Mac05], have to be counter-balanced with the generated pressure loss in the gas quenching apparatus, requiring an additional expense in energy from the ventilator system (hence requesting additional process costs).

Whereas the effect of the plate porosity over the pressure loss in the system can be evaluated in **Fig. 3-27**, according to standards from [IPA93], the impacting flow should ideally be perpendicular to the plate, and little subject to turbulences, to further reduce the overall pressure loss.

3.4.3 Heat transfer in spray quenching

3.4.3.1 Boiling phenomenon

During quenching of hot metal specimens with a vaporizable liquid, whose boiling temperature is below the temperature of the specimen surface, the boiling phenomenon occurs. It consists of a succession of heat transfer mechanisms, from the formation of a vapor film at the surface of the hot specimen, breaking in a transitional phase, as the temperature decreases below the Leidenfrost temperature. For temperature below the Leidenfrost point, nucleate boiling takes place, characterized by high heat transfer at the surface specimen, rapidly decreasing to reach a convective heat transfer phase at lower surface temperatures.

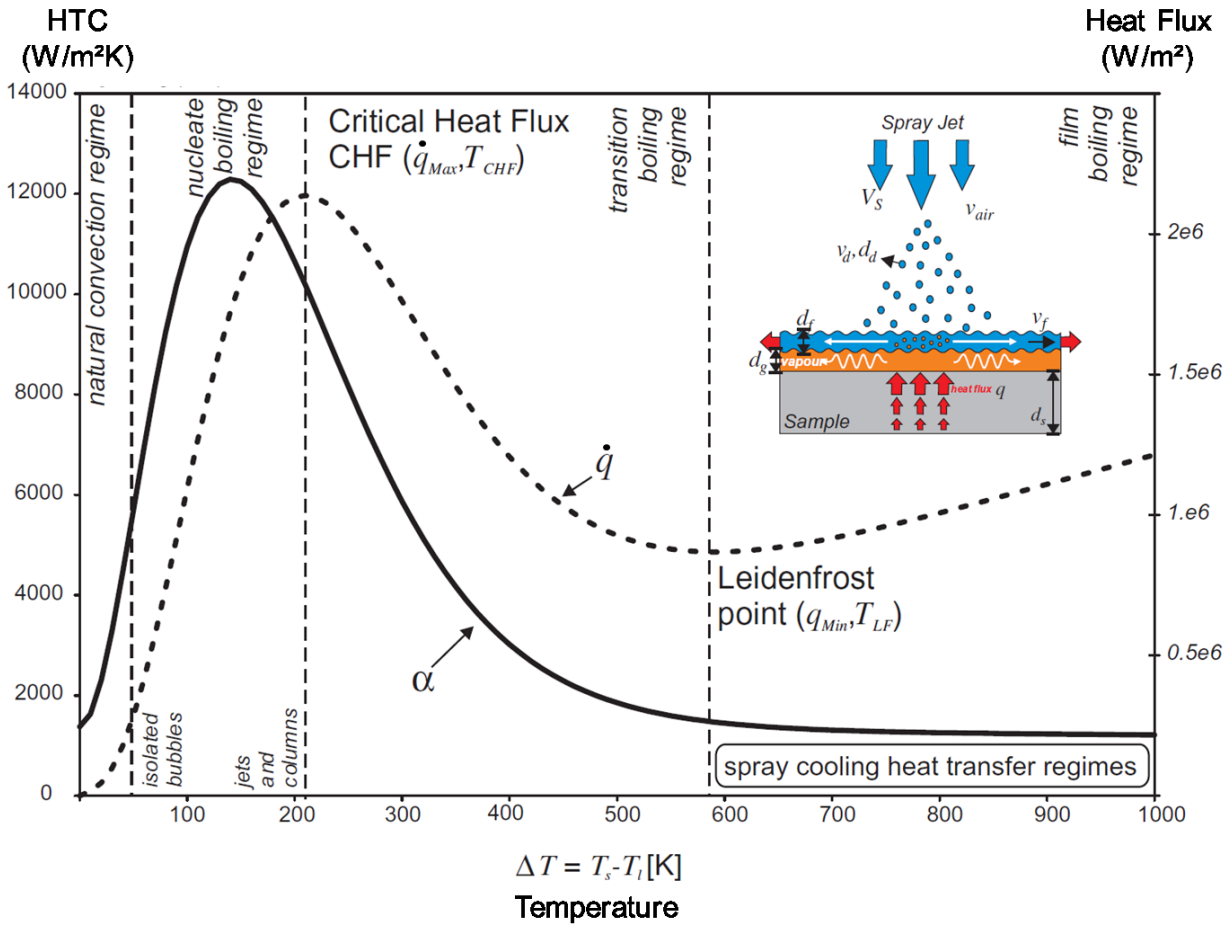

***Figure 3-28**: Spray cooling schema and boiling curve ($\dot{m}_w$ = 10 kg/m².s), adapted from [Wen08]*

Figure 3-28 summarizes the phases of the boiling phenomenon in two curves, depicting both the heat flux ($\dot{q}$) and the heat transfer coefficient (α), according to [Wen08].

3.4.3.2 Correlations

Various correlations offer the possibility to predict the heat transfer coefficient under specific conditions and according to a set of information depending on combinations of data connected to the quenchant and the quenched object.

Wendelstorf et al. [Wen08] introduce a correlation of the heat transfer coefficient (HTC) for spray quenching based on the temperature difference (ΔT) between the quenching medium and the quenched specimen, and the water mass flux ($\dot{m}_w$):

$$\begin{aligned} HTC\ (\Delta T, \dot{m}_w) \\ &= 190 \pm 25 + \tanh\left(\frac{\dot{m}_w}{8}\right) \\ &\cdot \left(140 \pm 4\dot{m}_w \left[1 - \frac{\Delta T \cdot \dot{m}_w}{72000 \pm 3500}\right] + 3.26 \right. \\ &\left. \pm 0.16\Delta T^2 \left[1 - \tanh\left(\frac{\Delta T}{128 \pm 1.6}\right)\right]\right), \end{aligned} \tag{3-27}$$

which evaluates the heat transfer coefficient in a tolerance interval.

Puschmann et al. [Pus00] consider evaporation quenching (also named *mist cooling* due to the fine droplets) as a process inherent to parameters such as

- the impingement density,
- the droplet diameter,
- the surface temperature,
- and the impact of the air flow (twin-fluid nozzle configuration),

and conclude that the heat transfer coefficient can take the following expression:

$$HTC\ (\dot{m}_w, v, d) = 16.8 \cdot \dot{m}_w \cdot v^{0.12} \cdot d^{-0.29}\,, \tag{3-28}$$

where v is the droplet velocity and d the droplet diameter [Pus03].

In evaporation quenching, the impinging spray droplets completely evaporate at the surface of the quenched specimen, without generating a steam film, between liquid and specimen, as conventionally observed during the boiling phenomenon. Thus, the Leidenfrost phenomenon takes place only at the droplet scale level; hence heat transfer coefficients are more stable during the cooling phase, and take higher values compared to spray or film cooling for similar water mass fluxes (**Fig. 3-29**).

Thereby the total heat flux can be substantially increased in comparison to conventional spray quenching techniques, using a minimum amount of quenchant [Pus03].

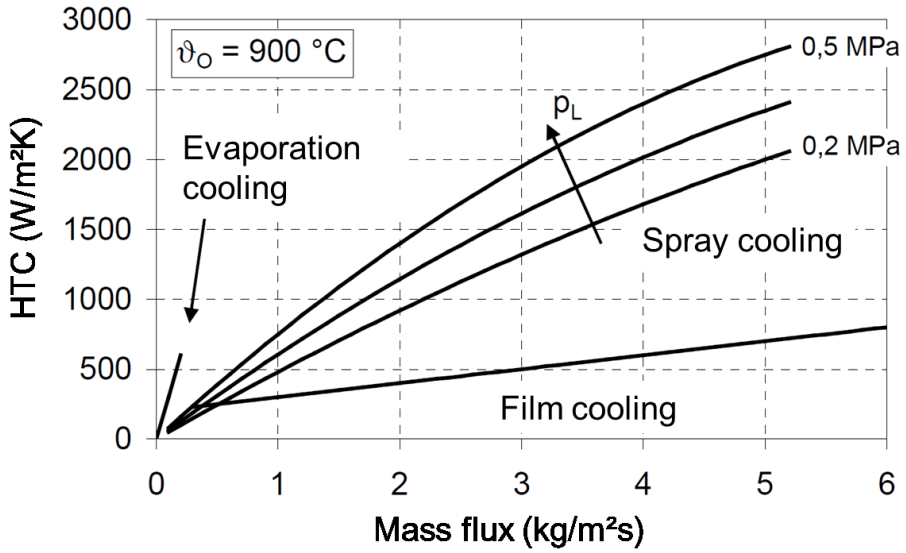

***Figure 3-29**: Values of heat transfer coefficients for various water mass flux considering evaporation cooling, film cooling, and spray cooling at various gas pressures (p_L), adapted from [Pus03]*

4 Measurements and numerical methods

4.1 Measurement conditions

The present work and the results described in the next chapter have required a set of common characteristics to frame the investigations, according to the physical context of experimental limitations. Hypotheses are made about the quenching parameters described in the introductive chapter:

- the investigated **parts** are set to small-sized (< 200 mm), simple (e.g., cylinder) and complex (e.g., bevel gears) geometries, commonly found in the heat treating automotive gas quenching industry;
- the quenching **medium** is limited to air or nitrogen under standard velocity range for industrial application. The pressure is set to atmospheric pressure for sake of compatibility with the experimental setup, and extended to higher pressures in numerical simulations;
- the quenching **environment** is limited to top-to-bottom quenching units, and batches whose size and dimensions have been detailed in Tab. 3-2 (Chapter 3.2.6).

4.1.1 Workpiece geometries and materials

4.1.1.1 Geometries

Industrial gas quenching applications mostly focus on gear technologies. From the characteristic geometries enumerated in Chapter 3.3.2, three specimen geometries, introduced in **Tab. 4-1** (bevel gear, helical gear, and ring gear), have been manufactured according to the geometrical challenges that they create in gas quenching applications:

- a **bevel gear**, whose head produces large recirculation zones harming the homogeneity of the heat transfer process;
- a **helical gear**, whose teeth are subject to various quenching intensities, locally (along a single tooth) or globally (inside the batch). Additional flow-controlling elements, such as flow ducts, help optimizing the heat transfer between the surrounding gas and the gear;
- a **ring gear**, whose arrangement in a batch influences the distortion risks encountered by the thin-walled specimen.

***Table 4-1**: Workpiece geometries*

Bevel gear	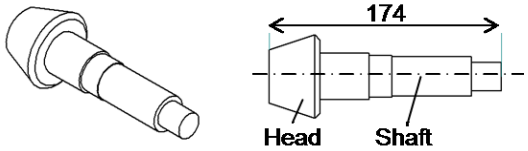		
Helical gear	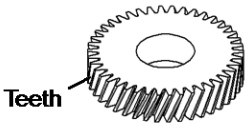	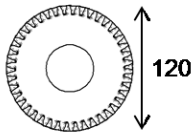	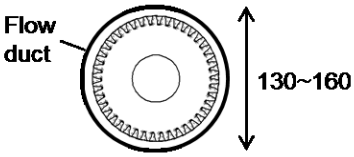
Ring gear	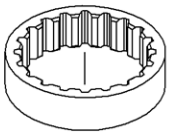	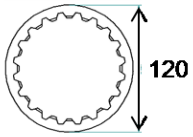	
Stepped shaft	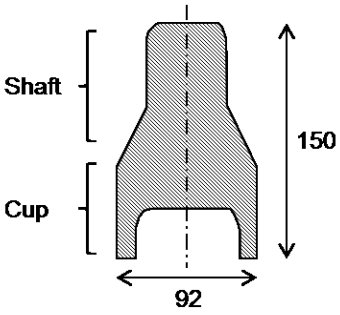	**Common rail**	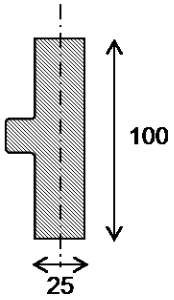

On the other hand, the two geometries in the bottom of Tab. 4-1 consist of forged geometries for automotive applications:

- a **stepped shaft** whose geometry comprises a shaft section and a cup section, of smaller wall-thickness;
- a **common rail**, smaller than the stepped shaft, and with a characteristic T-shape.

4.1.1.2 Materials

In the case of the gear specimens, the material provides specific characteristics concerning the heat conduction inside the solid, in order to evaluate the integral heat transfer coefficient (over the whole geometry), by the means of temperature measurements inside the specimen.

Table 4-2 (top) summarizes the materials of high heat conductivity, such as aluminum and copper alloys, that have been used to monitor the heat transfer coefficient under various experimental and industrial flow conditions.

***Table 4-2**: Workpiece materials*

	Ferrous alloys	Non-ferrous alloys	Applications
Bevel gear		- ENAW6082, aluminum alloy - Copper alloy	- Temperature measurement - HTC evaluation
Helical gear		- ENAW6082, aluminum alloy - Copper alloy	- Temperature measurement - HTC evaluation
Ring gear		- ENAW6082, aluminum alloy	- Temperature measurement - HTC evaluation
Stepped shaft	- 22MnSiCr-6-6-5, steel alloy - 38MnVS-6, steel alloy - 18CrNiMo-7-6, steel alloy - Austenitic steel	- ENAW6082, aluminum alloy	- Temperature measurement - HTC evaluation - Quenching scenarios
Common rail	- 22MnSiCr-6-6-5, steel alloy - 38MnVS-6, steel alloy		- Temperature measurement - HTC evaluation - Quenching scenarios

Concerning the two forged specimen found in Table 4-2 (bottom), the specified materials are directly related to mass production process, and affect the successive manufacturing and heat treatment steps occurring after forging and quenching:

- for the **stepped shaft**, the alloy 22MnSiCr-6-6-5 is a high-strength, ductile bainitic (HDB) steel, specifically developed for the forging of automotive parts. The alloy 36MnVS-6 is a ferritic-pearlitic, precipitation-hardening steel, whereas the alloy 18CrNiMo-7-6 is a case-hardening steel;
- due to its smaller dimension, the **common rail** specimen only features the high-strength, ductile bainitic and the precipitation-hardening steels.

4.1.2 Quenching units

4.1.2.1 Investigated parameter

Relevant parameters have been selected and exposed in **Tab. 4-3** to describe conventional quenching situations for industrial applications:

- the **chamber geometry**, set as the dimensions of the walls surrounding the quenched batch;
- the **workpieces**, specific to the industry branch;
- the **gas type** and **operating pressure**,
- the **gas velocity**,
- and the **Reynolds number**, all depending on the quenching unit technology.

***Table 4-3**: Investigated parameter ranges*

	Wind tunnel	Gas test chamber	Spray test chamber	Type A (industry)	Type B (industry)
Chamber geometry		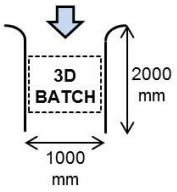	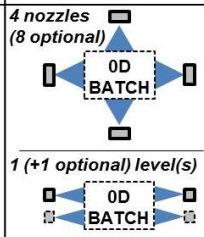	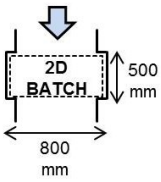	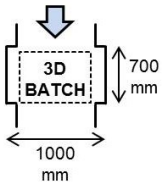
Workpieces	cylinders, gears (bevel, ring, helical)	cylinders, gears (bevel, ring, helical)	common-rail, stepped shaft	gears (ring, helical)	gears (bevel, ring, helical)
Gas type / pressure	Air, 1 bar	Air, 1 bar	Air (1-4 bar) + Water (0-5 L/min)	Air, 1 bar N_2, 1-10 bar	Air, 1 bar N_2, 1-10 bar
Mean axial velocity	0-20 m/s 0-22 m/s	0-15 m/s 10 m/s	0-20 m/s 10 m/s	0-12 m/s 10 m/s	0-15 m/s 10 m/s
Reynolds number	30.000-600.000	60.000-900.000	100-1.500, 25.000 (air only)	50.000-600.000	60.000-900.000

Experiment
Simulation

The ranges of velocities and pressures for the simulations in industrial applications have been chosen accordingly to the recent evolution of heat treatment gas quenching processes. Indeed, smaller, cost-saving technologies are leading the market with nitrogen-based recirculating units whose velocities and pressures remain respectively lower than 15 m/s at around 10 bar. At such conditions, a reduction of the gas pressure (decrease in quenching homogeneity) and velocity (decrease in quenching intensity) is compensated by improving the local control of the flow [Mac05] [Heu11b] [Kor16].

4.1.2.2 Gas quenching test chamber

Several quenching configurations have been investigated. In order to validate the experimental and numerical methods, a quenching test chamber seen in **Fig. 4-1** has been utilized, as described in [Sch07]. Design and construction of the test chamber aimed at giving optimal gas streaming conditions (aspect ratio close to 1) in comparison to conventional industrial gas quenching chambers [Mac05] [Sch09].

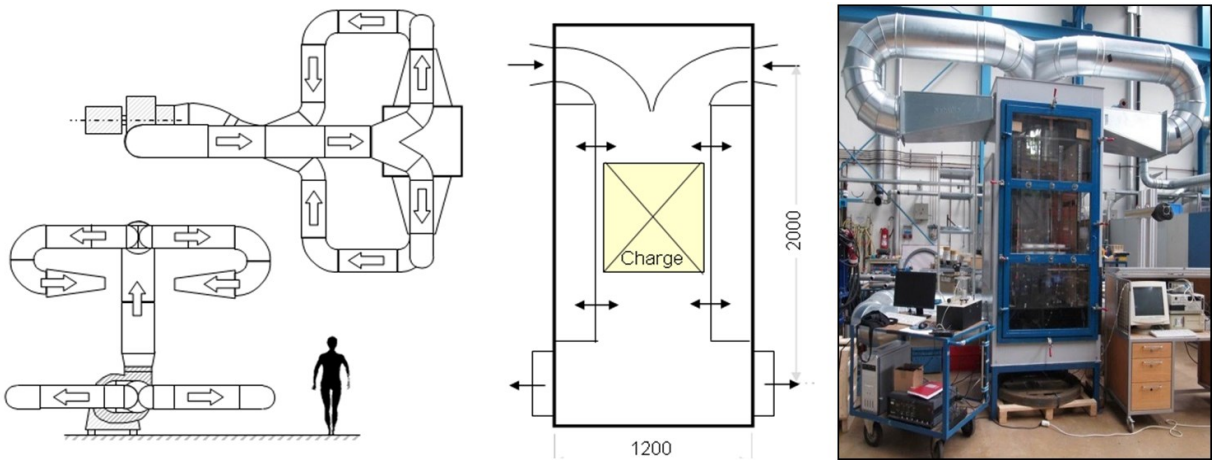

***Figure 4-1**: Test quenching chamber for the experimental investigation of batch distribution and flow conditioning, adapted from [Sch07]*

This experimental quenching chamber offers the space for the implementation of flow conditioners post- and past the charge, which can take the form of several layers featuring various part geometries. Experimental methods to assess flow and heat exchange properties have been tested and validated in the test-chamber. Numerical simulations have been validated using flow and heat transfer coefficient measurements performed in the test-chamber.

The quenching conditions offered by the test-chamber (top-to-bottom flow direction, air flow at atmospheric pressure) are also found in the industry, in particular in the case of field of nozzles, for impinging flows onto the surface of a batch.

4.1.2.3 Quenching unit Type A

Gas quenching processes for a single batch layer (2-dimensional design), shown in **Fig. 4-2**, has been described in [Heu11b]. This process configuration (Type A) offers the possibility for complex, flat specimen geometries (for instance, helical gears) to be quenched with a minor loss in end-quality, that is, low distortion and homogeneous microstructure.

Compared to a standard, multi-layered 3-dimensional batch, a 2-dimensional, single-layer batch is limited to small, flat specimen geometries, but leads to a significant reduction of the dimension of the quenching chamber. The coupling with a multi-zone furnace provides lower cycle times than conventional gas quenching processes, thus reducing production costs [Heu11b].

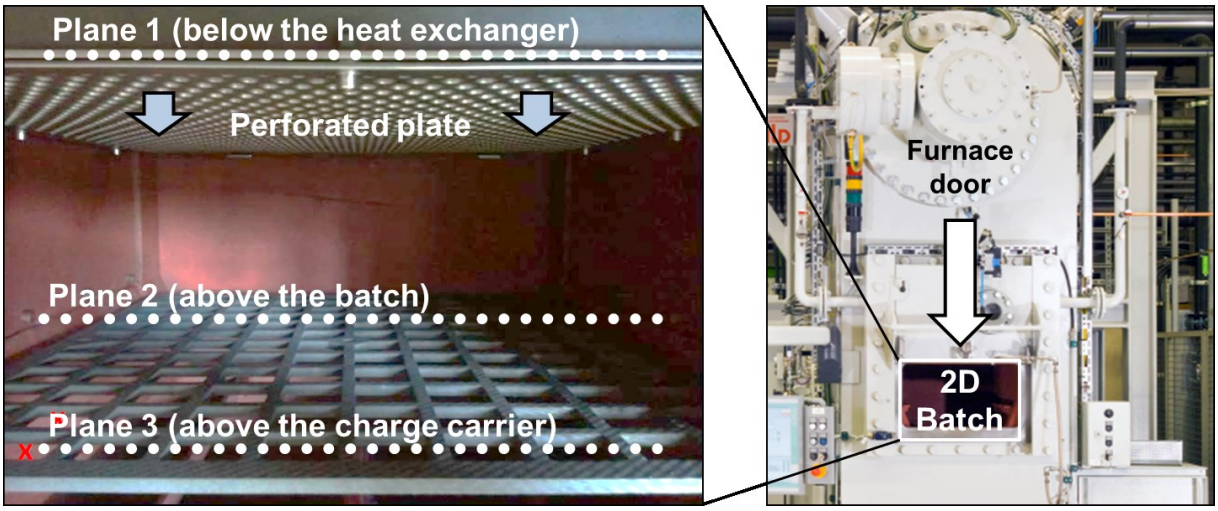

***Figure 4-2**: Inner view of a 2-dimensional, single-layer batch chamber (left) from a top-to-bottom gas quenching unit (right), Type A*

An inner view of this 2-dimensional quenching chamber is provided in Fig. 4-2 (left), where the top-to-bottom flow is indicated. Three planes for flow investigation have been defined, perpendicular to the gas flow. The gas typically flows through the heat exchanger, reaching *Plane 1* in the quenching chamber in a cooled state.

The cooled gas then passes through a perforated plate situated above the batch, whose top plane is defined as *Plane 2*, then flowing through the charge to reach the charge carrier (*Plane 3*), splitting afterwards into the reduced chamber section to be recycled. In order to optimize the flow pattern for the 2-dimensional batch-type quenching process described above, the gas flow was investigated with various mechanical structures at the three different measurement planes.

4.1.2.4 Quenching unit Type B

The 3-dimensional, top-to-bottom flow quenching chamber (Type B) is detailed in **Fig. 4-3**, coupled with a vacuum furnace. Compared to the test chamber (Fig.4-1) and the Type-A chamber (Fig. 4-2), the gas recirculation takes only place on one side. Various specimen geometries can be quenched in this quenching chamber, due to the possibility to arrange the batch in multiple layers, with the example of bevel gears, distributed in the batch carrier (Fig. 4-3, left). Three investigation planes are defined in a similar way than in Fig. 4-2, below the heat exchanger (*Plane 1*), above the batch (*Plane 2*), and above the charge carrier (*Plane 3*).

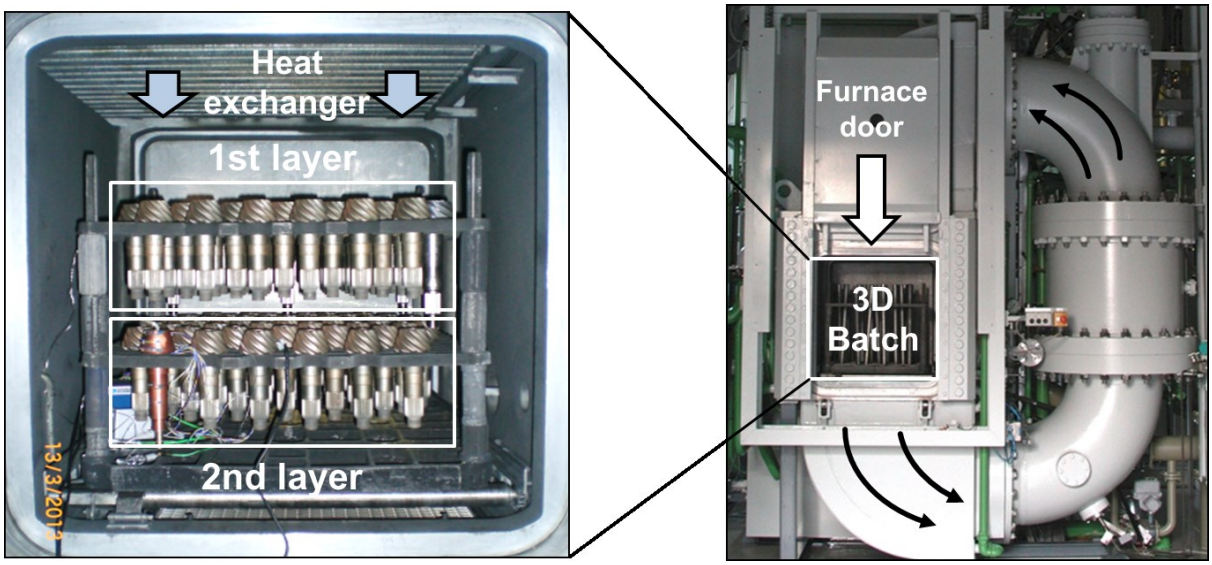

***Figure 4-3**: 3-dimensional, multiple-layer batch chamber (left) of a top-to-bottom gas quenching unit (right), Type B*

4.1.2.5 Flow conditioning solutions

Implemented on the three chamber types previously detailed, flow conditioning solutions take the form of:

- the **heat exchanger**, consisting of the walls surrounding the heat exchanger tubes bundle;
- **perforated plates**;
- and **cylindrical flow ducts**;

in the present work.

The standard shell surrounding the heat exchanger tubes bundle creates an unbalanced room between the tubes located near the wall and the shell, thus leading to heterogeneously distributed velocities, specifically at the edge of the quenching chamber. The adapted shell in the Type A quenching unit aims at correcting the unbalance by harmonizing the room between the tubes and the wall to obtain similar free areas for the flow at both sides, as seen in **Tab. 4-4**. Whereas the test chamber does not include a heat exchanger, no data has been provided for the heat exchanger implemented in the Type B quenching unit.

Perforated plates (with designation *RvD-L*, with *D* for *diameter* and *L* for *length*) are implemented below the heat exchanger of the Type A quenching unit (with adapted shell) to homogenize the velocity distribution above the quenched batch.

Three configurations (including two different plates) have been experimentally evaluated, and confronted to extended computed configurations such as

- a variation of the porosity from 22 to 100% at a constant perforated hole diameter of 10 mm;
- a variation of the perforated hole diameter from 8 to 12 mm at a constant porosity of 40%;
- a variation of the perforated hole diameter distribution from 8 to 16 mm at a constant porosity of 40%;

to find out the best solution to homogenize the flow.

The third flow conditioning approach investigated have seen cylindrical flow ducts utilized to fit the space around helical gears (of diameter 120 mm and thickness 30 mm), and focus the gas flow along the teeth.

The dimensional parameters of the investigated flow ducts are

- a diameter between 130 and 160 mm;
- an overall length *L* from 30 to 200 mm;
- and a length above the gear *l* from 0 to 60 mm.

***Table 4-4**: Flow conditioning parameters*

	Heat exchanger	**Perforated plate**	**Cylindrical flow duct**
Basic geometry	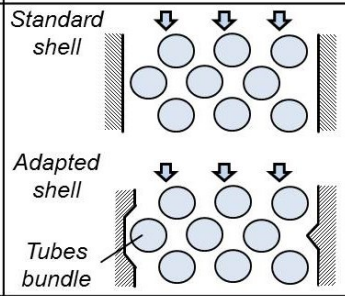	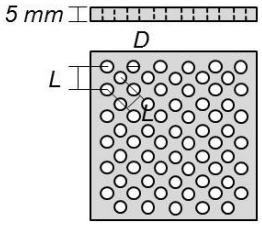	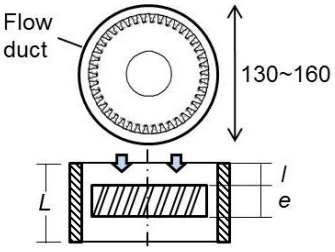
Configurations	- **Test chamber**: *no heat exchanger* - **Type A**: *standard + adapted shells* - **Type B**: *not specified/not investigated*	- **Test chamber**: *no plate* - **Type A**: *Rv10-15 + Rv10-18 (experimental), extended configurations (simulation)* - **Type B**: *no plate*	- **Helical gears**: *e = 30 mm, diameter = 120 mm* - **Flow duct**: *diameter = 130~160 mm, l = 0~60 mm, L = 30~200 mm*

4.2 Flow measurements

Flow measurements are herein covered for a subsonic, incompressible flow. A combination of measurement techniques, using Pitot and Prandtl tubes (single to multiple holes), and joule-heating via hot-wire anemometry, is used to evaluate 3-dimensional flow characteristics (velocity and turbulence). Through the use of automated multiple-axis positioning systems, velocity and turbulence distributions can be evaluated covering 1- to 2-dimensional areas.

4.2.1 Pressure probes

Pressure-based flow measurements use a minimum of two-point evaluation to compare the state of ambient pressure and dynamic pressure of the flow. Whereas the Pitot tube requires the use of a static element measuring the ambient pressure, the Prandtl measurement system features the two elements to directly provide the relative pressure, hence the velocity information of the flow [Nit06].

Figure 4-4 shows the 7-hole pressure probe, with a detail of the distributed holes and the decomposition of the main direction in the coordinate system of the probe, seen on the right. The 7-hole pressure probe allows the measurement of velocities and turbulences in a 70° incidence angle [Eve83]. The incidence angle varies, depending on the amount of pressure measurement points (5 to 12). The measurement frequency is limited to 100 Hz for this measurement technique, due to the constructive elements and dimensions failing to capture smaller velocity fluctuations. In this scope, 100 Hz has been used as the standard measurement frequency. This value is satisfactory to measure turbulence scales above 10 cm, which is appropriate for macro (chamber) or meso (batch) levels in gas quenching applications.

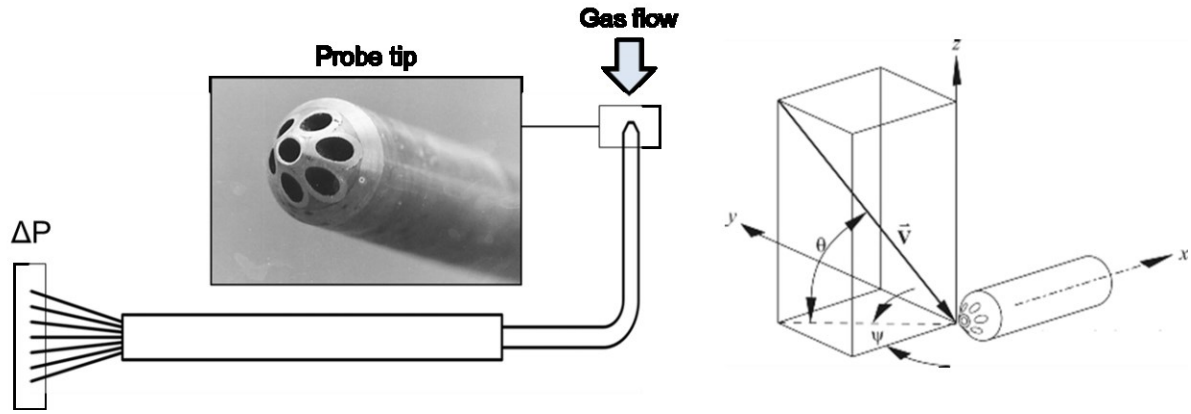

***Figure 4-4**: Description of the 7-hole pressure probe (source: Aeroprobe Inc.)*

The velocity is derived from the sensor measurement of the relative pressure using the Bernoulli equation,

$$\frac{\rho}{2}u_{\infty}^{2} = p_0 - p\,. \tag{4-1}$$

Temperature correction is implemented into the velocity calculation via the ideal gas equation

$$p = \rho \cdot R \cdot T_{\infty}\,, \tag{4-2}$$

where the velocity can be derived to the form

$$u = \sqrt{\frac{2(p_0 - p)RT_{\infty}}{p}}\,. \tag{4-3}$$

with R the universal gas constant.

4.2.2 Hot-wire anemometry

Hot-wire anemometry is the quantification of the velocity and fluctuations of a flow using a thin metal wire exposed to the flow stream. The energy spent to maintain it at a constant temperature is measured. This indirect technique to measure velocity is also named constant-temperature anemometry (CTA), depicted in **Fig. 4-5**.

As previously introduced, the turbulence grade can be derived from the standard deviation of the velocity at high-frequency measurements. The CTA system can work in ranges between kilo- and mega-Hertz, thus allowing finer measurements of turbulences at micro-scale, compared to pressure-based sensors.

As seen in Fig. 4-5, a thin wire (commonly few micrometers of tungsten) is connected between two tips, and coupled to a Wheatstone bridge maintaining it to a temperature greater than that of the streaming fluid, where the energy spent to maintain this temperature constant is monitored at the same time.

The heat-equation equilibrium leads to a linear relation between the temperature of the sensor and the electric resistance. Neglecting the effect of thermal radiation and the thermal conductivity in the two tips holding the tungsten wire, the heat balance is expressed as

$$\frac{U^2}{R_0} = A \cdot h(T_w - T_{\infty}) \tag{4-4}$$

where every term, except the voltage depending on the heat transfer occurring around the wire, is supposed constant.

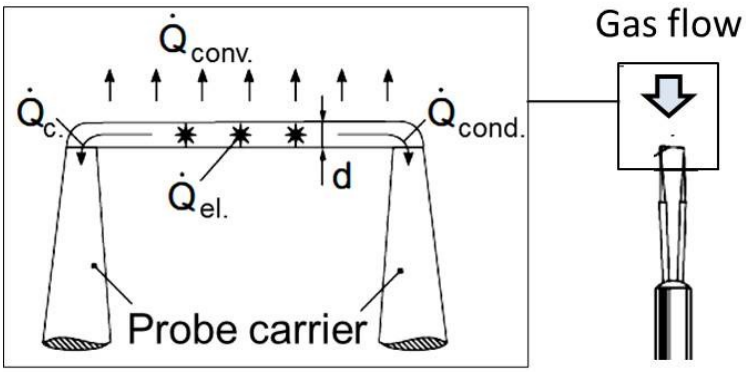

***Figure 4-5**: Representation of constant-temperature anemometry (right) with a closer view of the streamed wire and its heat balance (left), adapted from [Nit06]*

The convective heat flux of the wire surrounded by the gas flow is expressed by the relation between the dimensionless constants Nusselt and Reynolds number as described below,

$$Nu = A_0 + B_0 \cdot Re^n, \tag{4-5}$$

where A_0 *and* B_0 are geometrical and material properties involving the gas flow and the wire. The relation between electric voltage and gas flow velocity can be derived so that

$$U^2 = A + Bu^n\,, \tag{4-6}$$

depends on the constants described previously, where $n \sim 0.5$ [Nit06].
Considering the dimension of the system and the material properties,

$$Re_d = \frac{u * l}{\nu} = \frac{15\frac{m}{s} * 5 * 10^{-6}m}{15 * 10^{-6}\frac{m^2}{s}} = 5\,, \tag{4-7}$$

which confirms the laminar properties of the flow in the case of the streamed microscopic tungsten wire.

4.2.3 Measurement setup

Fluid velocity measurements inside of a quenching apparatus are carried out using hot-wire anemometry and 7-hole pressure probes. A control system, using *Virtual Instruments* (VIs) from the tool-box *Labview* (*National Instruments*), has been designed in order to operate a positioning system. It communicates with the acquisition card from the measurement tool, and collects the data/information during the measurement.

The solution is detailed in **Fig. 4-6**, highlighting the various devices and communication ways. The designed system allows high reproducible experiments and flexibility for the operator who can perform flow measurements over a 2-dimensional area.

Control loops written in *Labview* operate the two motors of the positioning system, where the probe is fixed. The flow information acquired by the probe are collected and analyzed by the pressure sensor, also operated using a *Labview* loop.

The system has been designed and validated in the test-chamber, and has been operated in the two industrial quenching chambers at high velocity gas flow, limited to atmospheric pressure conditions.

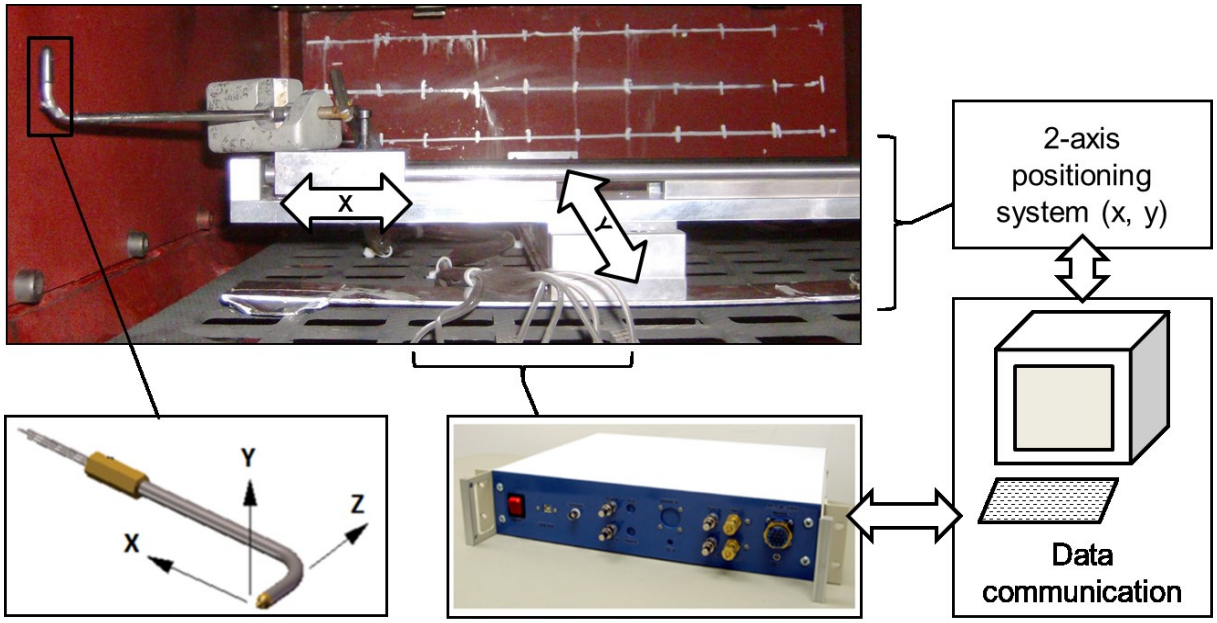

***Figure 4-6**: Communication between devices for the 2-axis positioning system, measurement and acquisition of velocity information in quenching apparatus*

4.3 Heat transfer measurements

4.3.1 Temperature measurement

4.3.1.1 Contact temperature measurement

Thermocouples provide contact temperature information using the electrical properties of materials via the Seebeck effect. **Figure 4-7** shows the two connected metal wires in contact with the surface of the investigated object. The conductive material is undergoing a temperature difference, which is electrically quantified between the two metals.

Various metal combinations provide specific temperature ranges that can be monitored, as well as properties (corrosion-resistance for instance) for the thermocouple. The combination Nickel-Chrome/Nickel (under the denomination *type K*) has been utilized in the present work, offering a temperature measurement range from -270 °C up to 1372 °C.

The time-constant of a thermocouple is directly proportional to the diameter of the tip, with values in the present work ranging from 0.8 second (for 0.5 mm diameter) up to 2 seconds (for 1 mm).

4.3.1.2 Remote temperature measurement

Thermography offers the possibility to perform distant, superficial temperature measurements on specifically treated surfaces in a large temperature range. This technique also provides higher measurement frequencies than those when using thermocouples (50 Hz versus 1.25 Hz). The measurement of the radiative emission of the warm body in the infrared range reduces the potential interference of the environment.

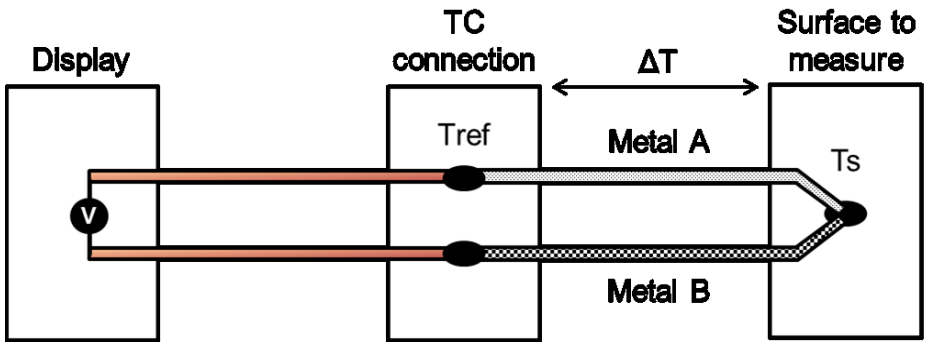

***Figure 4-7**: Description of a thermocouple (TC), evaluation the surface temperature (Ts) using a temperature reference (Tref)*

A test setup has been created to compare measurement techniques involving the sensors seen in **Fig. 4-8a**. The thermal camera has monitored a copper cylinder with various heat flux probes glued onto its surface. The Omega probe has a reduced influence on the local heat transfer during thermography measurement, as this probe is made of a transparent surface. The reflection of the object still affects the temperature measurement. The lower emissivity of the Captec probe (copper surface), however, proves the limit of the optic measurement technique, providing wrong information about the surface temperature.

4.3.2 Heat transfer coefficient measurement

The present work features two ways of measuring the heat transfer coefficient in heat treatment gas quenching: direct measurement through contact with the surface of the object and quantification of the heat flux; and indirect measurement, based on the cooling curve of the whole body, or a section of it.

4.3.2.1 Direct heat transfer measurement

The calculation of local heat transfer coefficients can be carried out by measurement of the heat flux at the surface of the object, using the heat flux probes represented in Fig. 4-8a.

The heat transfer coefficient can then be derived from the heat flux and temperature measurement at the surface of the object using the relation

$$h = \frac{\dot{q}}{(T_w - T_\infty)} \ . \tag{4-8}$$

Heat flux measurements at the object surface are carried out by the Captec and Omega sensors represented in Fig. 4-8a. The sensors are glued on the surface using thermal conductive material. The dimension of the sensor has a direct influence on the error factor during heat flux measurement. The bigger the surface, the more precise the measurement is, for a constant distributed heat transfer. Complex geometries cannot offer those conditions, thus compromises are needed concerning the dimension of the sensor.

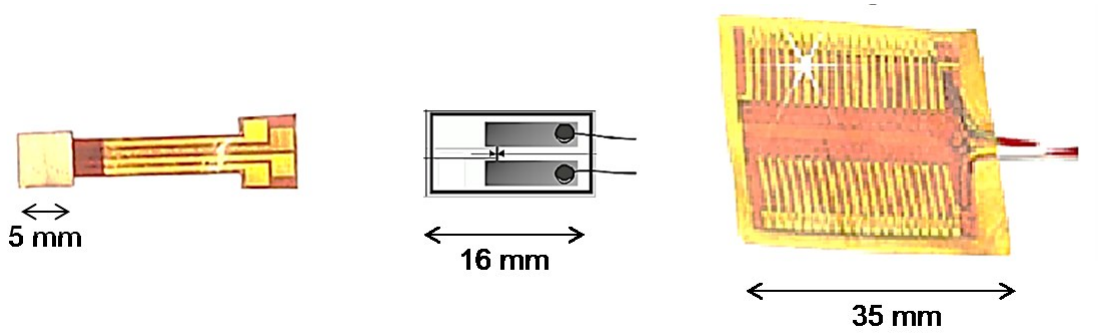

***Figure 4-8a**: Glue-on probes from the companies Captec (left), Dantec (center) and Omega (right) for the quantification of heat transfer via hot wire and superficial heat flux and temperature measurements*

The Captec sensor, seen in Fig. 4-8a (left), has a 5 x 5 mm² minimum dimension, where the heat flux is determined by temperature measurements at the two sides of the sensor (**Fig. 4-8b**), and calculation of the heat flux based on the known calibrated thermal barrier between the two surfaces.

The Omega probe offers a larger surface, thus less adapted to complex geometries. With multiple thermocouple connections at the two sides, the Omega probe however provides a greater precision than a Captec probe with similar surface. Both solutions integrate a thermocouple on the surface side, for measurement of the wall temperature.

As detailed previously, hot-wire anemometry also provides information on the heat transfer coefficient using the 0.9 mm-long tungsten wire, maintained at constant temperature.

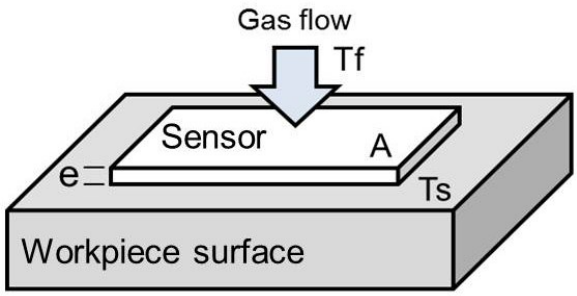

***Figure 4-8b**: Quantification of the heat transfer coefficient of a surface at temperature Ts, from a gas of temperature Tf, using heat flux measurement by a probe of area A and thickness e*

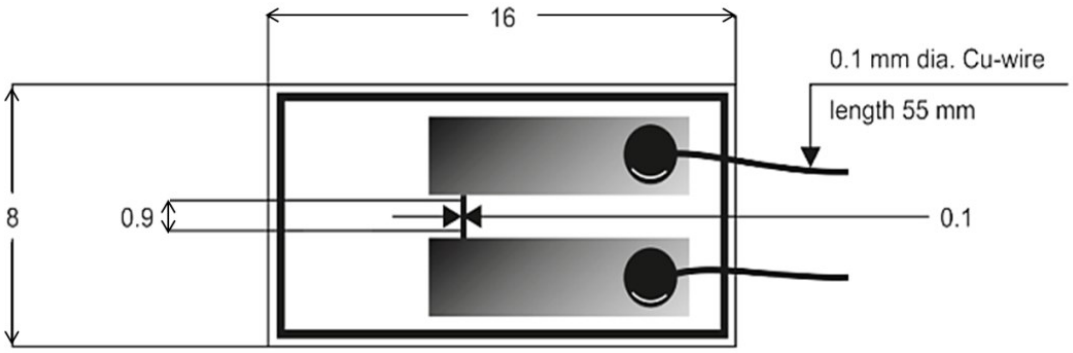

***Figure 4-9**: Glue-on probe for the velocity quantification in separation flows, also utilised for the measurement of heat transfer at the surface of the object (source: Dantec Dynamics)*

Hot-wire anemometry is also utilized to directly quantify the heat transfer, as seen in **Fig. 4-9**, with glue-on probes, where the heat transfer at the surface of the investigated object can be also measured. Such a technique offers an accurate and non-perturbing solution for the measurement of heat transfer coefficients, however requesting an initial, in-situ calibration.

Hot-wire anemometry features a less precise, more affordable way of quantifying the velocity in gas flow, and has been employed in the present work to verify measurements of pressure-based techniques.

4.3.2.2 Indirect heat transfer measurement

The lumped-capacitance method (LCM) is based on the assumption that:

$$Bi < 0.1 \tag{4-9}$$

According to the previous assumption, the thermal conduction in the workpiece is far greater than the heat transfer on the surface, in proportion to the characteristic length of the workpiece. Assessing the heat equilibrium in a workpiece:

$$\dot{q}_{out} = \dot{q}_{inner} \tag{4-10a}$$

$$hA(T_w - T_\infty) = -\rho C_p \frac{\partial T}{\partial t} V \tag{4-10b}$$

for quenching involving small heat transfer coefficients, thus when the assumption of a lumped-capacitance is verified, the heat transfer coefficient can be temporally integrated so that

$$ln\left(\frac{T_w(t) - T_\infty}{T_w(0) - T_\infty}\right) = -\frac{hA}{\rho C_p V} t\,. \tag{4-10c}$$

Integral heat transfer coefficients can therefore be obtained even for complex geometries, knowing the functional surface *A*, the volume *V*, the density ρ, and the specific heat capacity at constant pressure C_p based on a single temperature measurement in the specimen over the time.

4.3.3 Measurement setup

The automated positioning system, described in Chapter 4.2.3, has been extended for the measurement of heat transfer coefficients, using the integral method over an axially streamed copper cylinder (*Temperature probe*) represented in **Fig. 4-10**.

The complete control (positioning system and heating of the probe), communication and data acquisition (temperature of the probe and quenchant) is also operated by a *Virtual Instrument*.

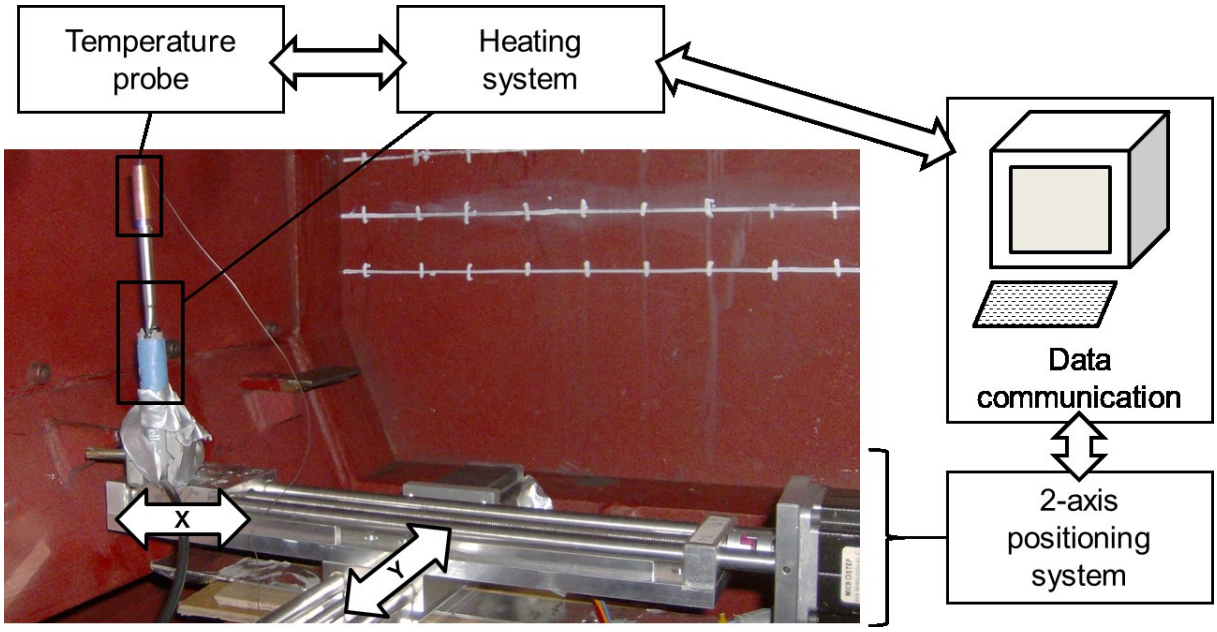

***Figure 4-10**: Communication between devices for the positioning, measurement, and acquisition of heat transfer coefficients using a cylindrical copper probe*

4.4 Microstructure evaluation

Quenching strategies need to be designed and optimized based on the assessed material and mechanical properties, allowing a re-adjustment of the gas flow parameters influencing the heat exchange.

The present work features property validation based on hardness and microscopic validation based on examination (light, electron microscopy). Both are destructive tests in the way that the probe requires a preparation phase involving the partial destruction with additional local pre-treatments (polishing, chemical solution). The tests are necessary to provide the state of microstructure inside the probe, at various scales.

4.4.1 Hardness

Hardness is the mechanical ability of a material to resist to a punctual or superficial plastic deformation. The hardness of an object is quantified (**Fig. 4-11**) using the depth of an indentation made by tools of various standardized geometrical shapes, under specific load and application rate. The harder the surface, the less depth an indentation will produce.

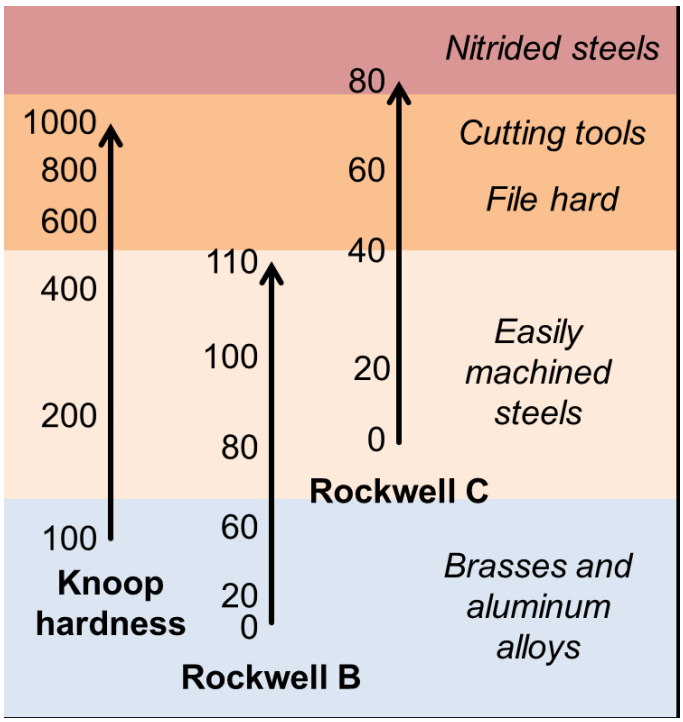

***Figure 4-11**: Comparison of several hardness scales, adapted from [Cal07b]*

Compared to other mechanical tests, hardness tests have the advantages of being simple to set-up and affordable, while involving light deformation of the surface of the material. It is possible to roughly estimate the tensile strength of the material from the hardness information under certain conditions [Cal07b].
The hardness scale is presented in Fig. 4-11 for conventionnal materials and heat treated steel grades, in the case of different measurements techniques (Knoop, Rockwell B and C).

4.4.2 Microscopy

4.4.2.1 Light microscopy

Light microscopy (LM) is typically used to observe the microstructure (grain size, boundaries, and regions of various material phases) by combining optical and illumination elements. Computer-assisted image post-treatment enhances the quality of the examination, and improves the microstructure diagnosis.
Abrasive papers and polishing techniques are used to prepare the probe, so that the investigated surface reaches a low roughness and high polished quality. The microstructure regions are revealed during the etching phase where chemical reagent is applied to the surface of the probe.

4.4.2.2 Scanning electron microscopy

In scanning electron microscopy (SEM) techniques, an electron beam is used to scan the probe and collect the scattering information of the surface of the specimen. The material should offer electrical conductivity to permit the use of SEM, which provides deeper and finer information about the microstructure properties than light microscopy technologies.

4.5 Numerical modeling and simulation

4.5.1 Computational fluid dynamics (CFD)

Numerical simulations are performed in order to support experimental work through extrapolated experimental conditions. Simulations offer the possibility to design experiments at various scales, and to decouple the phenomena involved during gas quenching processes. The fluid dynamics are thus modeled with the heat transfer mechanisms at micro, meso, and macro-scales.

Numerical simulations require a compromise between the computing power capability and the accuracy of the model in order to provide satisfying results.

4.5.1.1 Fluid motion

Before discretizing the definition of the problem according to the contextual spatial, temporal and physical environment, the momentum conservation/Navier-Stokes equation, governing the fluid motion is expressed under the form

$$\rho\left(\frac{\partial \boldsymbol{u}}{\partial t} + (\boldsymbol{u}\cdot\Delta)\boldsymbol{u}\right) = -\nabla p + \mu_L \Delta \boldsymbol{u} + (\lambda_L + \mu_L)\nabla(\nabla\cdot\boldsymbol{u}) + \boldsymbol{f}\,. \qquad (4\text{-}11)$$

Solving the equation requires high computational performances for resolving turbulence levels of through DNS (direct numerical simulation).

In order to model phenomena under higher turbulences or including more complex geometries, empirical truncations are utilized using RANS-(Reynolds-averaged Navier-Stokes) modeling, where the physical transport of mass, momentum and energy are computed in the form of the addition of the accumulation (time), convection (velocity) and diffusion (gradient) terms, eventually related to source terms (S_v, S_ϕ) in specific cases.

$$\frac{\partial \rho}{\partial t} + \frac{\partial \rho u_i}{\partial x_i} = 0\,, \qquad (4\text{-}12a)$$

$$\frac{\partial \rho u_i}{\partial t} + \frac{\partial}{\partial x_j}\left[\rho\left(u_j u_i + \overline{u'_\imath u'_\jmath}\right)\right] - \frac{\partial}{\partial x_j}\left[\eta\left(\frac{\partial u_i}{\partial x_j} + \frac{\partial u_j}{\partial x_i}\right)\right] + \frac{\partial p}{\partial x_i} = S_v\,, \qquad (4\text{-}12b)$$

$$\frac{\partial \rho \phi}{\partial t} + \frac{\partial}{\partial x_i}\left[\rho\left(u_i \phi + \overline{u'_\imath \phi'}\right)\right] - \frac{\partial}{\partial x_i}\left[\eta \frac{\partial \phi}{\partial x_i}\right] = S_\phi\,. \qquad (4\text{-}12c)$$

4.5.1.2 Turbulence modeling

Several turbulence models exist to resolve the derived Navier-Stokes equations with increasing complexity, needing more empirical inputs or computational performance. Zuckerman and Lior [Zuc06] did classify turbulence models for heat transfer application in impinging gas jet problems according to their effectivity and computational cost. In **Tab. 4-5**, the effects of turbulence models are demonstrated for the computation of heat transfer problems [Zuc06].

***Table 4-5**: Comparison of CFD turbulence models for impinging jet problems in terms of computational cost and accuracy, adapted from [Zuc06]*

Turbulence model	**Computational cost (time required)**	**Impinging HTC prediction**	**Secondary peak prediction**
k-epsilon	**** (low cost)	* (poor)	* (poor)
k-omega	**** (low moderate)	** (poor-fair)	** (poor-fair)
Realizable k-epsilon	**** (low)	** (poor-fair)	** (poor-fair)
Algebraic stress model	**** (low)	** (poor-fair)	* (poor)
Reynolds stress model	** (moderate-high)	* (poor)	** (fair)
Shear stress transport (SST)	*** (low-moderate)	*** (good)	** (fair)
v^2f	*** (moderate)	**** (excellent)	**** (excellent)
DNS/LES	* (extremely high)	**** (good-excellent)	**** (good-excellent)

RANS-modeling

In order to close the set of equations defined by the Navier-Stokes system above, the Reynolds stress-tensor has to be modeled. RANS-modeling satisfies this closing requirement using a 2-equation empirical turbulence system. Among the regular 2-equation turbulence models found in the literature, the k-omega-SST model offers a better solution for heat treatment applications, as mentioned in the literature dealing with industrial heat transfer phenomena [Men03a] [Zuc06] [Men09].

k-omega SST

In the conventional k-omega turbulence model [Men03b], two coupled transport equations, for the turbulent kinetic energy *k*, and the dissipation ratio *omega*, are solved. The extension of the k-omega model to a shear-stress transport model (k-omega-SST) offers a combination of the advantages brought by the conventional k-epsilon turbulence model in the free stream, whereas the k-omega model is applied only near the wall. The transition from one model to the other depends on the distance from the wall defined by the non-dimensional wall-distance y^+. Wall-functions are utilized [Men03a] in the case of the k-omega turbulence model to reduce the influence of the mesh refinements on the computational precision, especially in the case of heat transfer.

4.5.1.3 Heat transfer modeling

In the application of CFD-simulation for heat treatment, the quenching environment consists of the quenching chamber or gas supply, eventual flow conditioners or heat exchangers, and the charge to be quenched. Whereas inlet/outlet and transitional zones usually require a specific mesh refinement to ensure the convergence of the numerical scheme and the quality of the results, the area near the charge specifically requires a finer mesh to provide reliable data concerning the heat transport between the quenchant and the specimen.

Boundary layer

In the case of complex geometry modeling, the non-dimensional wall-distance y^+ may strongly vary from one area to another, thus producing non-physical heat transfer gradient. The regions near the wall, where the viscous forces dominate and produce the boundary layer, are seen in **Fig. 4-12**.

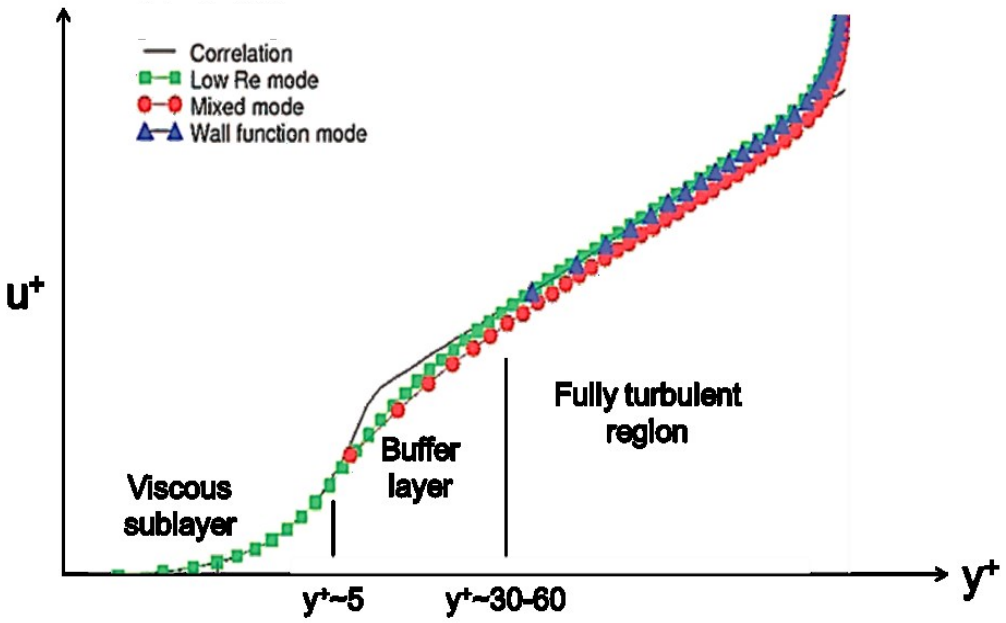

***Figure 4-12**: Relation between the non-dimensional velocity u^+ and the non-dimensional wall-distance y^+ for various turbulence models using the SST formulation, with the corresponding regions of the buffer layer, adapted from [Men09]*

In order to improve the results of the heat transfer simulation for complex geometries in CFD, wall-treatments are applied, as described in Menter et al. [Men09], to bridge the viscous (low-Re-modeling) and logarithmic (high-Re-modeling) areas of the boundary layer that are not satisfyingly computed.

The temperature correlation shown below, depending on the Γ-function from Kader [Kad81], is similarly applied for various physical values, and provides a blending function to allow the smooth transition between the regions of the boundary layer on the complex geometry [Men03b].

$$\frac{T_w - T}{T_\tau} = Pr \cdot y^+ \cdot e^{-\Gamma} + [2.12 \cdot ln(1 + y^+) + \beta(\mathrm{Pr})] \cdot e^{-1/\Gamma} \qquad (4\text{-}13a)$$

$$\Gamma = \frac{0.01(Pr \cdot y^+)^4}{1 + 5Pr^3 \cdot y^+} \qquad (4\text{-}13b)$$

Mesh refinement

The refinement of the mesh generated from the ground geometry (batch including quenching chamber) is required to offer a realistic physical environment to the computed flow. Grid independency tests are performed in the case of impinging gas quenching to determine the level of precision of the mesh that provides satisfying heat transfer conditions using the conjugate heat transfer solver.

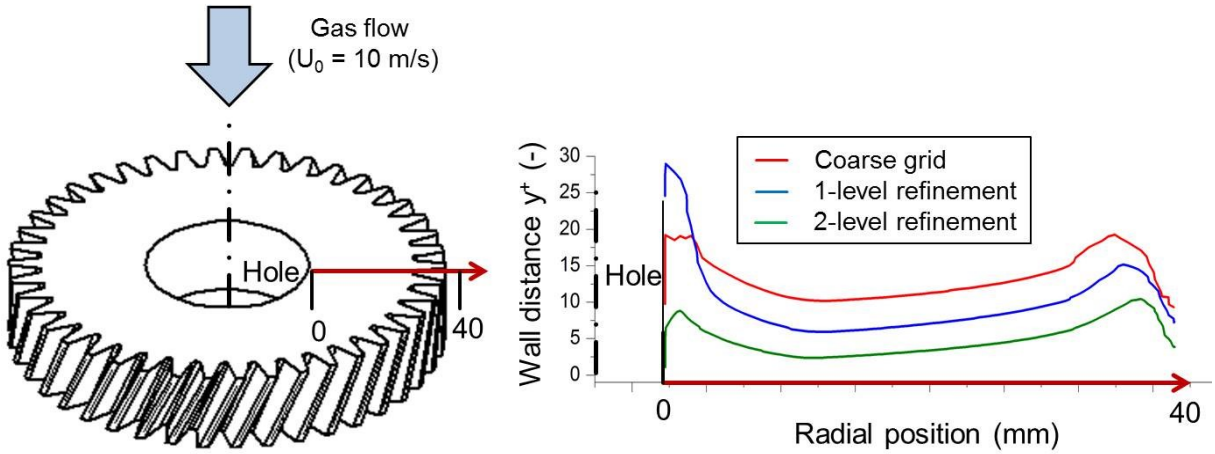

***Figure 4-13**: Refinement level evolution in the case of impinging gas quenching onto a helical gear specimen*

Figure 4-13 presents the influence of the mesh and the local surface refinements of the quenched object on the first cell spacing from the surface of the solid, y^+. Whereas the influence of the local grid size is demonstrated in Fig. 4-13 (right), with a linear trend between an increase in refinement level with a decrease in mean value of y^+ (from a coarse grid to higher refinement levels), local increases in y^+ are produced by the geometry variations of the helical gear specimen itself.

Both local and global variations of the y^+ values require a specific near-wall treatment responding to these variations in the heat transfer results, so that various specimen geometrical complexities can be numerically investigated.

4.5.1.4 CFD in OpenFOAM

Since its first open source release in 2004, the C++ library OpenFOAM has widely spread into the research and development community for computational fluid dynamics applications. The latest versions proved their effectivity for industrial case, and OpenFOAM is now a reliable alternative to commercial software solutions.

Through its highly tweakable interface, with its own coding language operating the C++ library in the background, and the GUI paraView besides, OpenFOAM benefits from bash-coding to run simulations and analysis routines, as well as further optimization coupling techniques.

Figure 4-14 presents the organization of a basic OpenFOAM solver *solidDisplacementFoam* extended for the computation of transient heat transfer problems.

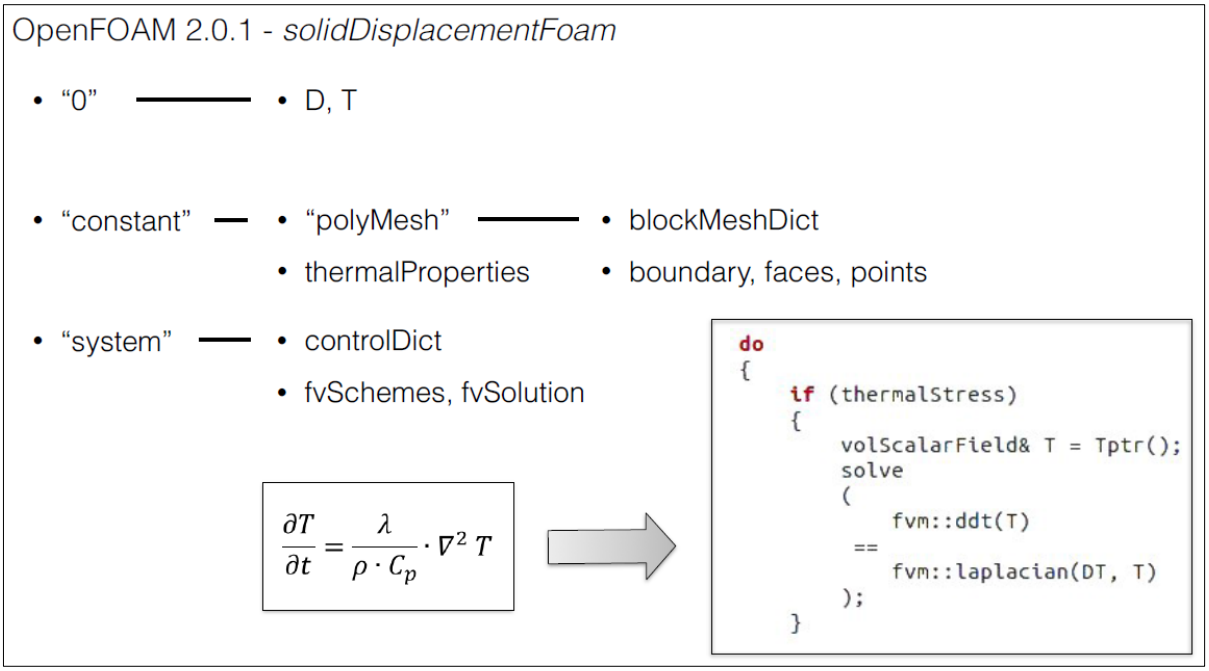

***Figure 4-14**: Folder tree of a simulation case involving the solver solidDisplacementFoam with heat transfer equation translated in C++-oriented OpenFOAM language*

From the main folder named according to the simulation project, three sub-folders define the pre-processing and the solver information to perform the simulation.

Pre-processing

Geometry, regions definition, and boundary conditions are distributed in the different sub-folders of an OpenFOAM case to set up the simulation:

- the folder **0** contains the physical values in single files (in Fig. 4-14, for instance, the temperature field T and the displacement field D into the body). The solver reads the information in each file (boundary conditions), and write into the folder case a new folder corresponding to the iteration (arbitrary or temporal) of the initial 0 folder;
- the folder **constant** gathers the simulation information that will only be read at the beginning of the simulation, geometry, regions, and their properties, as well as physical constants, type of turbulence, or gas modeling. The basic geometry in OpenFOAM is generated using a dictionary, blockMeshDict that is read using the blockMesh tool to convert points coordinates into discretized hexahedral mesh (points, vertices, faces, and finally boundaries).

Additional modifications of the mesh, with e.g., integration of external .stl complex geometries, can be performed using the tool snappyHexMesh that converts the hexahedral mesh into a tetrahedral mesh if more complex geometries have to be meshed inside the original mesh;

- the folder **system** provides the information about the method to solve the case. The solver name is mentioned in a control dictionary, controlDict, where information stands about additional libraries to be used (modified turbulence modeling for instance), the iteration information, and the time-step to record into the case folder. The files fvSchemes and fvSolution respectively define the numerical method for the solver to perform the simulation, e.g., transient or steady-state, first- or second-order upwind, etc, and the relaxation factors of the parameters. Various options (e.g., to split the computation between cores, or to perform post-processing sampling tasks) are also defined in the system sub-folder.

Solver

Solvers are defined in OpenFOAM as a library of C++ language, as seen in the case of transient heat transfer in Fig. 4-14 (bottom, right). There, the temperature volume-scalar field *T* is solved using the heat balance between heat conservation and temporal distribution in the body. The temperature conductivity is used in the C++ code as physical constant values for the material properties described on the left. The finite-volume method is utilized in this case of transient heat transfer in a solid body.

For conjugate heat transfer problems involving fluid dynamics, the basic solver *chtMultiRegionFoam* has been modified to allow the calculation of the heat transfer coefficient based on the heat flux calculated on the wall between the fluid and the solid region(s).

The solver proceeds as follow:

- the Navier-Stokes equations are first resolved in the fluid area using the previously defined turbulence model and SIMPLE algorithm (Semi-Implicit Method for Pressure-Linked Equations), iteratively solving both pressure and velocity equations in steady-state cases. Transient cases require Pressure-Implicit operators, thus PISO or PIMPLE algorithms. Depending on the mesh definition, non-orthogonality correctors might be needed.

Moreover, additional 'correcting' steps and stabilization methods (solution under-relaxation factors, geometric algebraic multi-grid -*GAMG*-) can also be utilized;

- once the energy equation is resolved, the temperature distribution inside the fluid area is set, related to the temperature surrounding the solid. A FVM solver evaluates the temperature inside the solid, using the Fourier equation.
- the heat transfer coefficient is calculated when both temperature fields are available before iterating.

Post-processing

OpenFOAM offers the external platform *ParaView* through command lines to visualize the outputs of the simulation, which are different lists of physical values attributed to locations in the mesh (e.g., cell-centers, points, faces). Various post-processing functions exist (sampling/averaging of a surface) to evaluate additional properties of the simulation results.

4.5.2 Transient heat transfer

Transient heat transfer in the finite-volume modeling of 3-dimensional, complex geometries is carried out using the implementation of the Fourier heat equation balancing the heat contained in a solid, and its temporal and spatial diffusion (with possible existing heat sources),

$$\rho c_p \frac{\partial T}{\partial t} - \nabla \cdot (\lambda \nabla T) = \dot{q} \tag{4-14}$$

The velocity of the heat diffusion of the solid (to or from its boundaries) is governed by the convective effect of the heat transfer coefficient, expressed using a 3rd order mixed (or *Robin*) boundary condition on the surface of the complex geometry.

4.5.2.1 Transient heat transfer in OpenFOAM

Heat exchange is defined at the surface of the solid as

$$\lambda \frac{\partial T}{\partial n} + h(T_w - T_\infty) = 0 \tag{4-15}$$

Vilums [Vil11] details the implementation of the 3rd order boundary condition of the form for the heat exchange described above in OpenFOAM. The validity of the solver modification has been tested on a simple setup involving an aluminum plate during forced convection from an impinging jet, using the commercial software *Comsol Multiphysics 3.4*.

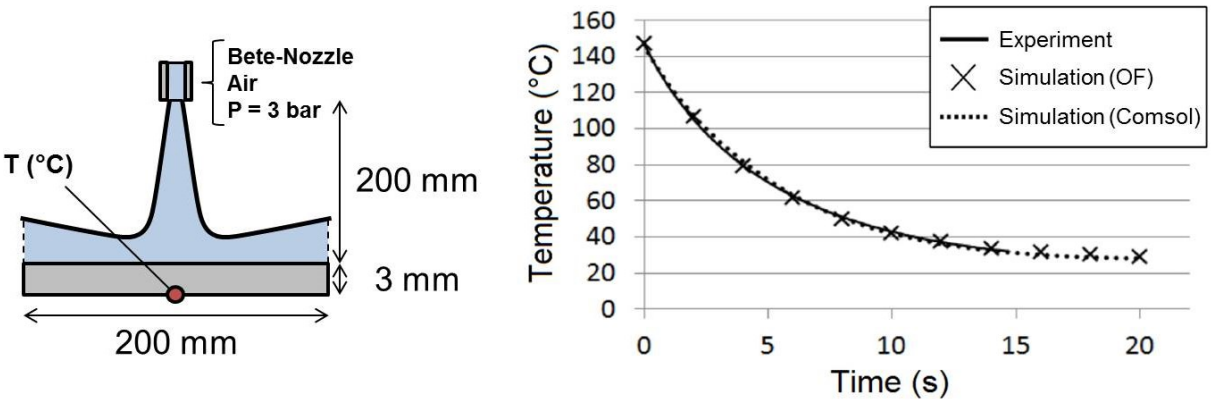

***Figure 4-15**: Validation of the OpenFOAM (OF) implementation of transient heat transfer with experimental configurations and the commercial-available solver (Comsol)*

Figure 4-15 compares experimental and simulation methods for the heat transfer coefficient evaluation at the center of an aluminum plate quenched using an air nozzle from the company Bete (*XA ef – pneumatic atomizing nozzle*). The experimental and both simulation results, using commercial (Comsol) and non-commercial (OpenFOAM) solvers, produce similar cooling curves, validating the use of the solvers for impinging air quenching techniques.

4.5.3 Pre-treatment and boundary conditions

4.5.3.1 Geometry modeling

Single specimen modeling

The complex specimen geometries are modeled based on characteristic geometries found in heat treatment gas quenching processes, as seen in Tab. 3-2 (Chapter 3.2.6), divided into three main categories: shafts (bevel gears), flat parts of high blocking grade (helical gears), and flat parts of low blocking grade (ring gears).

The boundary layer has to be carefully meshed around the complex geometry, as represented in **Fig. 4-16**. The complex modeling of a bevel gear is represented with y^+ values (first wall adjacent grid node), for the bevel gear streamed from the head (left side).

Figure 4-16 exhibits the range of y^+-values, from values located in the viscous layer ($y^+ < 2$), to values belonging to the blending area ($y^+ > 5$). The range is produced by a combination of a fine mesh added to the velocity fluctuations around the gear.

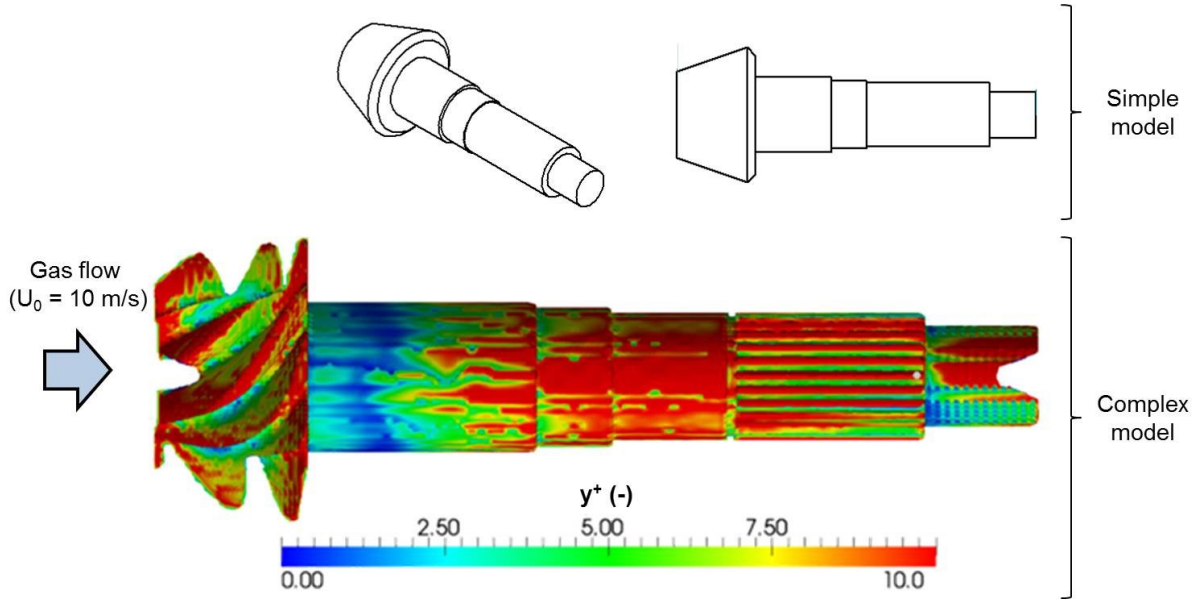

***Figure 4-16**: Distribution of the y^+ value at the first wall adjacent grid node of the surface of a bevel gear streamed from the head side*

Model simplification

Simplifying the bevel gear model (as in Fig. 4-16, top) spares a large amount of cells when modeling batch of several workpieces, and allows additional refinement levels in other areas of the quenching chamber for further geometrical integrations. A too coarse geometry might however disturb the flow and produce unwanted higher heat transfer coefficients [Mac05] [Buc14a].

The simplified model of the bevel gear, featuring a non-geared head pictured in Fig. 4-16 (top), succeeds in capturing the global trend of the heat transfer coefficient distribution along the gear [Buc14a]. The gas flow streaming produces a high heat transfer at the head surface, which largely decreases behind the head, in the recirculation area. The re-attachment point is in all cases similar and located at the geared shaft on the tail side, with however various intensities of heat transfer. In all cases, the heat transfer decreases along the shaft, up to the tail of the gear.

Chamber modeling

Simulations have been performed, modeling the flow in the test quenching chamber, and both industrial quenching chambers. A typical design of the chamber mesh is seen in **Fig. 4-17**. Figure 4-17 (left) presents a densified area for the mesh, which is where the perforated plates are located, to allow a fine modeling of the plate single holes.

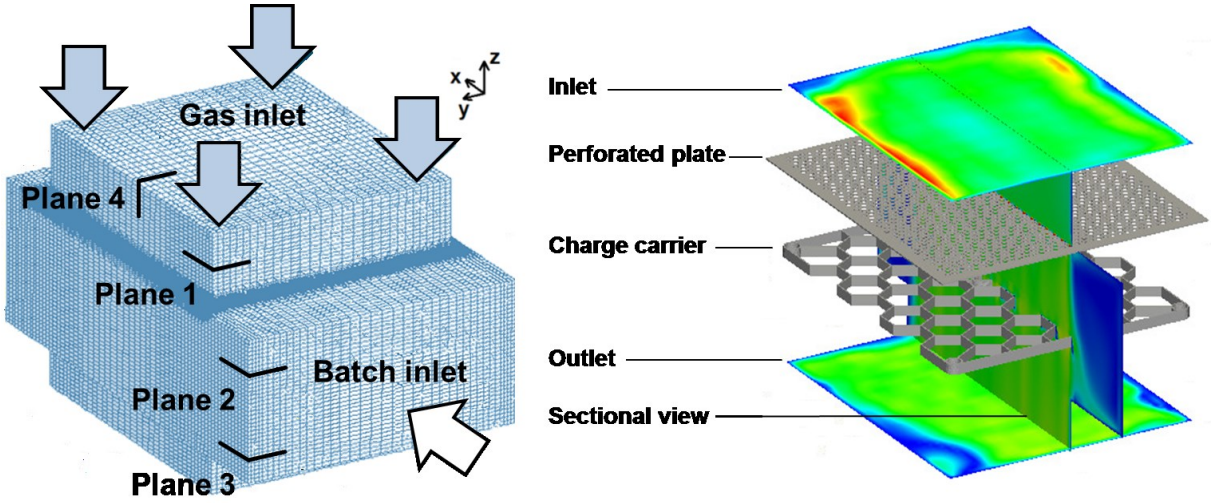

***Figure 4-17**: Meshed geometry (left), and implemented components with flow characteristics (right) of the quenching chamber*

Figure 4-17 (right) describes the boundary conditions of the inlet, at the top of the chamber, which consists in a realistic modeling of the flow conditions from the heat exchanger: 3-dimensional velocity and turbulent kinetic energy components have been measured, and the missing data have been interpolated to allow the implementation of the distributions into the simulation.

Flow conditioners are seen in Fig. 4-17, such as perforated plates and charge carrier, separately integrated to the mesh as single geometrical data (.stl). The batch made of single workpieces is also separately integrated above the charge carrier.

4.5.3.2 Inlet boundary conditions

In the simulation of one-directional gas quenching processes, the velocity inlet boundary conditions play a major role on the flow patterns and heat transfer issues during the simulation, besides the turbulence modeling and the pressure outlet boundary conditions.

In the present work, realistic velocity and turbulent kinetic energy distributions, in 3-dimension, have been taken into account through measurements in the investigated quenching chambers. Measurements have served the production of velocity and turbulence distributions in a 1024-point-resolution, covering a large portion of the functional area of the quenching unit, normal to the stream flow. The influence of the positioning system on the incoming flow has been numerically quantified, and had no major influence on the measurement system it supported.

Values from the calculated velocity and energy distributions have been interpolated to fit the measured distributions into the quantitative (mesh resolution), and qualitative (wall refinements) numerical grid, to perform the computational simulations with near-real flow conditions.

4.5.3.3 Material boundary conditions

For transient heat transfer simulations at high temperature (e.g., austenizing around 1200 °C), material properties (e.g., density or thermal conductivity) are depending on the temperature. For instance, in the case of the ferritic-pearlitic steel used during forging (38MnVS6), those values are significantly varying (between 10 and 50% for ΔT = 1000 °C) [Fis14]. A temperature-depending interpolation of the material properties (with data initially taken from [Fis14]) is therefore necessary to model realistic physical phenomena.

4.6 Methods validation

4.6.1 Velocity

Wind channel configurations (**Fig. 4-18**, left) have been tested for the validation and calibration of the glue-on, heat flux/heat transfer coefficient sensors, as described in [Sch13]. A copper specimen has been transversally and axially streamed over to compare with measurement results of the heat transfer coefficient [Wib03].

Velocity and turbulence level have been quantified in the wind channel, as seen in Fig. 4-18 (right). Increasing the ventilator frequency produces a higher mass flow rate of the gas, thus increasing the axial velocity in the center of the wind channel, as evaluated using CTA. An increase in ventilator performance produces an almost linear increase in mean velocity, with a decrease in the velocity range. The turbulence level is decreasing progressively as the velocity increases.

The velocity profile in the wind channel is shown in **Fig. 4-19**. A homogeneous velocity profile is found in the wind channel, offering optimal conditions to evaluate heat transfer of single specimen in gaseous flow.

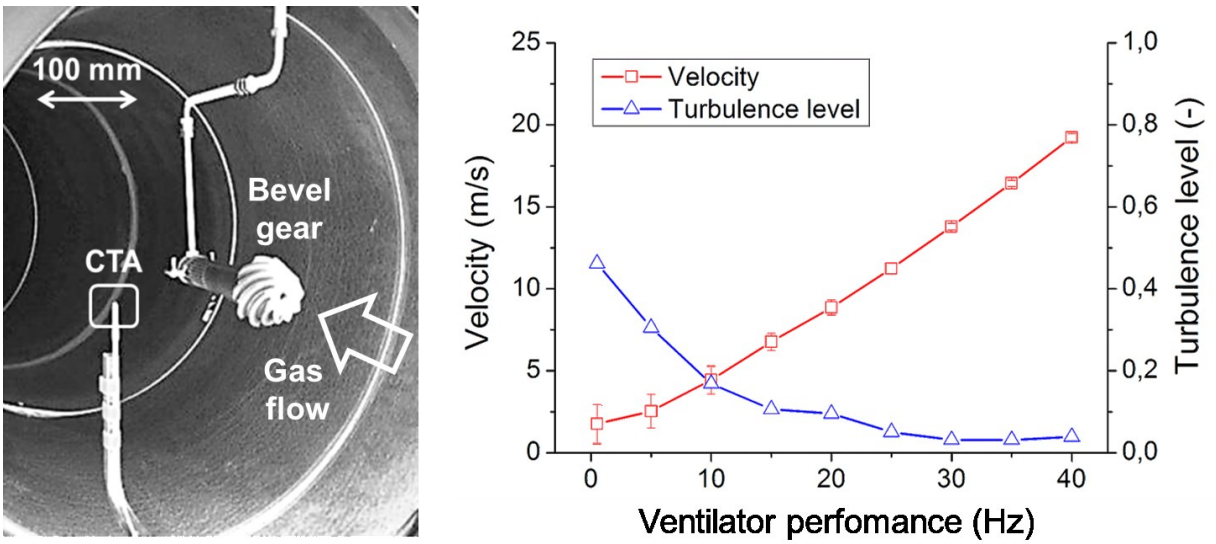

***Figure 4-18**: Experimental set-up of the wind channel featuring a bevel gear streamed from the head to the tail with hot-wire velocity and turbulence measurement device (left) and velocity and turbulence level related to the ventilator performance (right)*

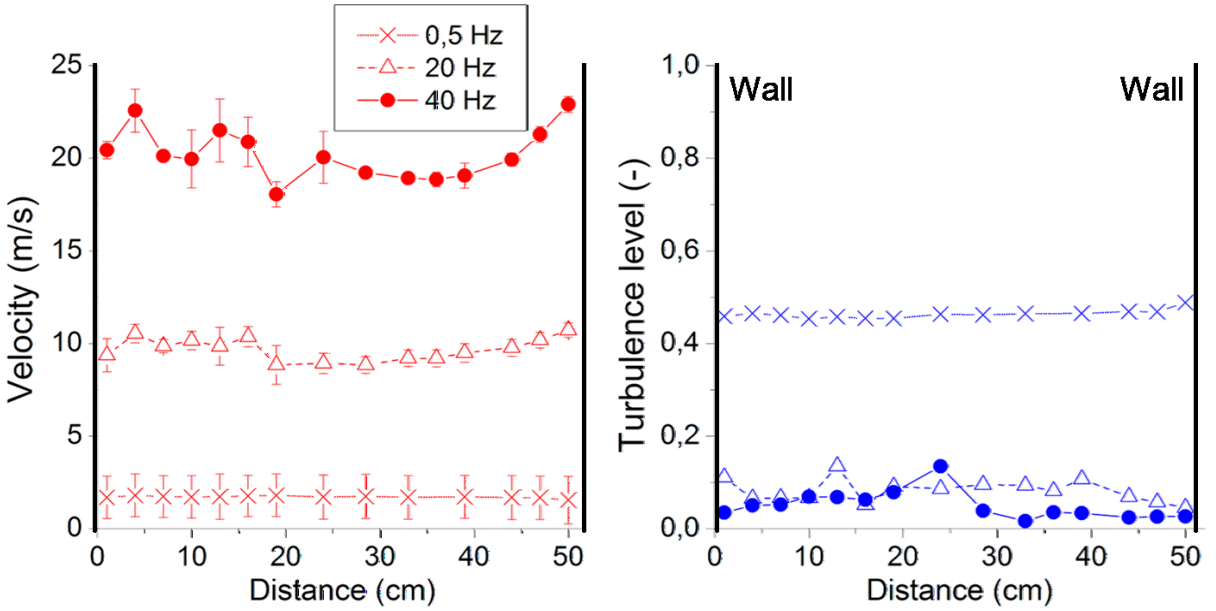

***Figure 4-19**: Velocity profile and turbulence level inside the wind channel at increasing ventilator performance across the channel*

4.6.2 Heat transfer

4.6.2.1 Measurement

Complex geometries, taking the forms of helical gears, shafts, or bevel gears, produce complex flows and turbulence, highly influencing the heat transfer coefficient. The geometries seen in **Fig. 4-20** have been investigated through experiments, with glue-on, heat-flux sensors situated on characteristic surfaces of the workpieces.

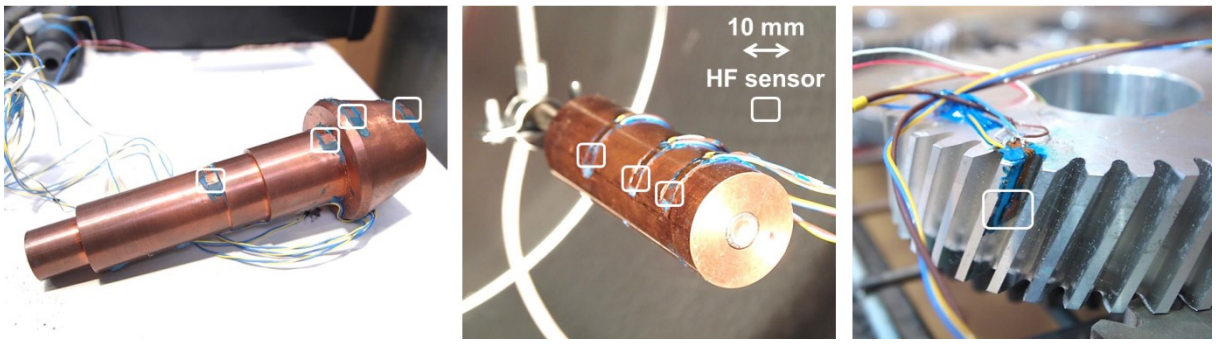

***Figure 4-20**: Investigated specimen from heat conductive material with heat flux sensor glued at various locations of the prepared surface*

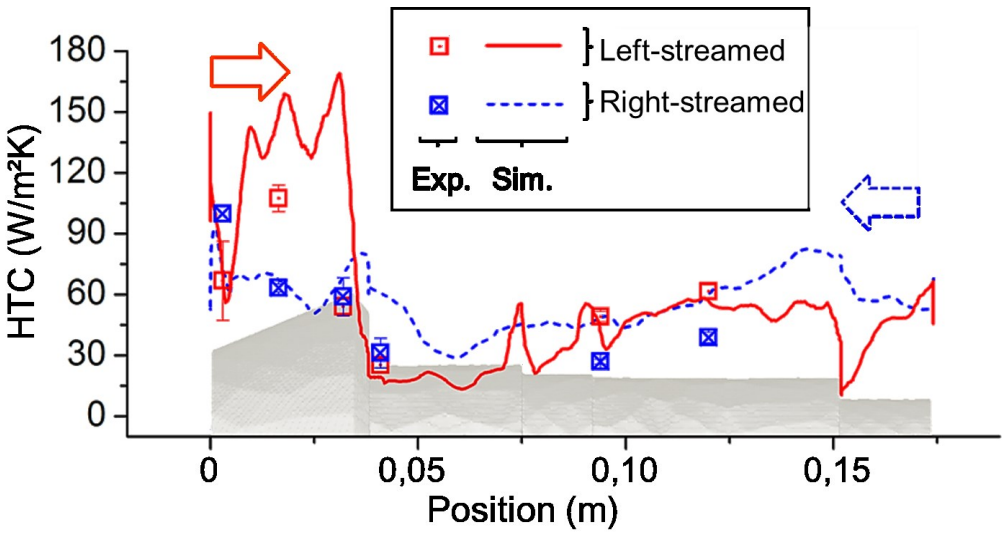

***Figure 4-21**: Local heat transfer coefficient distribution along a bevel gear streamed either from the left (head) or from the right (tail) side, and local HTCs measured by Captec heat flux sensors*

Figure 4-21 presents the comparison between simulation and measurement of heat transfer coefficients for a bevel gear streamed from either left (head) or right (tail) side. Captec sensors have been calibrated with respect to free convection conditions. The measured heat transfer coefficients follow the computed trend (axial flow simulation). The Captec sensor fails to predict an accurate value of the heat transfer coefficients in regions where strong gradients occur. This difference is due to the thickness of the sensor (0.5 mm) creating irregularities on the smooth specimen surface, hence disturbing the flow-field. The micro-perturbations and vortex formation caused around the sensor surface were previously described in [Hol99] and [Buc14a].

4.6.2.2 Simulation

Figure 4-22 features the results of the simulation of the heat transfer coefficient impinging onto the top surface of a helical gear, with verification of the heat transfer values using a Captec probe. The mesh quality is plotted in Fig. 4-22 (upper right), over the radial position on the top surface of the gear. Lower y^+ values indicate a higher refinement of the mesh, hence higher computational costs. The impact on the heat transfer coefficient along the surface is seen in Fig. 4-22 (bottom right), after using near-wall treatment solutions.

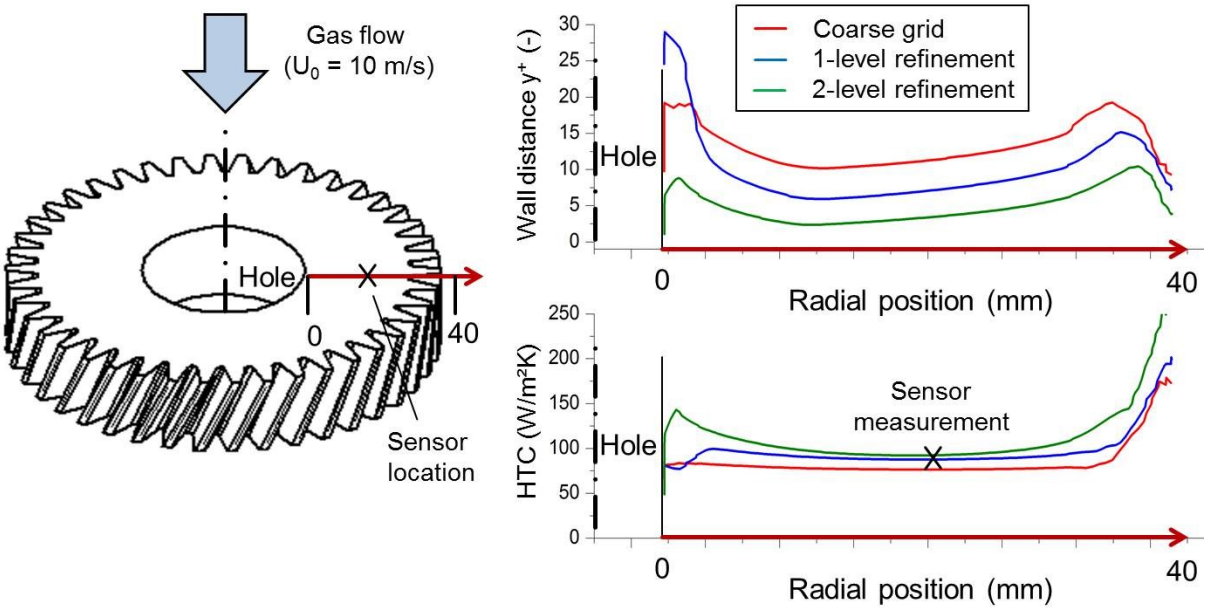

***Figure 4-22**: Grid independency test in the case of impinging gas quenching onto a helical gear specimen, verified by sensor measurements*

The values found by simulations using various grid refinement levels correspond to the measurements using the Captec probe, recommended for local measurements of the heat transfer coefficient. In areas where a wake zone occurs, the simulation still exhibits over-predicted values after computing the heat transfer coefficient, as seen in Fig. 4-22 (bottom right), at both edges of the computed location.

4.6.2.3 Correlation

Existing correlations in gaseous, turbulent heat transfer are limited to simple geometries. Characteristic lengths are commonly extracted from the diameter or length of a streamed cylinder (Eqs. 3-16) [Gni10a].

The correlation from Gnielinski [Gni10a] has been extended to complex geometries by taking into account the chord length of the geometry in the *Re*-number (usually the cylinder diameter or length), e.g., in the case of a cylinder, the sum of two radii and the length of an axial streamed cylinder. This approach, when applied to complex geometries, such as bevel or helical gears, presents satisfying agreement with measurements, as seen in **Fig. 4-23**.

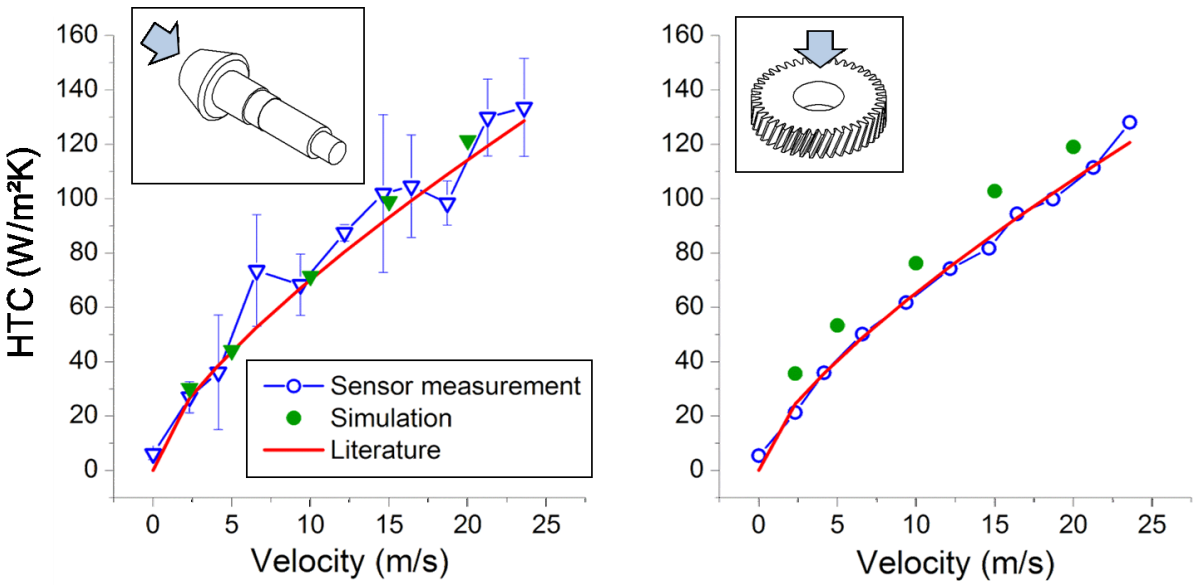

***Figure 4-23**: Results of the simulation and the measurement of the heat transfer coefficient as a function of the gas velocity, in comparison to literature ([Gni10a]) for the bevel (left) and helical gear (right)*

Whereas simulations of heat transfer in the case of the bevel gear (Fig. 4-23, left) match in average the measurements, the case of the helical gear (Fig. 4-23, right) still exhibits over-predictions in a range of 10-20%. Such error margins are also found in the literature for similar turbulence model (k-omega SST) [Zuc06].

4.6.2.4 Distribution

The method of an axially-streamed cylinder (described in Chapter 4.3.2 and 4.3.3) to measure the heat transfer coefficient distribution in quenching chambers has been evaluated, as presented in **Fig. 4-24**.

A corner of the test quenching chamber is represented in Fig. 4-24 (top left), as well as the integral heat transfer coefficient over the cylinder (bottom left), velocity (bottom right), and turbulent kinetic energy (top right) evaluated using the 7-hole pressure probe. The heat transfer coefficient values belong to the range reported in Tab. 3-1, for air quenching at relatively low velocities. Figure 4-24 shows the strong correlation of the heat transfer coefficient distribution with the velocity distribution, as both decreases along the center-to-corner direction. Higher heat transfer is measured close to the upper wall, as a consequence of a local increase in turbulent kinetic energy.

The cylinder probe demonstrates, in Fig. 4-24, the stronger influence of the velocity on the heat transfer coefficient, in comparison to the turbulent kinetic energy. However, in area of poor streaming conditions, high turbulences might improve the heat transfer coefficient, as shown herein.

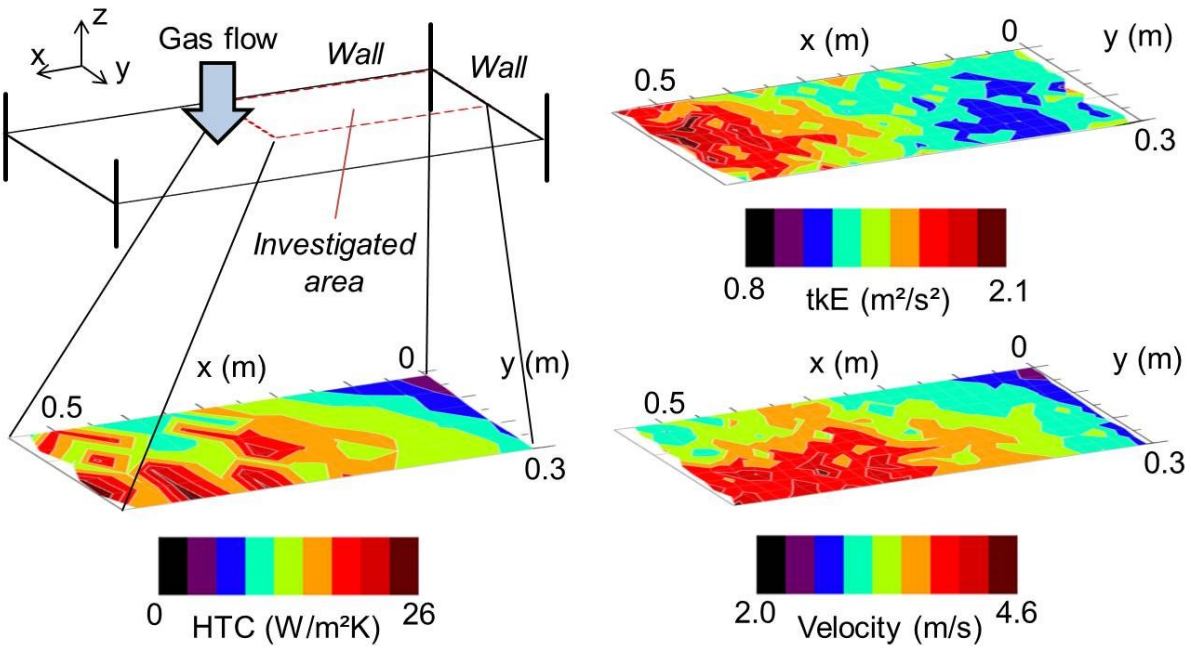

***Figure 4-24**: Influence of the turbulent kinetic energy (above, right) and the velocity distribution (below, right) on the integral heat transfer coefficient of a cylinder (below, left) evaluated in a section plane of the test chamber (above, left)*

4.7 Spray quenching evaluation methods

4.7.1 Droplet characterization

The performance of a twin-fluid, flat-spray nozzle introduced in Chapter 4.5.2 has been evaluated using a patternator measuring the water mass flux distribution sprayed, as seen in **Fig. 4-25** (center). Characteristic distributions as in Fig. 4-25 (right) are derived from positioning the patternator at various distances and angles under the spray nozzle (Fig. 4-25). The ellipse defined by the flat-spray is observed for a water flow rate of 0.45 L/min, with a main axis along the y-direction, as seen in Fig. 4-25 (right).

For lower water flow rates, the elliptical spray tends to a circular shape, as the distribution along the y-direction reduces to reach a range similar to the one along the x-direction. The water flow rates used in spray-quenching processes for heat treatment from the forming heat are largely above the critical value of 0.5 L/min, thus adopting the characteristic elliptical shape of a flat-spray.

4.7.2 Heat transfer characterization

To collect the temperature-depending heat transfer coefficient distributions during spray quenching, thermography has been combined to the lumped-capacitance method, locally adapted to a steel plate, to derive the heat transfer coefficients from the temperature measurements provided by the thermal camera (**Fig. 4-26**).

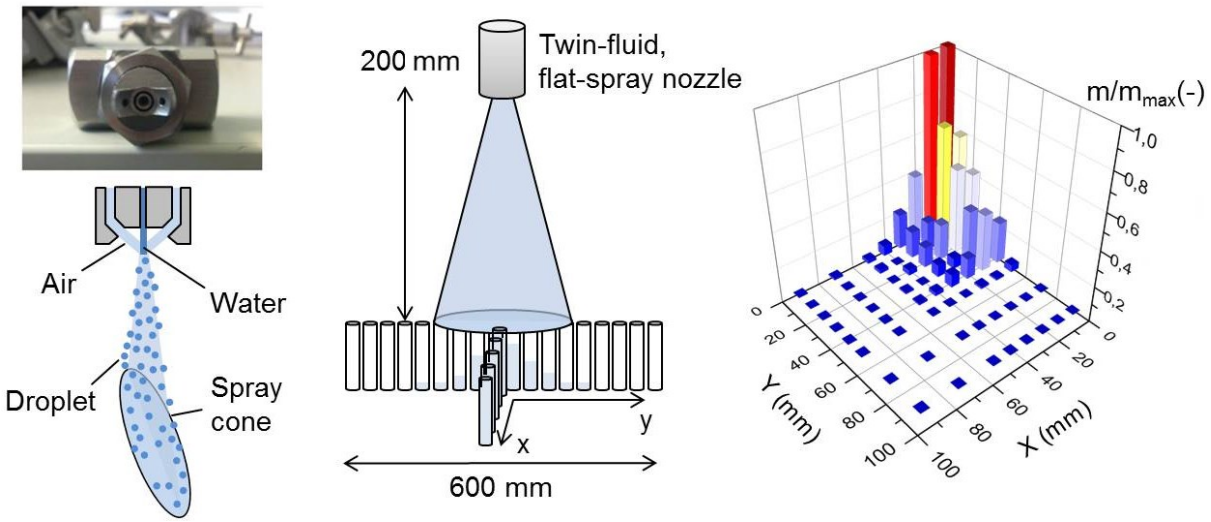

***Figure 4-25**: Experimental set-up to characterize the water distribution during spray process using a patternator, and result of the distribution at 0.45 L/min water flow rate at 3 bar air pressure.*

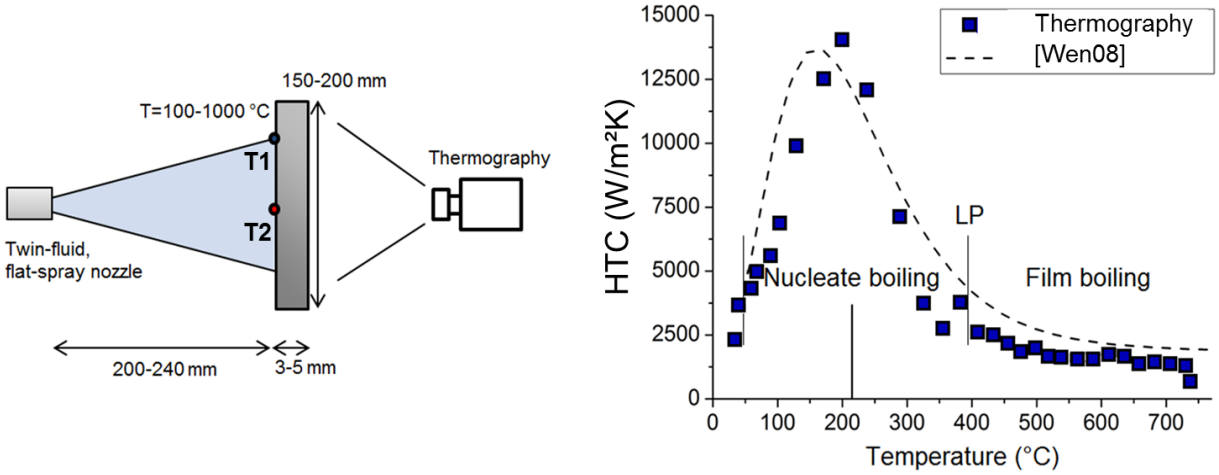

***Figure 4-26**: Experimental set-up to characterize heat transfer coefficients during spray-quenching of a steel plate using thermography and embedded thermocouples (left), and heat transfer coefficient (HTC) as a function of the surface temperature (derived from temperature measurements using thermography), compared to correlation [Wen08] at a water flow rate of 0.30 L/min at 3 bar air pressure (right)*

The lumped-capacitance method is based on the assumption that the effect of the inner heat conductivity in the specimen is higher than the effect of the convection taking place on the specimen surface (at *Biot-number < 0.1*). Furthermore, the high thermal conductivity of the plate (around 40 W/(m.K)) allows the temperature distribution during spray-quenching to be monitored on the other side of the black-painted plate (to increase the emissivity) using thermography. This measurement technique has been verified using thermocouples and surface mounted heat flux sensors (Chapter 4.5.2).

The derived heat transfer coefficients are expressed at the central impingement point for a water volume flow of 0.30 L/min in Fig. 4-26 as a function of the plate surface temperature. The results from the thermography derivation are compared to the correlation described in Eq. (3-27) [Wen08]. The characteristic boiling phenomenon occurring on the specimen surface during high temperature quenching, as also described in Chapter 3.4.3, is observed in Fig. 4-26 (right), split into the three successive phases: film boiling, nucleate boiling, and convection.

Whereas measurements on steel alloys deliver satisfying results in accordance with the correlation; aluminum alloys, due to higher thermal conductivity, deliver a more refined response to the lumped-capacitance, but cannot cover the full temperature range investigated, due to a lower melting point.

5 Results

5.1 Macro-level: flow in top-to bottom quenching units

5.1.1 Flow characteristics

The evolution of the flow distribution, in a gas quenching unit, depends on the geometry of the inner chamber, including expansions and cavities of the chamber, and space for furnace or batch-loading doors (Figs. 4-1, 4-2, 4-3).

Figure 5-1 presents the velocity components distribution in the x-, y-, and z-directions, measured at a section directly below the heat exchanger (*Plane 1*, at z = 0 mm in Fig. 4-17) in a quenching chamber without load.

From the local velocity measurements in these top-to-bottom, gas quenching units, observations are deduced in Fig. 5-1:

- the **x-direction** presents the lowest mean velocity component;
- the **y-direction** presents higher velocity in the direction of the expansion towards the furnace door (or *batch inlet*, as seen in Fig. 4-17), and the charge exit door, this effect might be reduced by increasing the thickness of both doors (hence reducing the cavity space);
- the **z-direction** exhibits the highest mean velocity, as it is the main flow direction in top-to-bottom quenching chambers. Higher velocity is found at the sides of the surface, as the flow close to the wall does not suffer from the high turbulence levels generated by the heat exchanger.

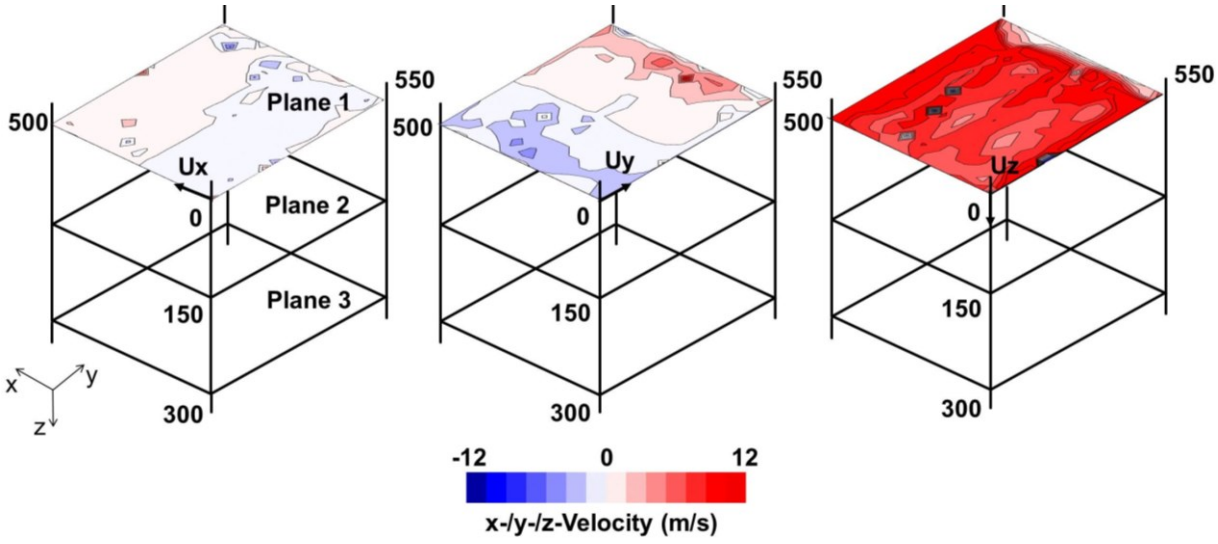

Figure 5-1: *Velocity distribution along the x- (left), y- (middle) and z-direction (right) below the heat exchanger (Plane 1, z = 0 mm)*

[Type A, measured, $\bar{u}$ = 12 m/s, p = 1 bar, Re = 380 000]

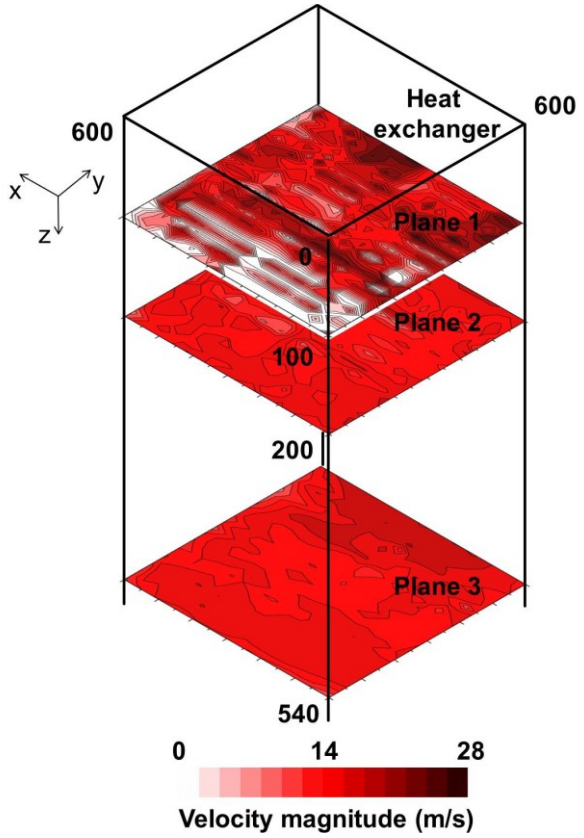

***Figure 5-2**: From left to right, velocity magnitude distribution measured in sections of the quenching chamber from top (Plane 1) to bottom (Plane 3)*
[Type B, measured, $\bar{u}$ = 15 m/s, p = 1 bar, Re = 700 000]

Figure 5-2 presents the evolution, from the top plane to the bottom plane, of the velocity magnitude in the gas quenching chamber (Type B). The top plane is situated in a narrower region of the chamber, 100 mm below the heat exchanger.

The heat exchanger strongly affects the gas flow distribution. Horizontal patterns of constant velocity magnitude are found with decreasing intensity, from the back (furnace access) to the front (batch loading) side. The heterogeneity of the velocity greatly decreases from the top plane to the middle plane, whereas the homogeneity only slightly improves from the middle to the bottom plane, as seen in Fig. 5-2. The areas of higher velocities located at the greater expansion of the quenching chamber (top/furnace door and bottom/batch-loading door) present an expansion towards the center of the quenching chamber, characterized by smaller velocity ranges.

The second investigated plane, presented in Fig. 5-2, is located right above the batch (in the investigated quenching chamber), and demonstrates a satisfying homogeneity that can still be improved by reducing the expansion space *feeding* the recirculation taking place at both doors location.

The normalized mean z-velocity, the normalized coefficient of variation (defined as the ratio of the standard deviation over the mean of a given value), and the normalized turbulent kinetic energy, are presented in **Fig. 5-3**. Considering the mean z-velocity, whereas an empty quenching chamber exhibits almost constant values (simulation and experiment), the mean value of the velocity greatly drops when the flow reaches the batch (at *Plane 3*), as the momentum becomes distributed over the transverse components, the flow is bypassing the charge.

The standard deviation of the velocity in the main z-direction is found to stay almost constant in the batch configuration, as the level of turbulence is transferred also to transverse components. For the empty configuration, the homogenization of the gas flow leads to the progressive reduction of the coefficient of variation, as to be seen in Fig. 5-3 (center), and already observed in Fig. 5-2. An equivalent trend is observed for the turbulent kinetic energy displayed in Fig. 5-3 (right), in the case of an empty quenching chamber, with decreasing turbulences during flow homogenization.

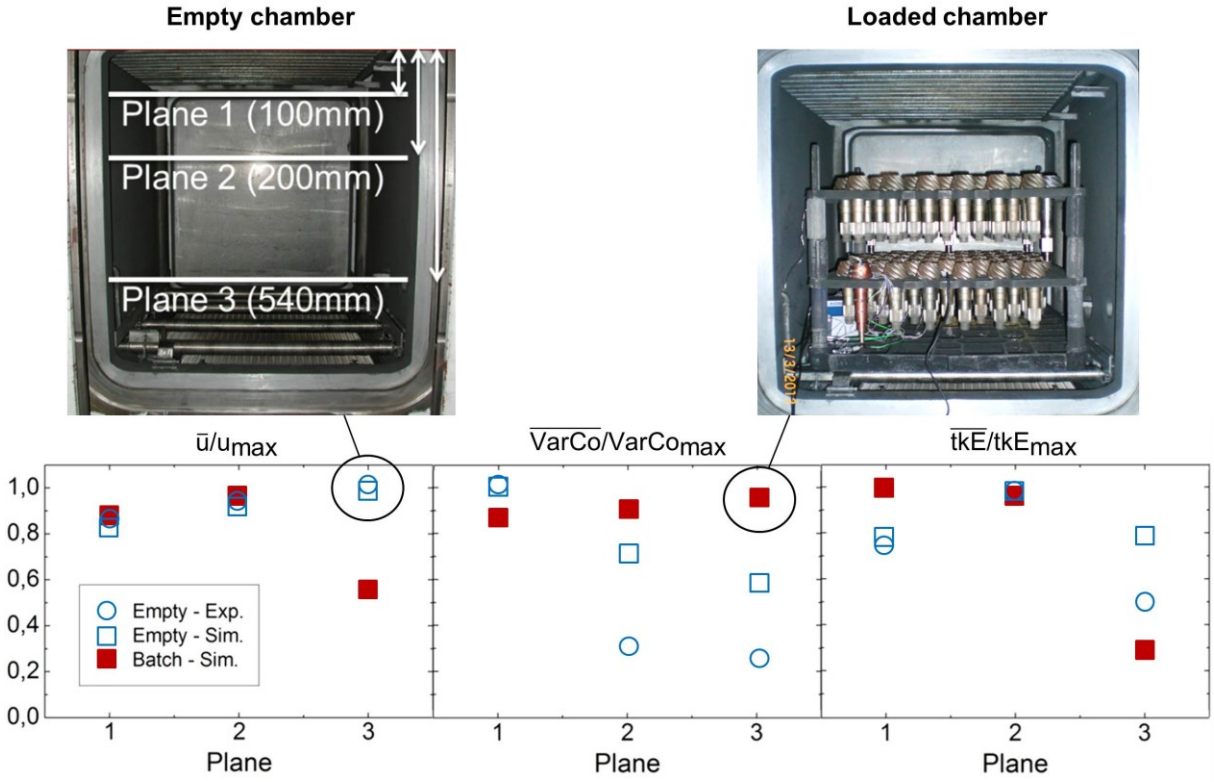

***Figure 5-3**: Results of the normalized axial, z-velocity (u_z), coefficient of variation (VarCo) and turbulent kinetic energy (tkE) at various planes (identified from Plane 1 to 3); measured and simulated*

[Type B, measured, $\bar{u}$ = 15 m/s, p = 1 bar, Re = 700 000]

Flow characteristics at a **macro scale**, in top-to-bottom gas quenching units, exhibit

- a *main vertical, flow-component* (z-direction), with high mean velocity, whereas both *horizontal, flow-components* (x- and y-directions, ten times lower than the z-direction) split according to the chamber near-symmetrical geometry,
- a *large influence of the gas-recycling technology* (e.g., heat exchanger), generating high flow inhomogeneity, progressively homogenizing (30 to 70% drop of the coefficient of variation) through the sub-levels of the quenching chamber.

5.1.2 Flow conditioning

5.1.2.1 Heat exchangers

Heat exchangers, in gas quenching process, are essential to cool down the recycled gas, and maintain the gas temperature difference between quenchant and batch during gas recirculation, thus enhancing the heat exchange at a given rate of heat transfer. They are usually [Alt08] [Heu13] arranged as parallel tubes bundle, located above the batch, as a compromise between constructive dimensions, flow homogeneity regeneration, and minimal temperature of the recycled gas.

This geometrical solution, however, strongly influences the flow structure past the heat exchanger. The fully developed, homogeneous flow, occurring without heat exchanger from the recycled gas flow, is strongly disturbed by large tubular arrangements of the heat exchangers.

Figure 5-4 (left) reproduces the velocity magnitude distribution, measured directly below the heat exchangers, *Plane 1*. The geometry of the heat exchanger disturbs the gas flow, and higher velocities are found mostly at the edge of the investigated area. The areas of higher velocities are however not evenly distributed, and maxima are found in the left section (x = 500), whereas minima are found on the opposite side (x = 0).

This flow dynamics unbalance is to be explained by the tubular arrangement of the heat exchanger. An asymmetry of the tube distribution produces more free area in the left side of the distribution leading to higher velocities, as seen in Fig. 5-4 (left).

Improved results for an alternative heat exchanger configuration (adapted shell around the tubes bundle) can be seen in Fig. 5-4 (right), with the distribution of the velocity magnitude located below the heat exchanger.

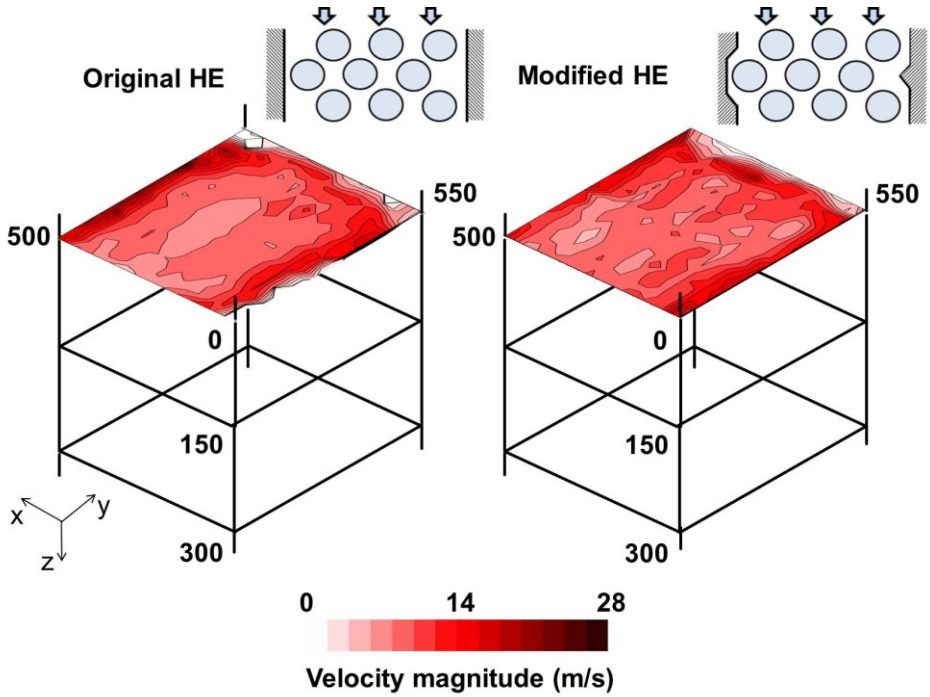

***Figure 5-4**: Velocity magnitude distribution at Plane 1 (z = 0 mm) for the original (left) and the modified (right) configuration of the heat exchanger*
[Type A, measured, $\bar{u}$ = 12 m/s, p = 1 bar, Re = 380 000]

Whereas the flow unbalance on the left and right side of the area has largely decreased, the velocity is found more homogeneous, and increases in the center of the plane, in comparison to the previous heat exchanger version shown in Fig. 5-4 (left). The then-optimized flow distribution, from the heat exchanger, impacts the perforated plate below. Perforated plates (as detailed in Chapter 3.4.2.2) aim at homogenizing the flow through the combination of multiple nozzles, consisted of the holes distributed among the plate above the batch.

The effects of heat exchangers are, however, globally positive to the flow homogeneity: previous observations [Tro98] stated the effectivity of flow conditioners where the major difference is a fine arrangement of thin plates, instead of more simple tubular arrangements, as in the corrected case described in Fig. 5-4. The room available downward the heat exchanger has a major influence on the ability of the gas flow to regenerate a developed profile. The measurement results of the velocity distributions, for the single components at various sections of the chamber (from top to bottom), are displayed in **Fig. 5-5** for the x-, y-, and z-components. A global trend of velocity homogenization is found from top to bottom of the chamber, for all the single components.

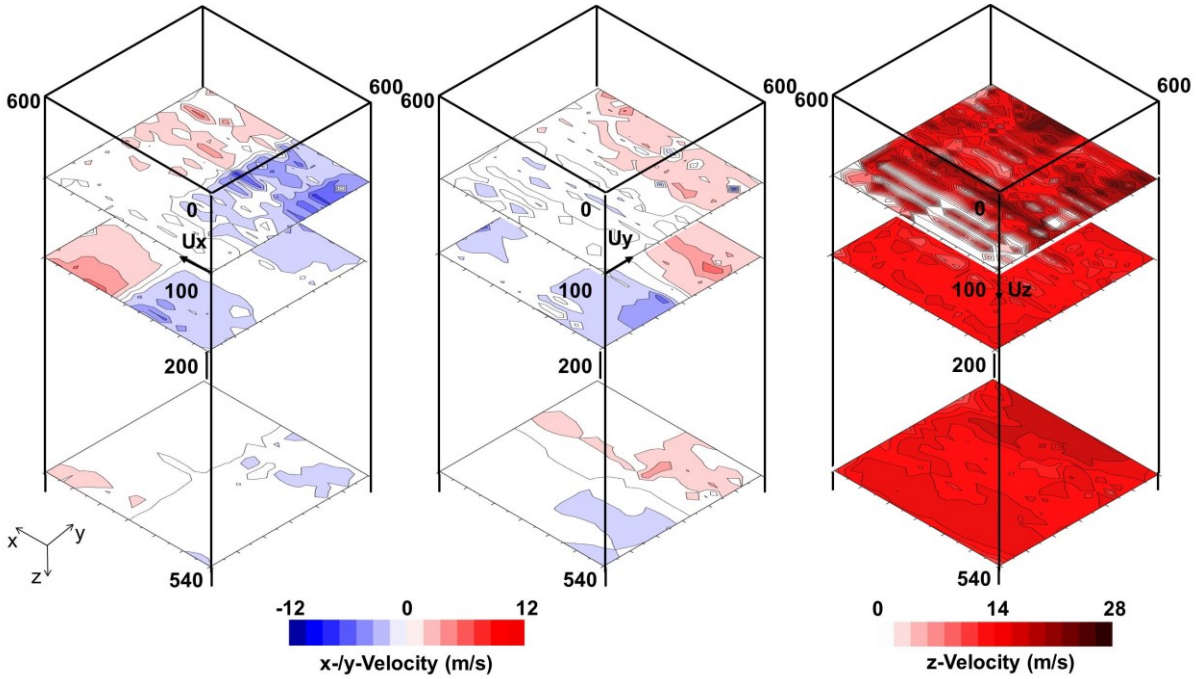

***Figure 5-5**: Velocity distribution along the x- (left), y- (center), and z-direction (right) at Plane 1 (below the heat exchanger), Plane 2 (above the batch), and Plane 3 (above the charge carrier) [Type B, measured, $\bar{u}$ = 15 m/s, p = 1 bar, Re = 700 000]*

As observed in the distribution of the main velocity (z-component) in all the sections, the geometry of the heat exchanger is strongly affecting the flow patterns at the various places, whereas the transverse x- and y-components are only affected at the top of the chamber. Whereas the top section presents an inhomogeneous distribution of transverse flow directions, related to the proximity of the heat exchanger generating turbulences, a clear flow separation is seen in the sections below between positive and negative velocity values, thus demonstrating a split of the gas flow to the sides.

The velocity magnitude, derived from the single velocity components, and the turbulent kinetic energy, are presented in **Fig. 5-6** for the various planes investigated. As stated previously, in top-to-bottom quenching flows, the velocity magnitude (left) only slightly deviates from the main flow direction (z-direction) seen in Fig. 5-5 (right), hence also following similar flow patterns (heat exchangers, recirculations).

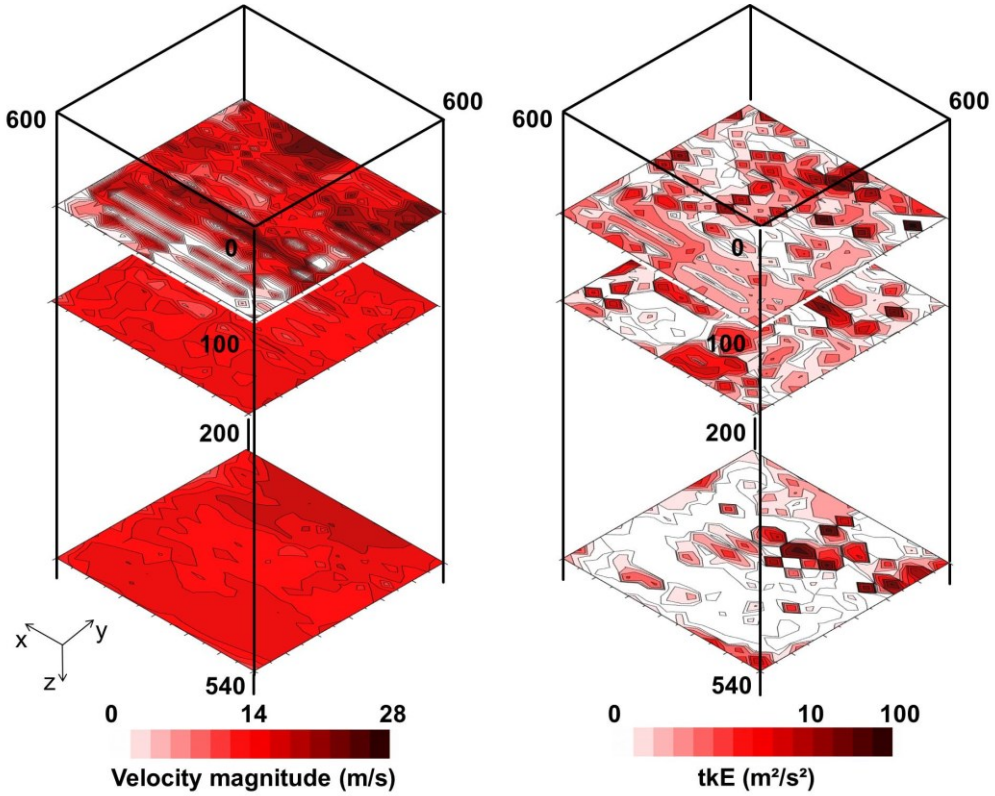

***Figure 5-6**: Velocity magnitude (left) and turbulent kinetic energy (right) distributions at Plane 1 (below the heat exchanger), Plane 2 (above the batch), and Plane 3 (above the charge carrier) [Type B, measured, $\bar{u}$ = 15 m/s, p = 1 bar, Re = 700 000]*

The turbulent kinetic energy represented in **Fig. 5-6** (right) decreases in intensity as the gas flows towards the bottom of the quenching chamber. Turbulent patterns are strongly influenced by the heat exchanger arrangement and geometry, as seen in Fig. 5-6 (top, right). Local areas of high kinetic energy are found where the single components are highly varying from their respective mean values. Whereas turbulent flows improve the heat exchange at the surface of quenched components, a local and unpredictability concentration of turbulences is often a drawback for the heat treatment process, due to the inhomogeneous cooling, further increasing the distortion risks.

5.1.2.2 Perforated plates

The flow homogeneity in gas quenching chambers, which is a key parameter in gas quenching process quality, may be corrected using additional flow conditioners, such as perforated plates. Perforated plates are evaluated with the focus of extending the experimental research of three various configurations by simulating a wider range of potential solutions for flow conditioners, as seen in **Fig. 5-7**, specifically at *Plane 2* (above the batch), as the flow homogenization above the batch has a critical impact on the heat transfer process, taking place inside the batch.

Experimental observations

The experimental observations of perforated plates situated below the heat exchanger cover three degrees of porosity, 26% (Rv10-18), 40% (Rv10-15), and 100% (no perforated plate), listed in **Tab. 5-1**.

Figure 5-7 exhibits the velocity magnitude distribution at the surface above the 2-dimensional batch for the three configurations measured. Difference is made between the center of the area and the edge, as seen in Fig. 5-7 (left). Whereas the initial distribution along the z-component in Fig. 5-4 (right) has a higher velocity at the edge, as also described in [War91], the high porosity of 100% (no perforated plate) leads to an increase in velocity at the center of the area, as seen in Fig. 5-7 (left), for a developed flow above the batch.

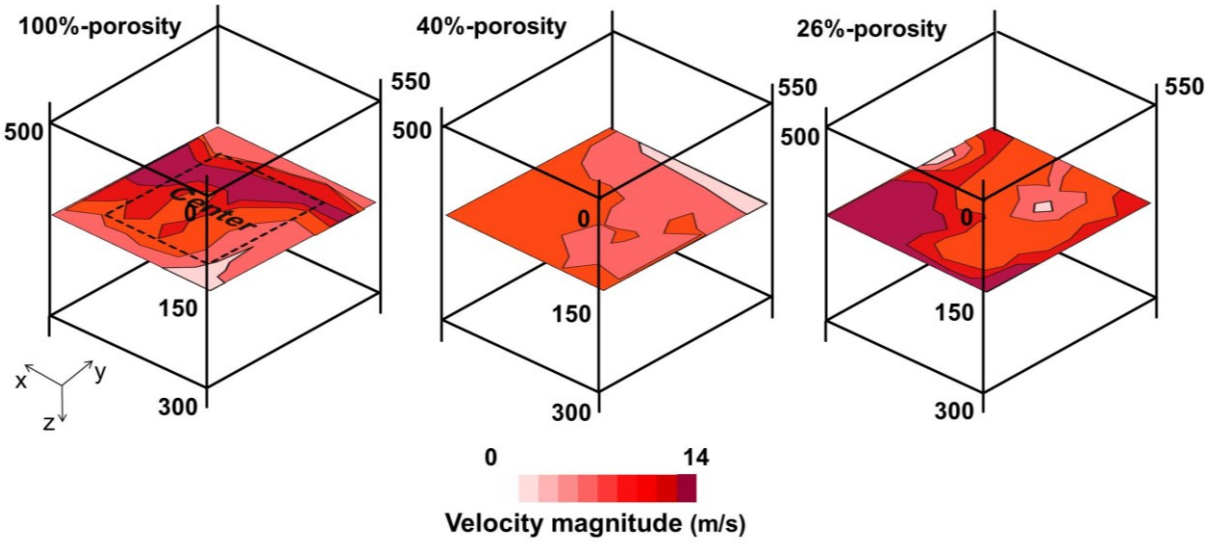

***Figure 5-7**: Velocity magnitude distribution for three configurations using perforated plates at Plane 2 (above the batch)*

[Type A, measured, $\bar{u}$ = 12 m/s, p = 1 bar, Re = 380 000]

***Table 5-1**: Velocity magnitude at Plane 2 for the three configurations (arithmetic mean, standard deviation, coefficient of variation) divided into center and edge of the plane [Type A, measured, $\bar{u}$ = 12 m/s, p = 1 bar, Re = 380 000]*

Plate (porosity)	Center Mean vel.	Center St.-dev.	Center Var. coef.	Edge Mean vel.	Edge St.-dev.	Edge Var. coef.	**Global Mean vel.**	**Global St.-dev.**	**Global Var. coef.**
no plate (100%)	11.81	1.96	0.17	10.07	2.73	0.27	11.15	2.82	0.22
Rv 10-15 (40%)	9.96	0.67	0.07	10.15	0.83	0.08	10.03	0.74	0.07
Rv 10-18 (26%)	11.6	1.51	0.13	12.64	2.33	0.18	11.99	1.92	0.16

Considering the center of *Plane 2*, the mean velocity without perforated plate is 17% higher than at the edge. As also mentioned in [DeB57], a low porosity leads to higher velocity at the edge, as the 9% increase shows, in the case of the Rv10-18 plate (porosity of 26%). The Rv10-15 plate demonstrated its highest homogeneity at *Plane 2*, with a center-to-edge difference below 2%, and a global variation coefficient below 7%, in comparison to the less homogeneous configurations, with Rv10-18 plate (16%), or without plate (22%) (Tab. 5-1).

The porosity has been chosen as a study parameter in this case, as the *Plane 2* distance from the plate is above an *H/D* ratio of 6 (*H/D > 6*). In this case, the heat transfer from an impinging jet is independent from the hole geometry [Col96]. Hence the perforated plate is assimilated to an array of round nozzles, whose single jets are optimally mixed when *H/D ~ 5* [Sch10b].

The measurements of the velocity components at various sections of the chamber, with and without perforated plate, are displayed in **Fig. 5-8**. Whereas the x-component (first row) does not show a high variation for the gas flow going downwards, the y-component (second row) is homogenizing, as demonstrated previously. The perforated plate of lower porosity (26%, Rv10-18, right column) presents the highest flow homogenization in the transverse components, whereas the main component is better handled at medium porosities (e.g., 40% for Rv10-15, central column).

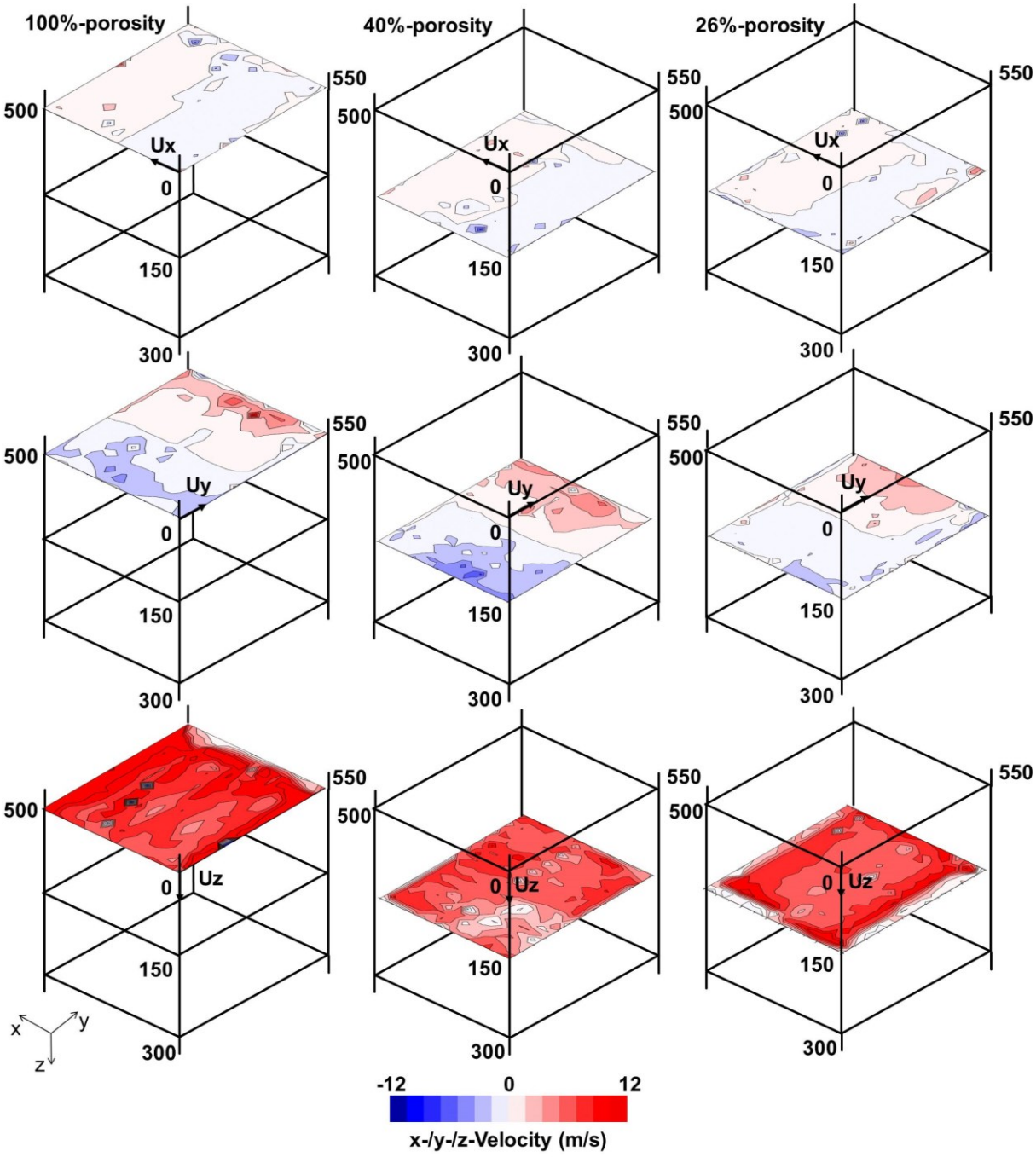

***Figure 5-8**: Velocity distribution along the x- (top), y- (middle) and z-direction (bottom) at Plane 1 (below the heat exchanger, no perforated plates), Plane 2 with a perforated plate of 40%-porosity, and Plane 2 with a perforated plate of 26%-porosity [Type A, measured, $\bar{u}$ = 12 m/s, p = 1 bar, Re = 380 000]*

The velocity magnitude, derived from the individual velocity components, as well as the turbulent kinetic energy have been evaluated and are presented in **Fig. 5-9** for the various planes and perforated plates. The velocity magnitude distributions qualitatively agree in all cases to the distributions of the main velocity (z-component) seen in Fig. 5-8 (bottom row).

The turbulent kinetic energy (Fig. 5-9, bottom) decreases with the gas flowing downward the quenching chamber. Concerning the perforated plates, medium porosities distribute the energy more evenly across the section of *Plane 2*, whereas a lower porosity tends to distribute the turbulent kinetic energy to the edge of the section, as also observed for the velocity magnitude distributions in Fig. 5-9 (top).

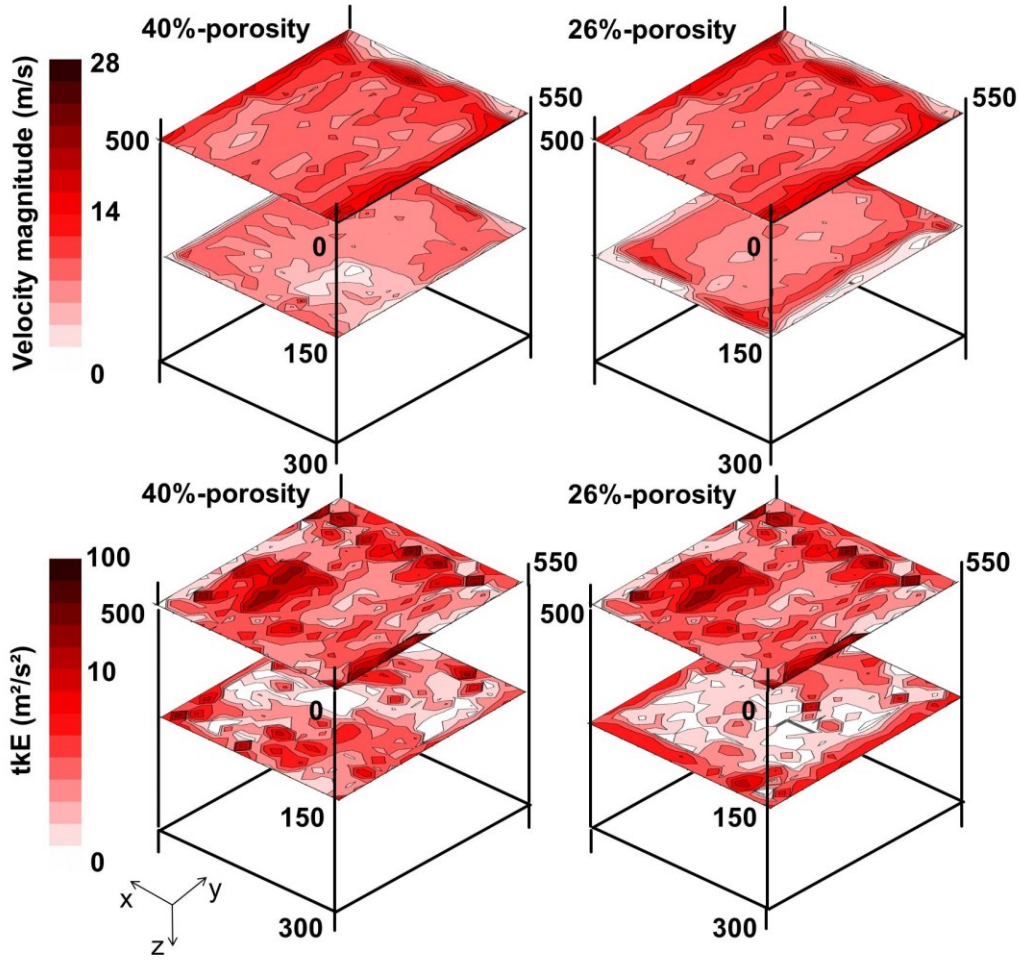

***Figure 5-9**: Velocity magnitude (top) and turbulent kinetic energy (bottom) distributions at Plane 1 (top) and Plane 2, for the Rv10-15 (left) and the Rv10-18 (right) perforated plates [Type A, measured, $\bar{u}$ = 12 m/s, p = 1 bar, Re = 380 000]*

The velocity magnitude and turbulent kinetic energy (Fig. 5-9) present similar trends as already described in Fig. 5-6. Whereas the velocity magnitude is almost identical to the velocity in the main flow direction, the turbulent kinetic energy is decreasing with the gas flowing downwards. The decrease in velocity magnitude, observed in Fig. 5-9 (top), compared to Fig. 5-6 (left), is compensated by a higher turbulent kinetic energy due to the smaller dimensions of the quenching chamber, as well as the structure of the heat exchanger, presenting a larger blocking grade.

Specific observations from the numerical simulations

Plane 2 (top of the batch) is located at a distance $5 < H/D < 6$, for $D = 10$ *mm*, below the perforated plate. A simulation-based parameter study has been carried out for specific plates with 10 mm-diameter holes, as seen in **Fig. 5-10** (Rv10-xx). For constant holes-diameter, the increasing porosity leads to a decreasing velocity in the main flow direction, whereas the homogeneity increases (decreasing variation coefficient, defined as the ratio of the standard deviation over the mean value, and velocity range, converging from 40%-porosity). A minimal porosity of 40% improves the flow homogeneity, as also found in [DeB57]. The average turbulent kinetic energy (tkE) decreases with increasing porosity. A high turbulent kinetic energy improves the heat transfer in the case of industrial gas quenching, thus an optimal configuration may be identified by a combination of high velocity, high homogeneity, and high turbulences, making the Rv10-15 perforated plate, in this particular 2-dimensional quenching, the optimal choice.

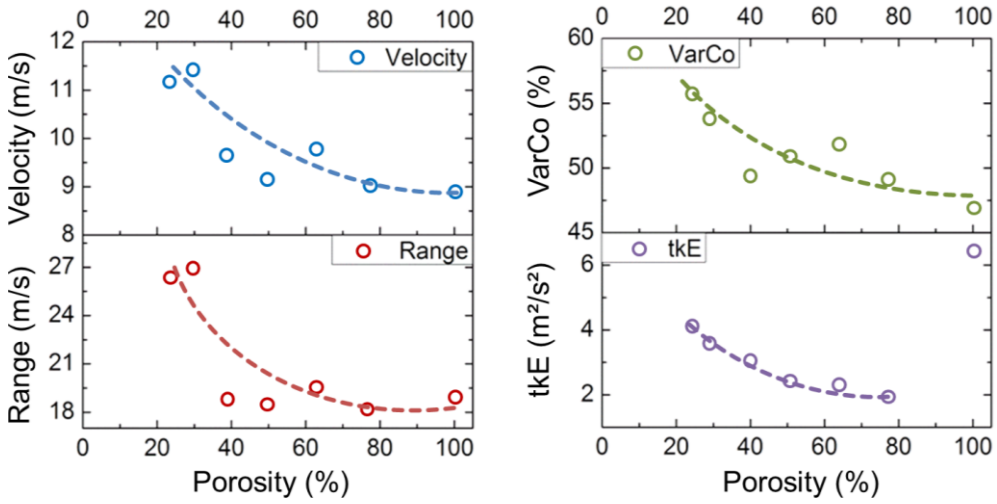

***Figure 5-10**: Flow characteristics (velocity, range, variation coefficient, and turbulent kinetic energy) for various plates with 10 mm-diameter perforated holes as a function of the porosity at Plane 2 [Type A, simulated, $\bar{u}$ = 10 m/s, p = 1 bar, Re = 320 000]*

The flow homogeneity is also investigated among the sections of the quenching chamber, from top to bottom (*Plane 4*), as represented in Fig. 4-17. **Figure 5-11** shows that a reduction of the porosity to 30% (third column) leads to an asymmetrical profile of the flow, focusing in the center of the chamber at *Plane 4*, as represented by the streamlines (Fig. 5-11, top). The recirculation zones take place inside the cavities of the quenching chamber, and reduce as the porosity increases. Whereas they remain local at a porosity of 50% (second column), the recirculation zones dramatically expand at 30% (third column), providing an undesirable velocity profile for gas quenching processes.

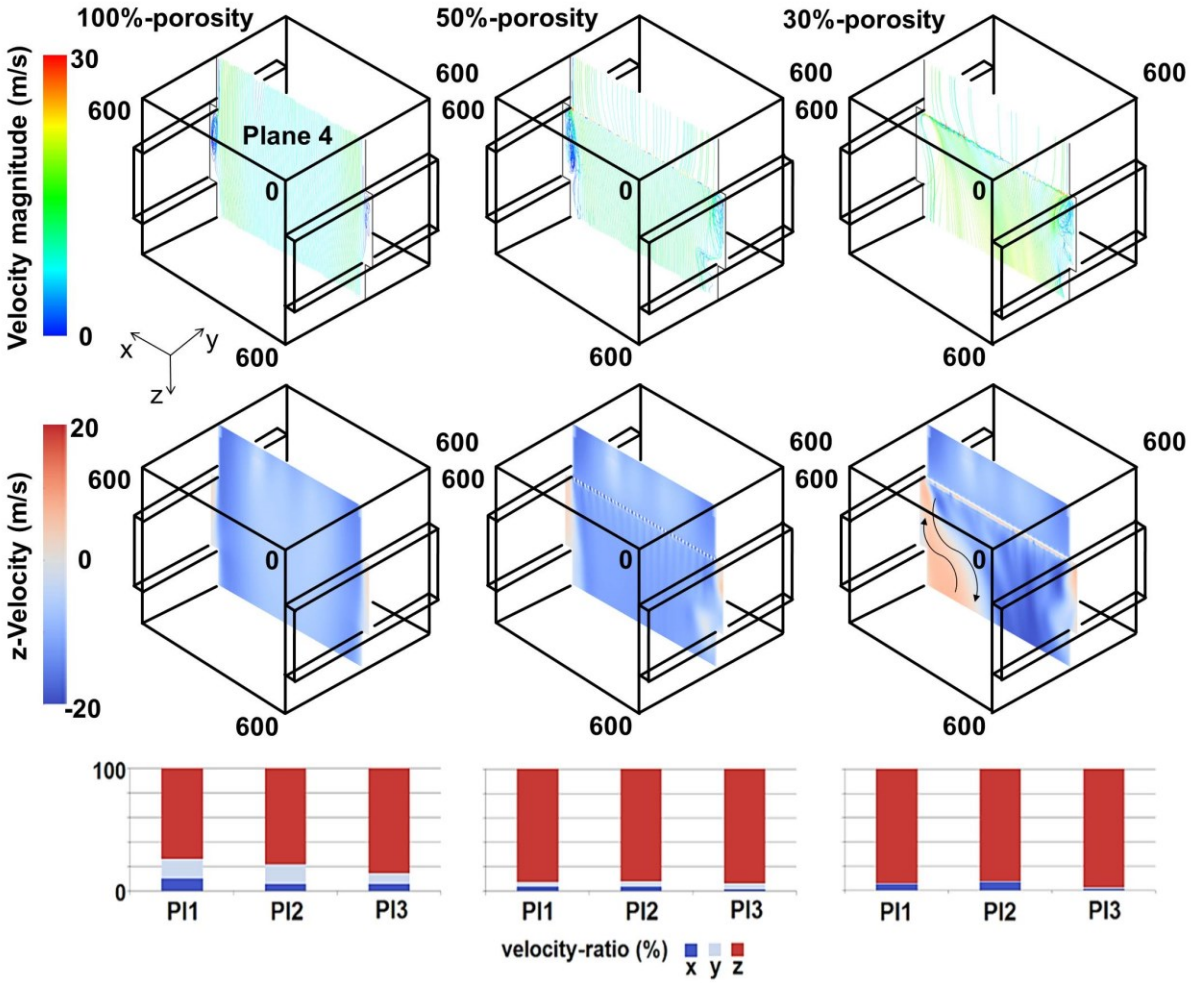

***Figure 5-11**: Velocity magnitude (top), z-velocity (middle), and ratio of the velocity components (bottom), as a function of the porosity, at the central section of the chamber, parallel to the gas flow*

[Type A, simulated, $\bar{u}$ = 10 m/s, p = 1 bar, Re = 320 000]

The expansion of the recirculation zone is located where the fastest velocity and highest turbulence reaches the perforated plate, improving the flow through the plate. Further comparisons in Fig. 5-11 (bottom) presents the influence of the chamber configuration on the components of the velocity. The influence of the component in the x-direction remains stable for the various porosity levels, due to the geometrical expansion of the chamber into batch and furnace inlets; whereas the component in the y-direction is affected by the porosity, as to be seen in Fig. 5-11 (bottom), due to the expansion of the recirculation zones.

The measurements and the simulations confirm the positive influence of perforated plates on improving the flow distribution homogeneity. Perforated plates ranging from 40% to 65% porosity and with holes-diameter having the optimal ratio *H/D ~ 5-6* provide flow patterns to ensure the most homogeneous quenching process.

Flow conditioning solutions at a **macro scale**, in top-to-bottom quenching chambers, may take the form of design criteria affecting

- the *expansion* of the chamber area from the heat exchanger above should be limited to avoid the creation of recirculation areas,
- the *heat exchanger*, whose effect on the flow homogeneity can be in-situ quantified, and adapted to produce a homogeneous and intensive flow distribution above the batch (an industrial case lead to reduce the coefficient of variation from 39% to 31% by optimizing the heat exchanger shape),
- *perforated plates*, whose geometry (hole diameter, distribution, and overall porosity) provide an effective incoming flow homogenization, especially in reduced chamber dimensions, with the following guideline:
    - 40% to 65% porosity
    - ratio *H/D ~ 5-6*

5.2 Meso-level: structure of the batch

5.2.1 Multi-layered batch arrangements

Conventional applications of heat treatment gas quenching cover 3-dimensional batches of small workpieces (cylindrical gears, flat gears) to decrease the process time per part. Variations of the batch arrangement have been investigated for various complex part geometries with additional flow conditioners, for single or group of parts to obtain further efficiency improvements.

5.2.1.1 Bevel gear

3-dimensional arrangements of bevel gears are compared in **Fig. 5-12**, on the basis of the integral heat transfer coefficient on the bevel gear specimens. The measurements took place in the gas quenching test chamber. The effects of the charge density, amount of layers, and layer offset, have been taken into account during the experimental observations.

The effect of the batch density is shown in Fig. 5-12 (left). The increase in charge density (distance between parts from three to two diameters) is found to improve both mean heat transfer coefficient and standard deviation in the measurements results. The second layer of bevel gears is quenching more homogeneously due to the protective effect of the first layer, in Fig. 5-12 (right), as also observed by [Mac05].

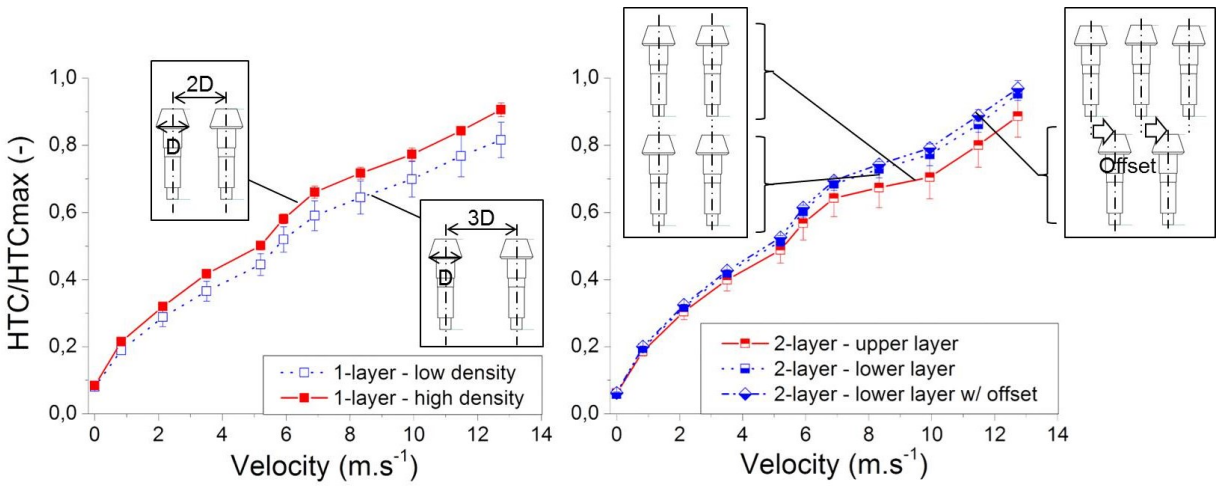

***Figure 5-12**: Effect of batch density (left) and layers offset (right) on the heat transfer intensity (HTC) and homogeneity (standard deviation) for bevel gear specimens [Test chamber, measured, $\bar{u}$ = 0-14 m/s, p = 1 bar, Re = 890 000, HTCmax = 65 W/m²K]*

The heat transfer in the second layer is furthermore enhanced when implementing an offset of the parts at the second layer, as also seen in Fig. 5-12 (right). Large batches of bevel gears require a high batch density and an offset of the second layer, while avoiding a too high density or further layers, causing a higher pressure loss that harms the ventilator performances. [Mac05] suggests the use of dummy cylinders as first layer to ensure the global quenching homogeneity between layers.
As observed by [Mac05] and [Buc14a], the charge carrier has a positive influence on the average value of the heat transfer, increasing the heat transfer coefficient for multiple-layer configurations. However, the carrier grid leads to increasing the standard deviation of the heat transfer coefficient, thus the heterogeneity of the quenching of a bevel gear specimen.

5.2.1.2 Helical gear

The arrangement of batches of helical gears has been investigated in a series of simulations for several configurations summarized in **Fig. 5-13**:

- configuration 1 features two layers of helical gears, arranged in line, one under another;
- configuration 2 features an offset of the second layer, as pictured;
- configuration 3 comprises the use of long flow ducts across both layers;
- configuration 4 features the use of an individual flow duct around each gear specimen of a two-layer batch without offset.

The results can be seen in Fig. 5-13 (right) for the mean heat transfer coefficient at the upper and bottom layers. Concerning the intensity of the heat transfer, the longer flow duct fails to reach the effectivity of the configurations with shorter flow ducts, or even without flow ducts. This configuration is also discarded because of the highest coefficient of variation observed, out of all configurations computed and extensively evaluated in [Buc14b].
Whereas the configuration with smaller, 30 mm-long flow ducts and without offset of the bottom layer reaches the effectivity of the configurations without flow duct, Fig. 5-13 exhibits the high potential of a batch arrangement featuring small, individual flow ducts, and the offset of the second layer.
Also for 3-layer batches, the maximum mean heat transfer coefficient, with smallest coefficient of variation, is found for the configuration involving individual flow ducts and an offset of the second layer.

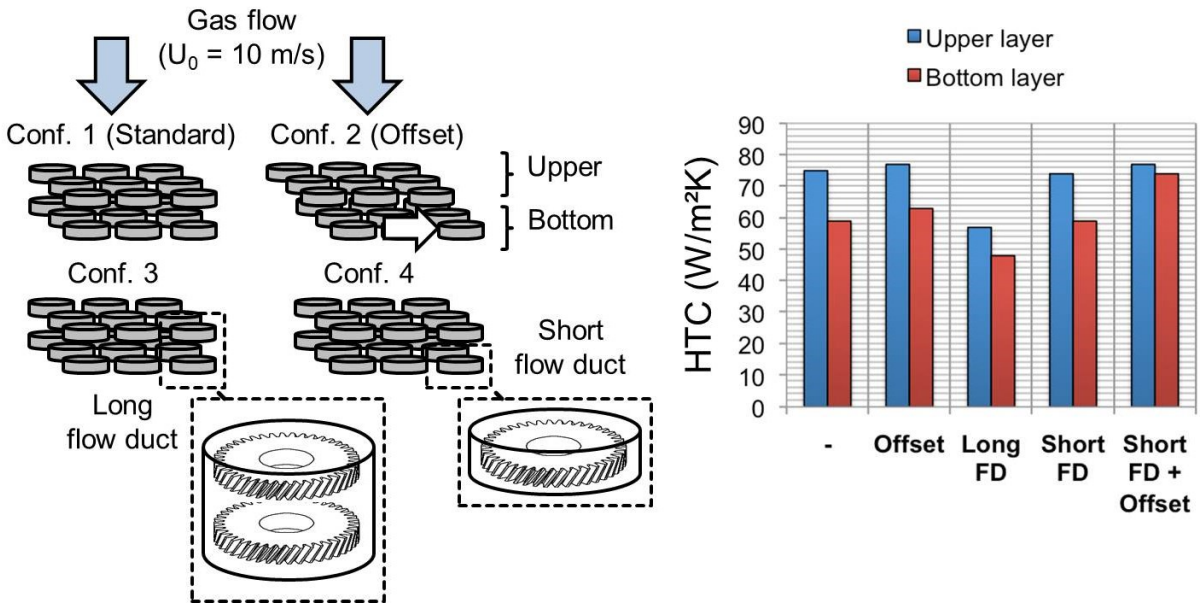

***Figure 5-13**: Mean heat transfer coefficients of 2-layer batch configurations involving helical gears; configuration 1 is standard, configuration 2 consists of an offset of the bottom layer, configuration 3 involves long flow duct for the two layers and configuration 4, flow ducts around single specimens*
[Test chamber, simulated, $\bar{u}$ = 10 m/s, p = 1 bar, Re = 700 000]

Short, individual flow-ducts, dimensioned according to the gear size, focus the gas flow in the teeth region, and are found to effectively improve the heat transfer of the whole helical gear at every layer of a 3-layer batch. An offset of the second layer is requested to condition the gas flow, so that the second and eventually third layers can be quenched with higher cooling rates.

The results achieved on the **meso scale** indicate that both heat transfer homogeneity and intensity are improved in multi-layered batches of gear specimens by

- *setting an offset of the sub-layers* of the batch (around 5% increase in quenching intensity),
  - corresponding to half the distance between the specimen centers,
  - in a single direction,
- and *enclosing the specimen in cylindrical solutions (flow ducts)* intensifying the gas flow close to the specimen surface (major increase in quenching intensity at the bottom layer),
  - with a cylinder length nearly equal to the specimen length,
  - with a wall-to-specimen distance between 5 and 10 mm.

5.2.2 Single-layered batch arrangements

5.2.2.1 Bevel gear

Batch configurations produce additional effects to the gas flow around workpieces, in comparison to configurations involving single parts. Such effects can be, for instance, the neighboring effect of other workpieces, the effects of the charge carrier, or the effect of the environment of the quenching chamber depending on the workpiece position.

Bevel gears are challenging part geometries for batch configurations in gas quenching. The head/pinion of the gear creates a high blocking grade for the impacting gas flow on the top of the batch. The shaft of the gear is smaller in diameter, and longer than the head, increasing the distortion risks due to the dimensions.

In Fig. 5-12, the measured integral heat transfer coefficient showed that a low batch density increases the quenching heterogeneity (standard deviation), while remaining less effective in terms of HTC intensity, in comparison with a high batch density.

Whereas bevel gears appear to be challenging parts for the quenching of single workpieces, the arrangement in highly densified batch minimizes the flow irregularities produced by the flow channeling and impinging gas stream. As already observed [Heu13a], top-to-bottom gas flow is sufficient in 2-dimensional arrangement of bevel gear to reach satisfying quenching homogeneity, thus avoiding distortion risks.

5.2.2.2 Helical gear

The teeth region of the helical gear is critical during the quenching process. Gas flow recirculation strongly affects the quenching homogeneity and intensity in impinging flows. The tooth lying in the closest gap between two gears is investigated in **Fig. 5-14** (top). The heat transfer coefficient distribution is computed along the two sides of the tooth: the impinging side (left), and the rear side (right). Various distances between both gears have been analyzed in a series of simulation runs, ranging from 0 mm (gears in contact) to 20 mm (neglectible flow disturbance of the neighboring gear).

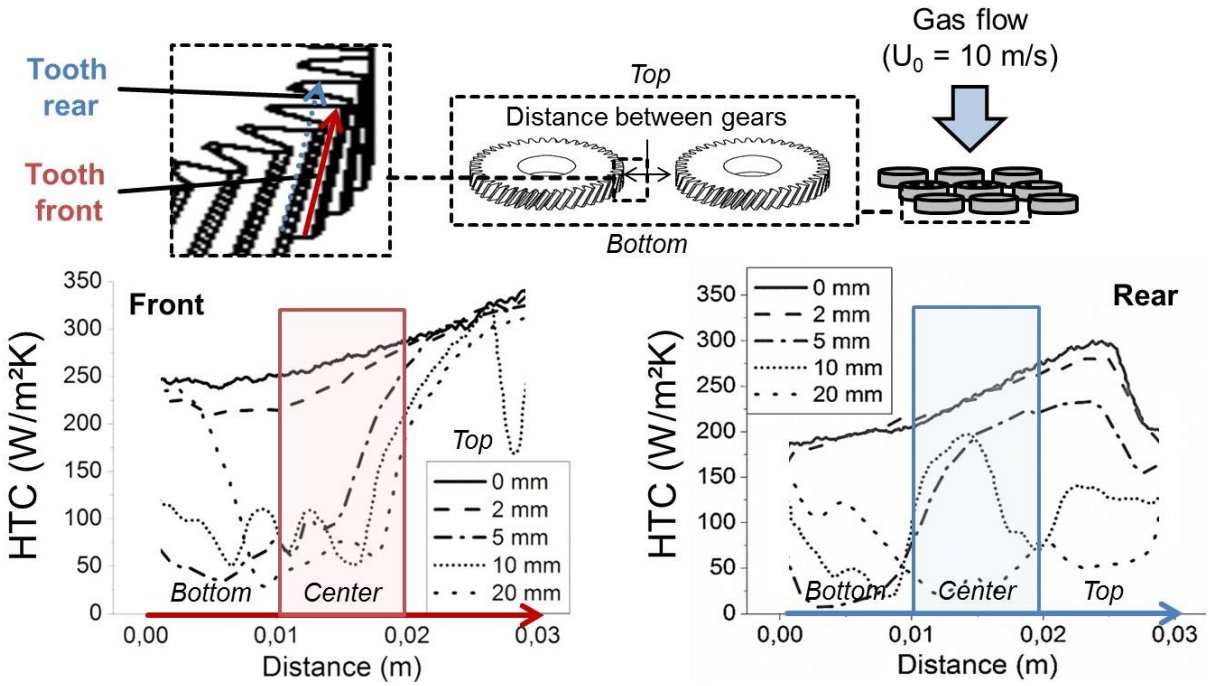

***Figure 5-14**: Computed heat transfer coefficients (HTC) along the front (left) and rear (right) side of a gear tooth for various batch densities (distance between gears) [Test chamber, simulated, $\bar{u}$ = 10 m/s, p = 1 bar, Re = 700 000]*

As it can be seen in Fig. 5-14 (left) at the front side of the tooth, the widest distance between the gears (20 mm) provides the lowest homogeneity of the heat transfer coefficient distribution, characterized by higher heat transfer at the top and bottom section of the tooth, whereas the center of the tooth remains barely affected by the flow. Decreasing the distance between gears leads, on both front and rear sides of the tooth, to a positive increase in heat transfer intensity and homogeneity, with both sides demonstrating only limited heat transfer coefficient gradients, specifically for close distances (0 and 2 mm). However, the distance between gears for 2-dimensional batches has to be maintained large enough to avoid such local heat transfer variations between teeth (as seen in Fig. 5-14, below 20 mm). The local benefits mentioned previously are indeed a drawback for the quenching homogeneity of the whole gear, as the rest of the teeth are quenching worse.

The average heat transfer coefficient and the HTC range, presented in Fig. 5-14, are shown in **Fig. 5-15**, as a function of the distance between gears. The sampled data are located in the same area described in Fig. 5-14, in the closest region between neighboring gears.

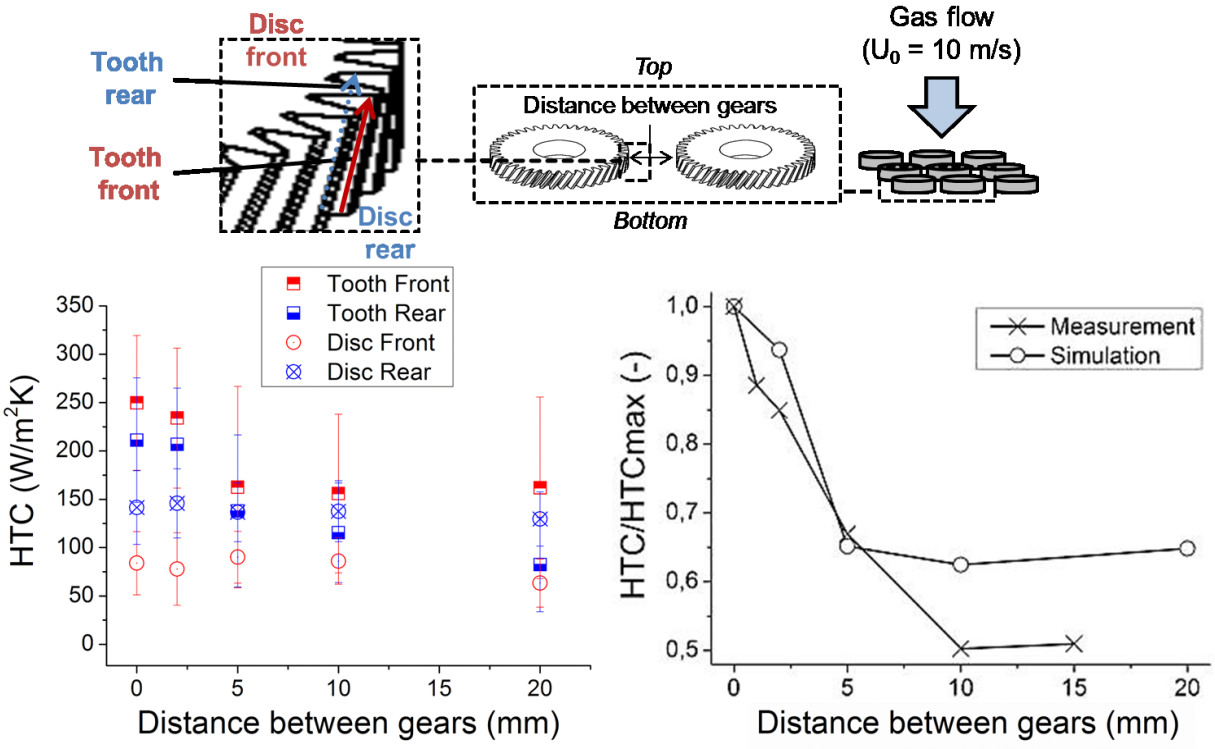

***Figure 5-15**: Simulated average heat transfer coefficients of a helical gear (left), and averaged heat transfer coefficient comparison (right) between measurement and simulation of a tooth as a function of the distance between gears*
[Test chamber, measured and simulated, $\bar{u}$ = 10 m/s, p = 1 bar, Re = 700 000]

The front and rear sides of a helical gear are also covered in the data shown in Fig. 5-15. Whereas the density in the batch affects the heat transfer of the front and rear side of the gear in a +/-20% range, a high heat transfer is found for close distances between gears. The heat exchange is decreasing as the distance increases, until the value of 10-15 mm, where the heat transfer coefficient reaches a constant minimum.
Figure 5-15 (right) presents the comparison between measurements and simulations over the distance between gears on the heat transfer rate. All capture the trend found previously, with stabilization of the heat transfer rate in the same 10-15 mm distance. Simulations are found to slightly diverge from the measurements, as seen in Fig. 5-15 for large gear distances.
Batch arrangements involving helical gears, producing high blocking grades, require a minimal distance between gears of 10 mm in order to maintain similar quenching intensities and homogeneities in the teeth regions. The blocking grade has not proved any major influence on the heat transfer rate, neither at the front nor at the rear side of the helical gear.

5.2.2.3 Ring gear

Rings offer low blocking grades and high sensitivity to distortion. With additional teeth regions, ring gears are highly challenging workpieces in gas quenching, when willing to ensure quality of the mechanical process, and reproducibility of the production. Gas quenching is of interest for ring gears as both method and workpiece combine their advantages: low distortion potential for gas quenching and low blocking grade for ring gears.

Figure 5-16 (left) presents the effect of the flow rate (in terms of ventilator performance) on the integral heat transfer of a ring gear, for measurements done in the test chamber. In comparison with the correlation detailed in Chapter 4.6.2.3, an error margin of around 20% can be found. The error margin is to be explained by the high turbulence level in the quenching chamber, thus increasing the heat exchange at the surface of the gear. This effect has not been observed in the experiments for the single gear in a wind channel.

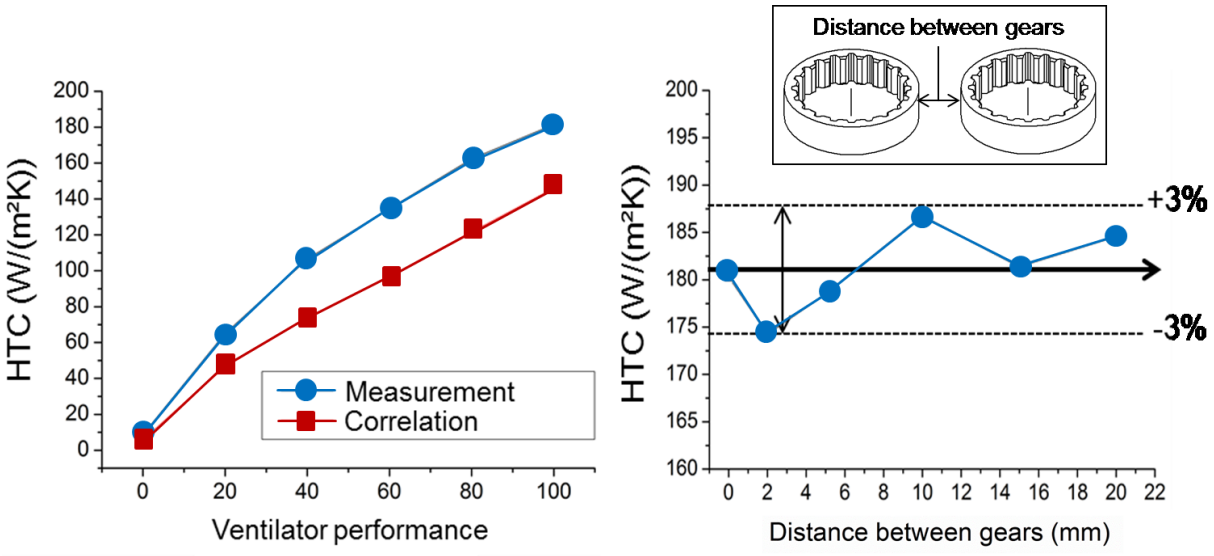

***Figure 5-16**: Measurement results of the integral heat transfer over a single ring gear compared with correlation (Chapter 4.6.2.3) at various ventilator performances (left) and effect of the distance in batch of ring gears over the heat transfer at 100% ventilator performance*

[Test chamber, measured, $\bar{u}$ = 0-14 m/s, p = 1 bar, Re = 890 000]

Figure 5-16 (right) shows the relation between the distance and the tangential heat transfer coefficient measured between two neighboring ring gears (0 mm means the two gears are in contact). Increasing the distance from the situation where the two ring gears are in contact does not influence the heat transfer coefficient, as seen in Fig. 5-16 (right).

The local heat transfer coefficient scatters in a +/-3% range around the average value. The distance between ring gears in a batch does not influence the heat transfer coefficient because of the low blocking grade of such workpieces so that the density of parts can be set the highest for 2-dimensional and 3-dimensional batch of ring gears.

The investigation of the flow and heat transfer at the **meso scale** for single-layered batch indicates that

- heat transfer homogeneity and intensity are improved for gear specimens by providing a *minimum space between specimens* to lessen the mutual interaction between the neighboring specimens, especially in the teeth region, over the gas flow,
    - of at least 5 mm for flat gears (outer gearing),
    - yet not relevant for ring gears (low blocking rate of the batch).

5.3 Micro-level: flow control for single specimens

5.3.1 Heat treatment homogenization using impinging jets

5.3.1.1 Ultrasound-assisted gas quenching

The use of pulsating or oscillating flows within impinging gas quenching has been investigated to assess the potential of local pressure variations to increase the intensity and homogeneity of the heat transfer at the surface of metal specimens.

The investigated flow configuration on a flat plate is a combination of a gas nozzle with an acoustic sound field. The local HTC distribution on the flat plate is evaluated using temperature measurements and the lumped-capacitance method (at *Biot-number < 0.1*), as well as glue-on heat flux sensors. The experiments are carried out in temperature configurations close to ambient conditions (*80 °C < T < 120 °C*, using the aluminum plate arrangement), in parallel with simulations.

The characteristic HTC distribution found for an impinging jet (**Fig. 5-17**, right) is in agreement with the literature [Zuc06], with a high peak in heat transfer at the stagnation point (center of the impinging jet), quickly decreasing as the jet expands radially outwards.

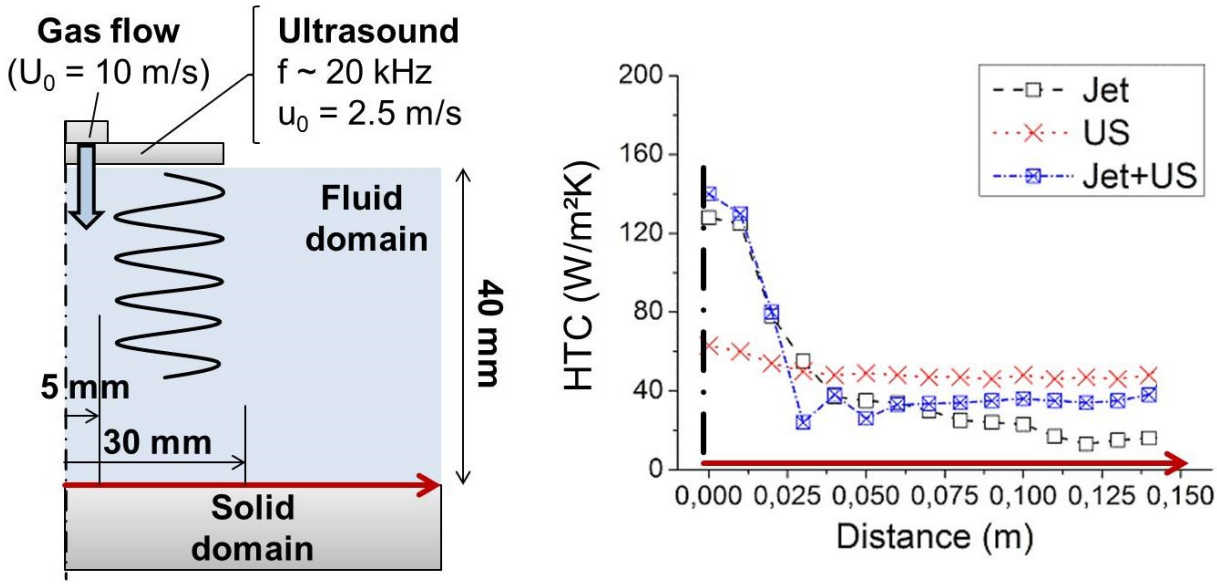

***Figure 5-17**: Simulation setup (left) and local heat transfer coefficient distribution for three flow configurations (gas jet, ultrasound, and jet with ultrasound) (right) [Test chamber, simulated, $\bar{u}$ = 10 m/s, p = 1 bar, Re = 25 000]*

The sound effect on the heat transfer is also reported in Fig. 5-17, with a smoother distribution than the sole impinging jet, and an almost constant heat transfer in the direction of the expansion. The combination of both techniques produces a higher peak in the center, whereas the expanded jet, influenced by the ultrasound, maintains a higher, more constant heat transfer coefficient along the expansion path.
Simulations and measurements of integral heat transfer coefficient demonstrate a qualitative agreement, as seen in **Fig. 5-18**. The integral evaluation of the heat transfer over the plate confirms the slight improvement brought by the combination of impinging jet and ultrasound in both simulated and measured cases.
The combination of gas flow and ultrasound proves interesting improvement of the heat transfer homogeneity, and a slight increase in intensity for the specimen and configuration investigated.

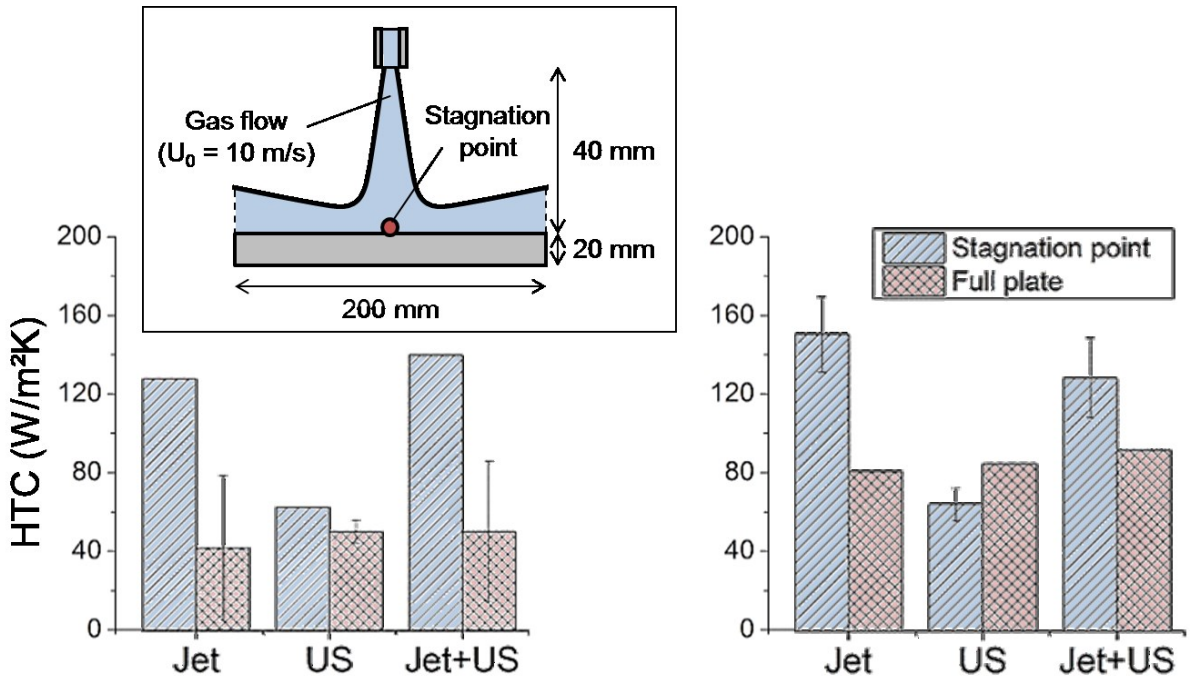

***Figure 5-18**: Comparison of simulation (left) and measurement (right) results concerning the local and integral heat transfer on the aluminum plate*
[Test chamber, simulated and measured, $\bar{u}$ = 10 m/s, p = 1 bar, Re = 25 000]

5.3.1.2 Nozzle field distribution

A process-integrated spray-quenching field has been evaluated in order to perform a controlled quenching of individual specimens from the processing heat (1100 to 1250 °C), as seen in **Fig. 5-19** for a forging process line. The forging/quenching process described in Fig. 5-19 (right) features the quenching unit made of a nozzle field pictured in Fig. 5-19 (left), integrating a ring-sensor monitoring the specimen microstructure during the quenching process [Hin12a].

Temperature-depending heat transfer coefficient distributions, based on local thermography measurements, are derived for various spraying parameters. These HTCs are implemented into a transient heat transfer simulation as boundary conditions on the surface of complex geometries (such as the stepped shaft and the common rail seen in Fig. 19, left). Additional elements interacting with the spray (such as the ring-sensor) are taken into account, as seen in the simulation results of **Fig. 5-20** for the common rail specimen.

Due to the integration of the microstructure sensor (ring shape) in the quenching process [Hin12a] [Rei14] (Fig. 5-19 top left for the stepped shaft, bottom left for the common rail), the quenching configuration needs to be adapted, where four nozzles surround the stepped shaft, positioned so that the flow targets the massive part of the shaft, where the heat is concentrated.

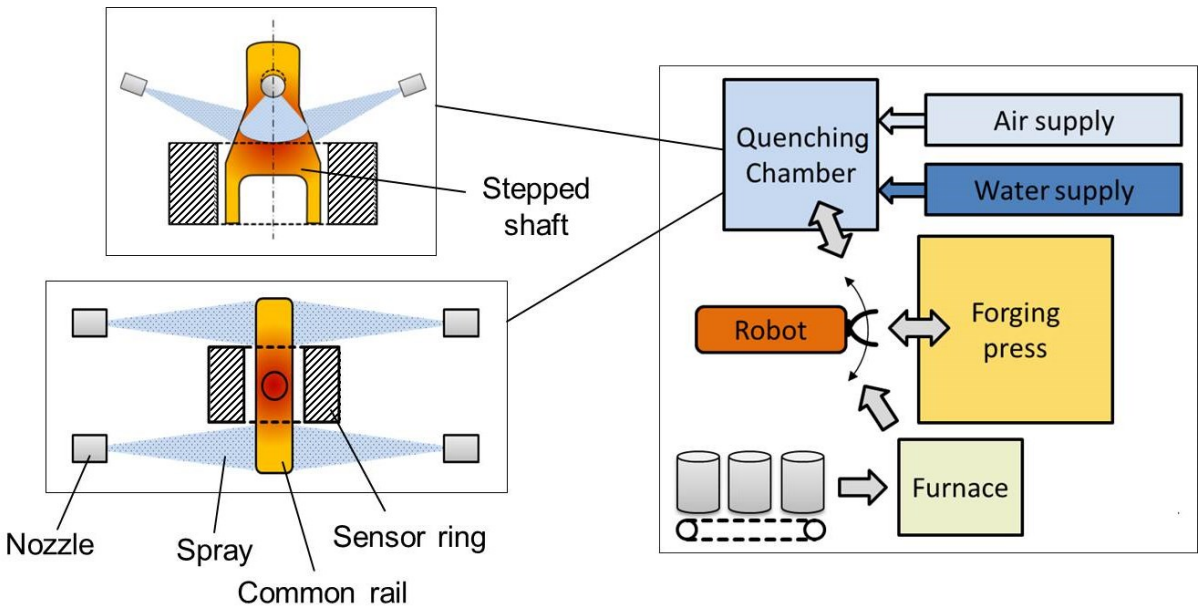

***Figure 5-19**: Spray-field (left) integrated into the quenching cell unit with its location within the forging unit (right)*

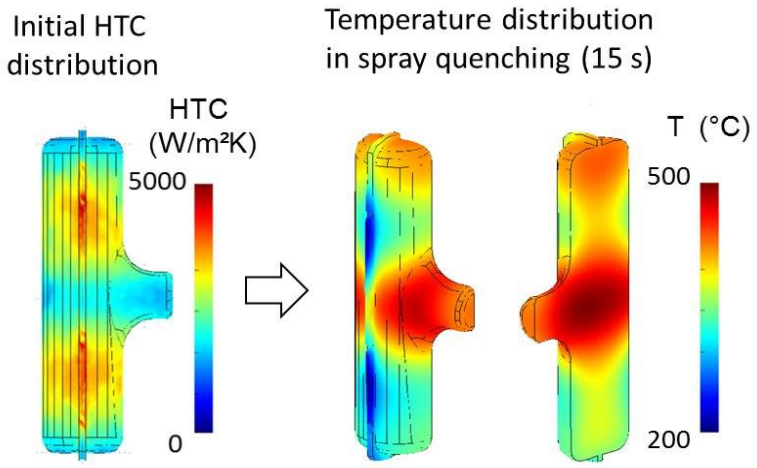

***Figure 5-20**: Quenching configuration for the common rail surrounded by a ring-sensor with simulation results of the HTC (left) and temperature (right) after 15 seconds of spray quenching*

[Test chamber, simulated, $\dot{V}$ = 4 L/min, p = 3 bar, Re = 1 200]

The ring sensor protects the lower section of the shaft (cup) from losing its internal energy due to the rapid quenching, thus avoiding a phase transformation into martensite, in comparison with an unbalanced flow distribution.

The simulation of a slow rotation (0.25 rps) of the stepped shaft specimen under spray quenching and without the protective action of the ring sensor has demonstrated improvements in quenching homogeneity [Buc15]. However, this solution was discarded due to the additional process costs for similar results obtained using the heat relaxation inside the specimen.

The heat transfer coefficient distribution on the shaft specimen surface is shown in **Fig. 5-21** (left), increasing with time as the temperature of the surface decreases, according to the boiling phenomenon undergone by the water in case of spray-quenching.

The flat spray, oriented horizontally compared to the specimen rotational axis, allows a reduction of the rapid quenching action to the massive part of the shaft, as also seen on the HTC distribution in Fig. 5-21. The transient simulation results are shown in Fig. 5-21 (right), with the temperature distribution inside the stepped shaft after 30 s of spray quenching.

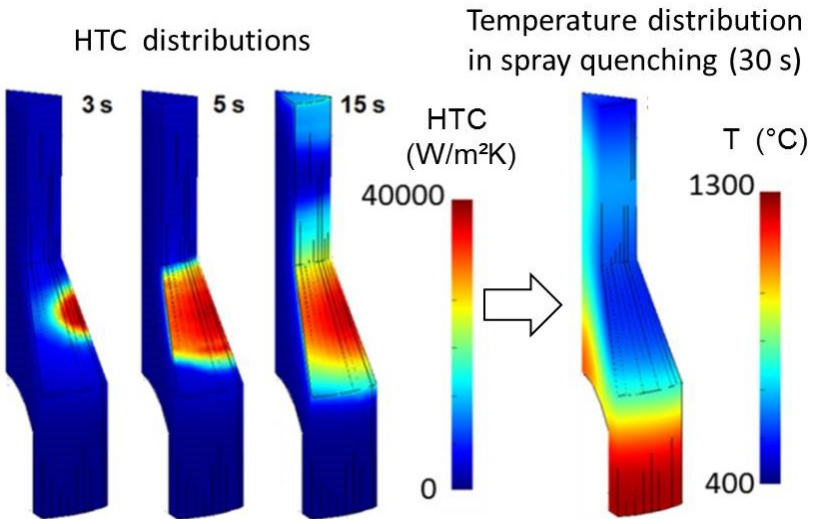

***Figure 5-21**: Selected quenching configuration for the stepped shaft surrounded by a ring-sensor with simulation results of the HTC (left) and temperature (right) at various times during spray quenching*

[Test chamber, simulated, $\dot{V}$ = 4 L/min, p = 3 bar, Re = 1 200]

The distribution is almost homogeneous inside the shaft section, whereas the cup section at t = 30 s is still warm. The effect of inner heat conduction through the specimen, occurring during the second phase of homogeneous bainitizing, leads to a smooth re-distribution of the remaining heat in the cup section into the rest of the stepped shaft.

Investigation results at the **micro scale** show that heat treatment homogenization can be improved by

- *using additional jet corrective methods*, such as ultrasound (quenching homogeneity and intensity improved by around 10%),
- or *improving the design of quench field for single specimen*, for instance by
  - fully integrating the existing process chain (sensors, process cycle, unit cell, automation), thus sparing process time and costs,
  - rotating the specimen around its symmetrical axis to tackle the high HTC gradients existing in impinging jet quenching (improved quenching homogeneity),
  - and implementing constructive flow-conditioning solution to protect thin areas from high HTCs, to lead the gas flow, or to produce turbulences (improved quenching time and homogeneity).

5.3.2 Gas flow around single gears

5.3.2.1 Flow structure around bevel gears

Bevel gears are assimilated to shafts with a pinion head which has a strong influence on the incoming gas flow. The measured distribution of the gas velocity around a single bevel gear streamed along is seen in **Fig. 5-22** with two directions of the flow, either from the tail or from the head side of the gear. The recirculation zone observed near the head side is indeed larger when the gas streams from the head side, compared to the shaft side. Geometry irregularities, such as variations in the shaft diameter, produce a decrease in velocity due to small recirculation zones, as also observed in Fig. 5-22.

The influence of the streaming velocity on the heat transfer of the bevel gear is presented in **Fig. 5-23**. The negative influence of the larger recirculation zone is observed through the lower heat transfer coefficient measured behind the streamed head of the bevel gear in Fig. 5-23 (left). The range of heat transfer coefficients along the bevel gear increases with the streaming velocity in this case, as well as the standard deviation for the local values measured by the single sensors.

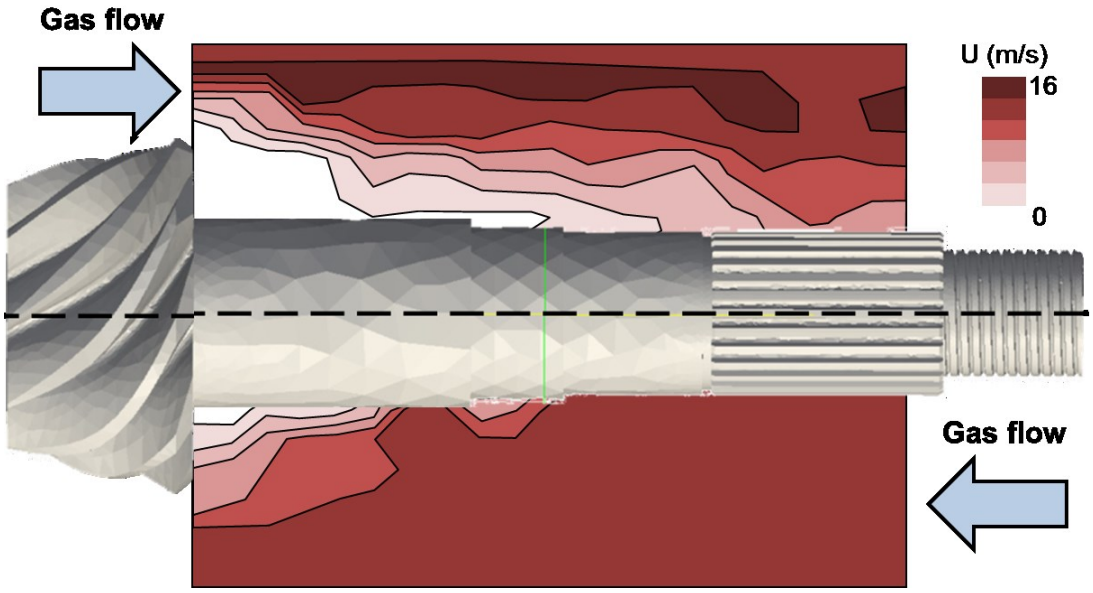

***Figure 5-22**: Velocity distributed around the bevel gear streamed from the head side (top) and the shaft side (bottom) measured by CTA*
[Wind tunnel, measured, $\bar{u}$ = 15 m/s, p = 1 bar, Re = 115 000]

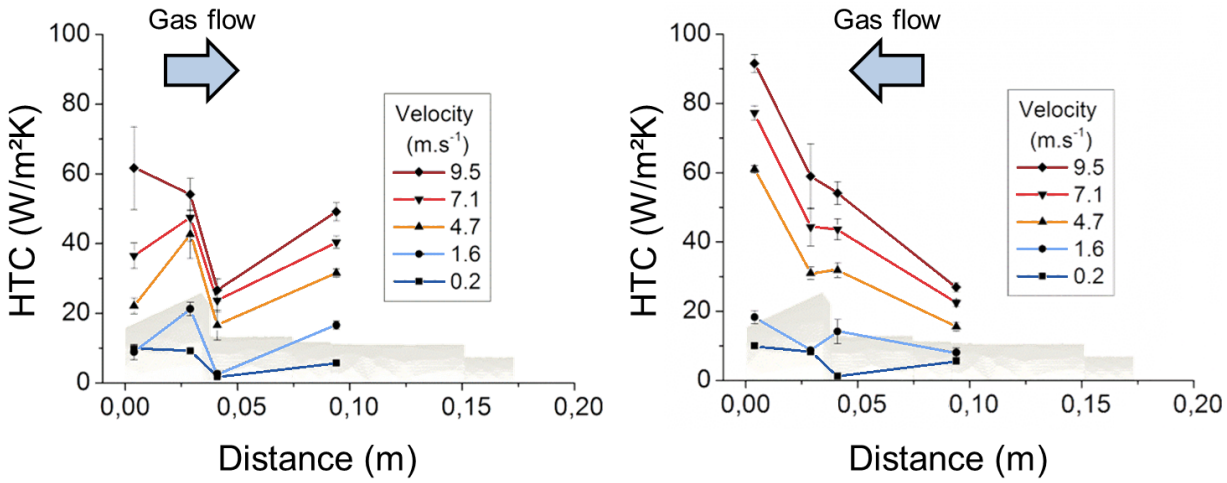

***Figure 5-23**: Influence of the axial velocity on the local heat transfer coefficient of a bevel gear streamed along from the head (left) and from the shaft (right) sides [Wind tunnel, measured, $\bar{u}$ = 15 m/s, p = 1 bar, Re = 115 000]*

The heat transfer coefficients reach their initial values after re-attachment of the recirculation zone for all the velocities considered in Fig. 5-23 (left). In the opposite streaming conditions, the local heat transfer coefficients (Fig. 5-23, right) present lower standard deviations. However, the global heat transfer coefficient increases progressively, even though a small recirculation zone takes place behind the head. Simulations proved the increase in heat transfer in this location due to the combination of medium or low velocities with high turbulent kinetic energy, produced by the bevel gear pinion geometry.

Figure 5-24 (left) demonstrates both the increase in mean heat transfer and standard deviation (vertical bars) with the velocity. However, the coefficient of variation, defined as the ratio of the standard deviation over the mean velocity, drastically decreases in the velocity range 5 to 10 m/s, stabilizing afterwards for increasing velocity, as the standard deviation increases slower than the related velocity.

Figure 5-24 (right) summarizes the local variation of heat transfer coefficient along a bevel gear streamed from the left/head side at increasing velocity. The local effect of the gas velocity is found in the increase in inhomogeneity of the heat transfer coefficient distribution, as shown in Fig. 5-24, reaching its local maximum at the front of the bevel gear, which is also the separation point of the recirculation zone.

The reattachment of this zone only occurs behind the head of the bevel gear, as the velocity domains show in Fig. 5-22, along its smaller-diameter shaft. As well, this reattachment point is velocity-dependent as also found by [Wib05].

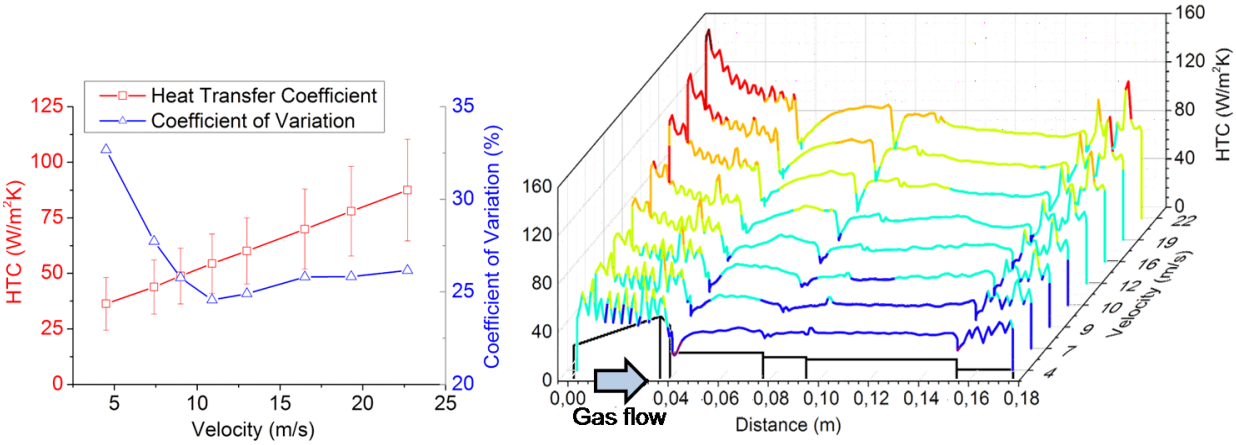

***Figure 5-24**: Mean heat transfer coefficient, standard deviation and coefficient of variation of the local heat transfer (left), and gas velocity related local heat transfer coefficient along the full-modeled bevel gear geometry featuring the simulation (right) [Wind tunnel, measured, $\bar{u}$ = 4-22 m/s, p = 1 bar, Re = 170 000]*

5.3.2.2 Flow structure around helical gears

Figure 5-25 presents some streamlines and the velocity magnitude around a helical gear, with a heat transfer coefficient distribution at its surface. Large recirculations are taking place behind the impinged surface, whereas smaller recirculations occur on the teeth surface, where the flow is producing a more intensive heat transfer, reaching approximately a third of the tooth length.

When considering the teeth of gears streamed from the disc surface, they suffer from the development of an early recirculation zone, shown by the simulation in Fig. 5-25 (left), where the heat transfer coefficient, exposed to the incoming flow in the front tooth, decreases dramatically along the axis to the back to stabilize to lower values in the range of 50 W/(m²K). Such recirculation zones have also been observed in the work of [Pel05], involving high-pressure gas quenching with Helium (20 bar) of a single gear.

5.3.2.3 Flow conditioning around helical gears

Simulations have been performed for a single helical gear in various flow configurations involving flow conditioners (cylindrical flow ducts) around the specimen [Buc14b]. The flow ducts are intended to focus the flow around the gear, as to prevent the radial spreading of the flow during impingement on the gear front side.

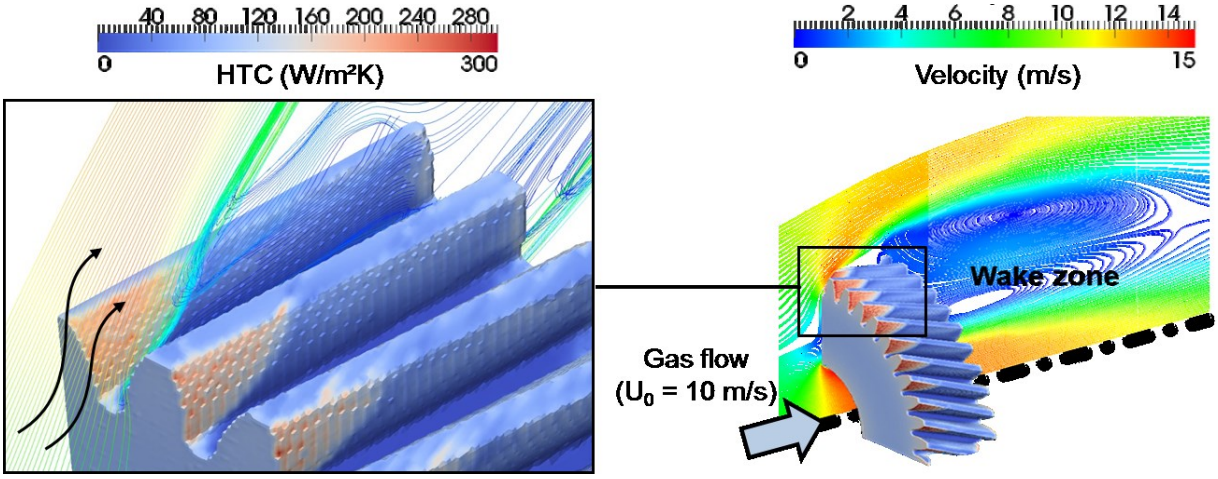

***Figure 5-25**: Streamlines and velocity magnitude around a helical gear with heat transfer coefficient distribution at its surface*
[Wind tunnel, simulated, $\bar{u}$ = 10 m/s, p = 1 bar, Re = 75 000]

The influence of the flow duct diameter on the local heat transfer at four key positions of the helical gear is investigated, as seen in **Fig. 5-26** for a ratio *e/L = 1* (gear thickness over flow duct length). The top surface (disc front) and the bottom surface of the gear (disc rear), as well as the streamed surface (tooth front), and the reverse side of the tooth (tooth rear) are investigated in detail.

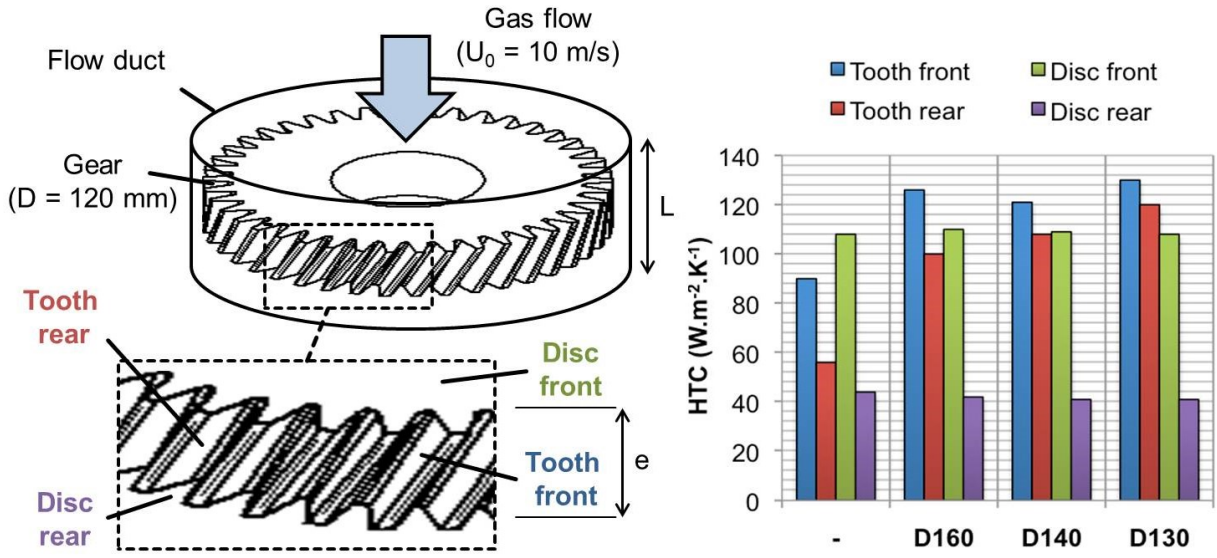

***Figure 5-26**: Computed average heat transfer coefficient at specific locations of the gear for various flow-duct diameters (from 130 to 160 mm) with e/L = 1*
[Wind tunnel, simulated, $\bar{u}$ = 10 m/s, p = 1 bar, Re = 75 000]

The intensity and the uniformity of the heat transfer coefficient distribution, over those surfaces, play a major role on the achieved quality of the workpiece during the heat treatment process. The gas flow within heat transfer simulations have been computed, involving configurations of flow ducts (diameter from 130 to 160 mm) around single helical gears (diameter 120 mm), as summarized in Fig. 5-26 under the various mentioned configurations: without flow duct, with a 160 mm-diameter cylindrical flow duct, then varying the diameter to 140 mm and 130 mm, around the 120 mm-diameter helical gear. The height of the cylindrical flow duct has been kept constant, equal to the gear height ($e/L = 1$).

Both the mean heat transfer coefficient and the coefficient of variation have been evaluated at four locations of the helical gear. Introducing a flow duct, and reducing its diameter, decreases the size and the intensity of the recirculation zone, observed e.g. in Fig. 5-25. The velocity is increasing and more uniformly distributed in the tooth area. In Fig. 5-26, the effect of flow uniformization and intensification correlate positively with an improved heat transfer.

The introduction of flow ducts intensifies the heat transfer, except for the rear surface of the gear, with the smallest duct diameter obtaining the best improvement. The homogeneity of the heat transfer distribution (low coefficient of variation) is found to reach its maximum for the 130 mm-diameter cylinder.

In the flow ducts investigation at batch level, the 140 mm-diameter cylinder was used as a compromise between high and homogeneous heat transfer coefficient distribution for the investigated regions of the gear.

Local heat transfer coefficient have been computed along the helical gear tooth, at both impinged and rear sides for the various flow-duct configurations, to evaluate the influence of a reduction of the free room available for the streaming gas flow. The section of the tooth exposed to the impinging flow is quenched more intensively and homogeneously with the reduction of the cylinder diameter, as described in **Fig. 5-27**. The area undergoing the recirculation in Fig. 5-27, characterized by higher heat transfer, is expanding as the flow duct diameter reduces. The use of a flow duct influences positively the heat transfer on the rear side of the tooth, as seen in Fig. 5-27. Reducing the flow duct diameter enlarge the peak in heat transfer coefficient situated at the front side of the tooth, while intensifying the heat transfer along the tooth.

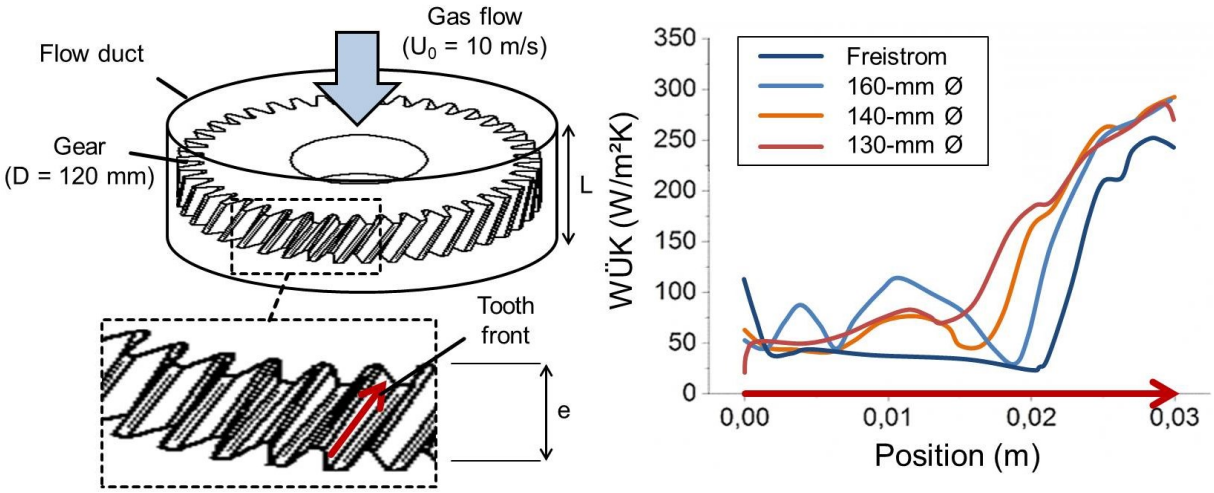

***Figure 5-27**: Computed local heat transfer coefficient distributed along the gear tooth at the impinged side for various flow-duct diameters (from 130 to 160 mm) with e/L = 1 [Wind tunnel, simulated, $\bar{u}$ = 10 m/s, p = 1 bar, Re = 75 000]*

Complex specimen geometries in gas quenching produce high variations of the heat transfer coefficient due to flow disturbances, either caused by the combination of high velocity + high turbulence (high increase in HTC), or by the combination of low velocity + high turbulence (lower increase in HTC).

Homogeneity and intensity in heat transfer of single gear specimens at the **micro scale** can be improved by

- *fitting the gas pressure and velocity* to the quenching unit and quenched workpiece (to reduce macroscopic flow irregularities through the quenching unit),
- *varying flow directions and velocity*, according to the specimen geometry (using flexible reversing flow techniques),
- or *adapting external flow conditioning elements to single specimen*, such as cylindrical ducts, to locally focus the gas flow (providing large improvements of the quenching intensity and homogeneity in the teeth region).

5.3.3 Process-integrated stepped quenching

5.3.3.1 Heat treatment from the forging heat

The process cell described in Chapter 5.3.1.2 (Fig. 5-19, right) has been operated to perform integrated heat treatment of forged components under various process parameters (austenizing temperature and time, quenching technique -*spray or gas jet*-, intensity and time). The heat treated components have been evaluated using hardness measurement and microstructure observation (light microscopy and scanning-electron microscopy). The central section of a stepped shaft after gas and spray quenching is seen in **Fig. 5-28**, with the results of microstructure observation using light (left), and scanning-electron microscopy (right). As an example, the images of the specimen (Fig. 5-28, Core or *hot-spot* and Surface or *cold-spot*), present the characteristic, needle-like phase arrangement of a bainitic microstructure, both with high similarities.

Comparable experiments and analyses have been performed for various steel grades and specimen geometries [Buc15], as listed in **Tab. 5-2** for the common-rail, and **Tab. 5-3** for the stepped shaft. Tab. 5-2 presents the results of various quenching scenarios performed in a 4-nozzle field (2 x 2-arrangement, no rotation) for the common-rail specimen. The hardness Vickers values (HV30) at key positions in the central section of the specimen are evaluated for the analysis of the homogeneity of the resulting microstructure after quenching.

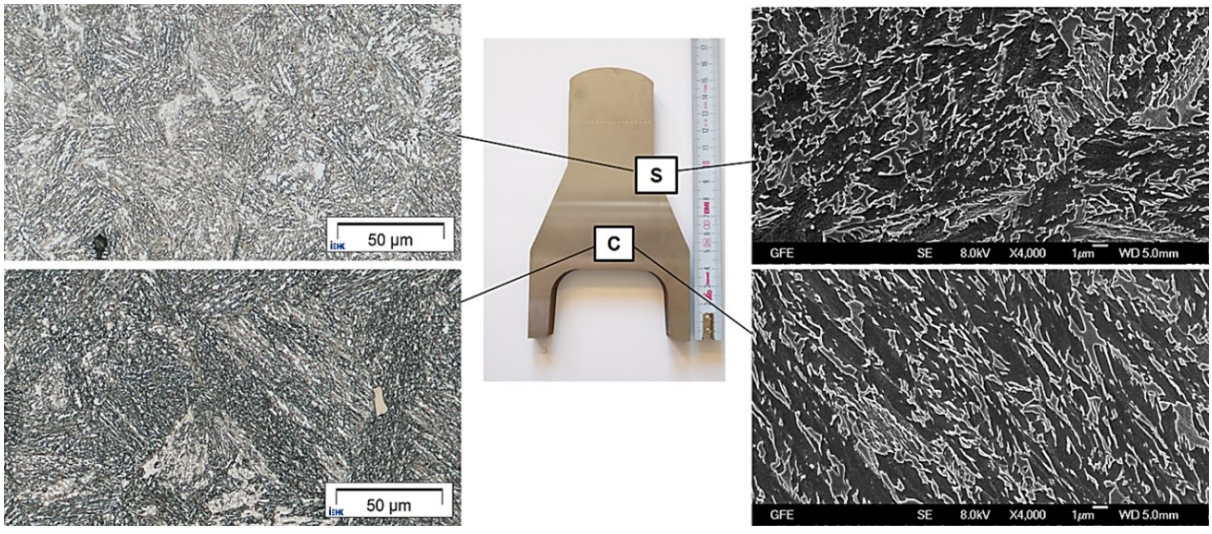

***Figure 5-28**: Micrographs using light microscopy (left) and scanning electron microscopy (right) at two positions (core C, and surface S) of the shaft after gas and spray quenching*

***Table 5-2**: Various quenching scenarios (spray-field arrangement and heat transfer coefficient profile) and results (HV30-hardness and microstructure quality at two locations of the specimen) for the common-rail of various steel grades*

Material	Quenching scenario	Hardness (HV30)	Microstructure
AFP	HTC *AFP1* Free conv. 10 t	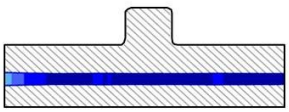	**Top/Bot./Mid.:** homogeneous, F/P
AFP	HTC *AFP3* Spray 8.000 300 10 Air p. Free conv. t 15s 40s	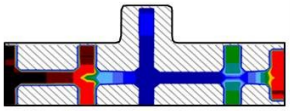	**Top/Bot.:** heterogeneous, Ma/B **Mid.:** homogeneous, F/P
HDB	HTC *HDB1* Air p. 300 10 Free conv. t 60s	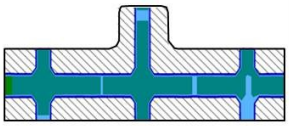	**Top/Bot./Mid.:** homogeneous, bainite
HDB	HTC *HDB3* Air p. 300 10 Free conv. t 100s	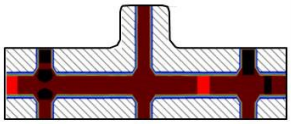	**Top/Bot./Mid.:** homogeneous, Ma/B

***Table 5-3**: Various quenching scenarios (spray-field arrangement and heat transfer coefficient profile) and results (HV30-hardness and microstructure quality at two locations of the specimen) for the stepped shaft of HDB steel grade*

Material	Quenching scenario	Hardness (HV30)	Microstructure
HDB	HTC *HDB1* Air p. 250 10 Free conv. t 100s	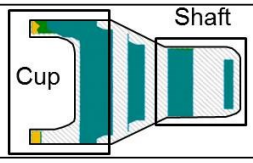	**Cup:** heterogeneous,Ma/B **Shaft:** homogeneous, bainite
HDB	HTC *HDB3* Spray 8.000 300 10 Air p. Free conv. t 25s 2min	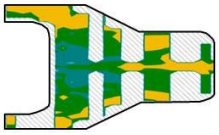	**Cup:** heterogeneous,Ma/B **Shaft:** heterogeneous,Ma/B
HDB	HTC *HDB4* Spray 8.000 300 10 Air p. Free c. Air p. t 22s 2min 20min	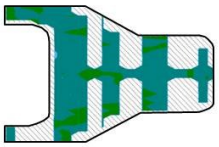	**Cup/Shaft:** homogeneous, bainite
HDB	HTC *HDB5* Spray 8.000 300 10 Air p. Free conv. t 22s 2min	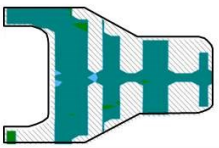	**Cup/Shaft:** homogeneous, bainite

The scale, seen in Tab. 5-2 (right), defines the targeted bainitic microstructure colored in green. Harder and softer microstructures (martensite and ferrite/perlite) are represented in red/black and blue, respectively. Whereas free convection and spray-quenching provide either a too weak, or too strong quenching for the small forged specimen, the pressured-air arrangement, using four nozzles around the specimen, succeeds in providing a homogenous bainitic microstructure, where the optimal quenching process time remains in a 60 to 80 s range, as seen in Tab. 5-2.

A 4-step quenching process applied to the stepped shaft, with successively spray-quenching, pressurized air, free convection, and a final pressured-air phase, succeeds in bainitizing homogeneously the massive specimen, as seen in Tab. 5-3, hence obtaining improved mechanical properties from the integrated quenching in the forging process-chain.

Whereas the first scenario in Tab. 5-3 (top) succeeds in bainitizing most of the stepped shaft specimen strictly with a gas-quenching-based, 8-nozzle configuration (seen in Chapter 3.3.2), the cup section undergoes a strong martensitic transformation, as revealed by both hardness and microscopy tests. As detailed previously in Fig. 5-21, the ring-sensor provides a positive, shield effect to the cup section of the stepped shaft, which is seen on the rest of the quenching scenario described in Tab. 5-3.

Quenching the specimen using spray, as in the second scenario presented in Tab. 5-3, produces higher, instable heat transfer coefficients past the Leidenfrost point due to the boiling phenomenon, occurring onto the surface of the specimen. A too long period of spray-quenching leads to the formation of martensitic microstructures at the surface of the specimen (martensite shell). The reduction of the spray-quenching duration, from 25 to 22 s, as seen in the scenario 2 and 3 in Tab. 5-3, provides better results for the production of a homogeneous bainitic microstructure into the stepped shaft specimen. Concerning the third quenching scenario described in Tab. 5-3, the trace of ferritic/pearlitic microstructure into the core of the stepped shaft has been reduced after performing a final gas-quenching step, seen in Tab. 5-3 (bottom).

The 4-step quenching scenario, seen at the bottom of Tab. 5-3, consists of an initial spray-quenching from the forging heat for 22 seconds, followed by a first relaxation using gas-quenching, and a second, stronger heat relaxation, using free convection. A final gas-quenching phase offers slight improvements of the final microstructure quality, as seen in the final hardness distribution of the stepped shaft.

Tested strategies for the batch production of forged specimens are shown in **Fig. 5-29**, for the two specimen geometries under investigation (common rail and stepped shaft) covering three steel grades (AFP for precipitation hardening ferritic-pearlitic, HDB for high-strength ductile bainite, and CHS or 18CrNiMo7-6 for case-hardening steels) and various quenching strategies. Mean and standard deviation of the Vickers Hardness (HV30) distribution evaluate the potential of producing a homogeneous bainite microstructure.

For the common rail specimen, spray-quenching produces hardness values in the bainite range for the AFP steel grade. The global heterogeneity of the microstructure, varying from ferritic/pearlitic to martensitic ranges, discards its application for small specimens with this steel grade. The final production has been carried out using single free convection in the case of AFP-steel common rails, to ensure satisfying microstructure homogeneity. Higher process potentials are found for the common rail from HDB steel grades, as seen in Fig. 5-29 (left). Gas quenching provides this specific steel grade a high homogeneity (<10%), with hardness values within the range of bainite. Increasing the quenching duration leads to an increase in mean hardness and standard deviation. Concerning the stepped shaft specimen, the larger volume, in comparison to the common rail, provides a better process-control for steel grades including late-starting bainite domains.

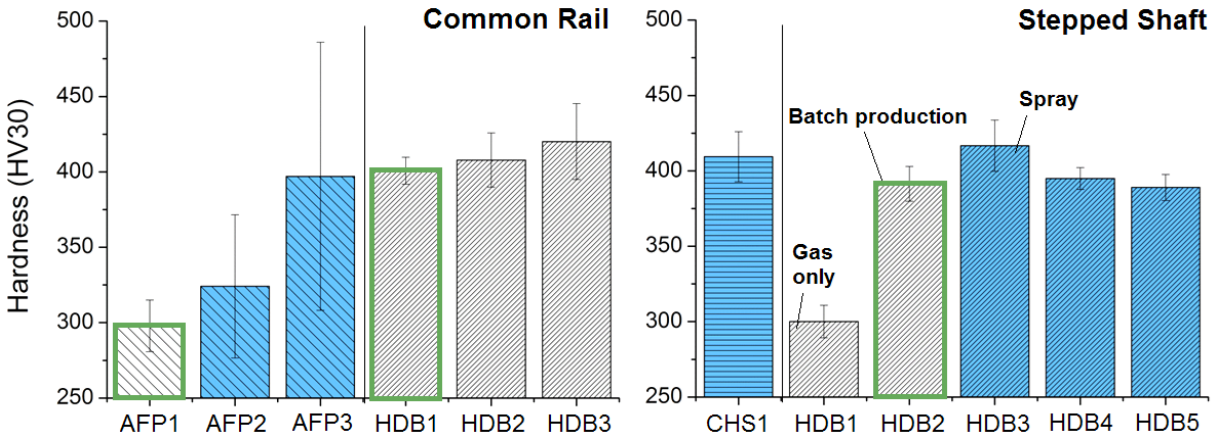

***Figure 5-29**: Mean surface hardness measured for various quenching scenarios (gas-only in gray, spray in blue) involving the three steel grades and the two investigated specimen (common rail, left and stepped shaft, right).*

Whereas AFP steel grades could not be homogeneously bainitized for this size of specimen, due to the high Biot number, case-hardening and HDB steels, as seen in Fig. 5-29 (right), demonstrate high bainitizing potentials with HV values in the bainite range. The size of the specimen leads to large heat relaxation phases, thus providing a high microstructure homogeneity, as seen in the standard deviations exhibited in Fig. 5-29 (right), so that spray quenching can be operated with better results than with gas-quenching only, or in comparison to smaller-sized specimens.

5.3.3.2 Heat treatment during machining

As investigated in [Ego14], machining at elevated specimen temperatures (*hot-machining*) and heat treatment exhibit a combination potential. In-situ bainitizing during machining has been tested for a stepped shaft specimens of HDB-steel. The integrated gas quenching field, as presented in Fig. 5-19, is adapted to perform the quenching strategy presented in **Fig. 5-30** (left), consisting of a quenching from the austenized state (45 min at 950 °C) to lower the specimen surface temperature to 400 °C, before the bainite nose. A specimen surface temperature of around 400 °C has been found to be optimal to perform hot-machining on a bainite microstructure [Ego14]. The temperature of the specimen surface has been monitored using thermal camera during the process.

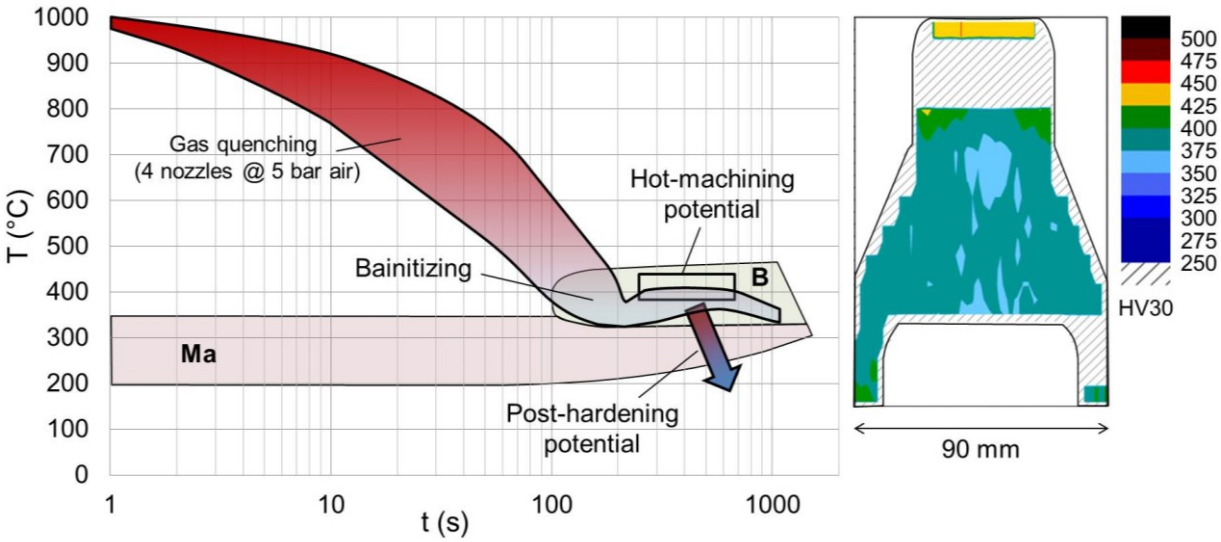

***Figure 5-30**: Gas quenching strategy of a hot machined, then bainitized stepped shaft (left), with resulting hardness distribution (right)*

The process window displayed in Fig. 5-30 (left) offers around 300 seconds to machine the shaft along the cup area, later on to continue the heat treatment by isothermally bainitizing the rest of the specimen. Additional heat treatment steps are possible, such as the shell-hardening of the machined surface of the shaft by quenching the specimen using gas quenching in a final step.
The hardness of the resulting heat treatment is represented in Fig. 5-30 (right), via the Vickers hardness (HV30) distribution, demonstrating the effectivity of homogeneous bainitizing in most of the stepped shaft. The cup area, sensible to martensite transformation, has been preserved from severe quenching effects, also during the machining. The top of the shaft has undergone a martensite transformation, due to the cold contact of the specimen-holder in the turning machine, which could not be avoided, due to constructive restrictions of the experimental setup.

The quenching process of single specimens (**micro scale**) is improved by the use of temporally and spatially controlled gas and spray quenching, integrated into the manufacturing process as demonstrated in

- *triggering the heat treatment directly from the forging heat*,
  - effectively adapting the quenching apparatus to various specimen geometries,
  - successfully adapting the quenching steps to the variety of materials (especially in the case of homogeneous bainitizing),
- and *carrying out the heat treatment during machining by*,
  - integrating the quenching apparatus to the turning machine for single specimen (lean manufacturing),
  - spatially (adapted nozzle field), and temporally (specimen rotation, stepped quenching) controlling the heat transfer,
  - successfully bainitizing the specimen during the turning process.

6 Conclusions

6.1 Summary and concluding remarks

Improvements in the spatial and temporal control of the quenching process, over the three process scales (macro, meso, and micro) are necessary to accelerate the adoption of gas and spray quenching as a cost-effective, heat treatment process for the manufacturing of gear components from high-performance steel alloys.

Macro-level: flow in top-to-bottom quenching units

Top-to-bottom gas quenching units, conventionally used for gears heat treatment, exhibit specific flow characteristics related to the chamber geometry, with a large influence of the gas-recycling technology (e.g., heat exchanger). The flow distribution, progressively homogenizing throughout the sub-levels of the quenching chamber, can be improved using flow conditioning techniques, modifying the form of the heat exchanger or the chamber itself, or using flow conditioners, as e.g. perforated plates above the batch, whose geometry (hole diameter, distribution, and overall porosity) provides an effective flow control in reduced chamber dimensions.

Meso-level: structure of the batch

During heat treatment gas quenching, batches consisting of multiple layer of gears undergo complex heat transfer mechanisms, whose homogeneity and intensity are improved by setting an offset of the sub-layers of the batch, as well as enclosing the specimen in cylindrical flow guidance solutions, intensifying the gas flow close to the specimen surface. In single-layered batch of gears, providing a minimal room between specimens lessens the mutual interaction between the neighboring specimens over the gas flow, thus improving the spatial control of the quenching process.

Micro-level: flow control for single specimen

Single specimens are subject to quenching heterogeneity due to the local gas flow disturbances. Homogeneity and intensity in heat transfer of single specimens can be improved by adapting external flow conditioning elements to the specimen, such as cylindrical ducts, to focus and locally intensify the gas flow.

Besides spatial quenching control, gas quenching control over the time can be operated by varying the flow directions and velocity, according to the specimen geometry, as well as using impinging jets with corrective methods (such as ultrasound), or a quenching field integrated into a lean process chain (sensors, process cycle, unit cell, automation).

6.2 Perspectives of heat treatment gas quenching

Simulation tools for the virtualization of quenching processes

Simulation tools demonstrated their capacity to provide relevant results to diagnose quenching processes (gas and spray), and provide technical improvements for industrial quenching applications. The potential of intuitive open-source solutions for CFD and heat transfer simulations gives attractive perspectives to the industry.

Process-integration of gas quenching in modern manufacturing processes

The successful integration of heat treatment gas quenching in an automated lean manufacturing production line, for forging and machining, demonstrates its great potential for on-demand production, process automation and time reduction, as well as energy cost saving solutions.

With an improved spatial and temporal control of the heat treatment process, gas and spray quenching offers the requested process flexibility, parametering, and monitoring, as well as safety and environmental compliance to embrace the values of the *Industry 4.0* world.

Flow-conditioning limits in heat treatment gas quenching

Several micro- (e.g., using individual flow conditioners) to macro-solutions (e.g., on the gas-recycling solutions) were evaluated and tested with positive results. However the geometry of the quenched specimen largely influences the local flow uniformity, hence the heat transfer. Gas quenching, besides being limited by the material and size of the specimen, is limited to specific shapes depending on the direction, intensity, and conditioning of the gas flow.

Gas quenching as heat treatment solution for tomorrow

Whereas gas quenching offers the requirements of a green, cost-saving, and safe solution for the future of heat treatment process, its drawbacks, namely the limitation induced by the material and size of heat treated specimens, still remain a challenge for the manufacturing industry.

Developments are carried out to develop both the cooling homogeneity in the current gas quenching techniques (at micro-, meso-, and macro-scale), and improve the metal alloys to comply with the gas quenching limitations. Further research for compatible steels and various alloys are therefore necessary to extend the application fields of heat treatment gas quenching.

7 List of publications and supervised works

7.1 List of publications

Reviewed papers

- Bucquet T., Hoja T., Waldeck S., Sander S., Fritsching U.; “Process-integrated gas- and spray-quenching for high-strength ductile forged components“, International Journal of Material Forming (2017), DOI: 10.1007/s12289-016-1336-1
- Bucquet T., Fritsching U.; “Flow conditioning in heat treatment gas quenching“, International Journal of Microstructure and Materials Properties 11.3/4 (2016), pp. 262-276, DOI: 10.1504/IJMMP.2016.079151
- Bruchwald O., Frackowiak W., Bucquet T., Huskic A., Reimche W., Maier H. J.; “In-situ-Erfassung der Werkstoffumwandlung und Gefügeausbildung von Schmiedebauteilen im Abkühlpfad“, HTM J. Heat Treatm. Mat. 70 (2015) 3, pp. 150-161, DOI: 10.3139/105.110259
- Bucquet T., Fritsching U.; “Flow Optimization to Enhance Gas Quenching Efficiency for Helical Gears Specimen“, Modeling and Numerical Simulation of Material Science 4 (2014) 4, pp. 143-152
- Fischer M., Dickert H. H., Bleck W., Huskic A., Kazhai M., Hadifi T., Bouguecha A., Behrens B.-A., Labanova N., Felde A., Liewald M., Egorov F., Garbrecht M., Brinksmeier E., Reimche W., Bruchwald O., Frackowiak W., Maier H. J., Bucquet T., Hinrichs B., Fritsching U., Hoja T., Hoffmann F., Zoch H.-W.; “Ecoforge: Energieeffiziente Prozesskette von Hochleistungs-Schmiedebauteilen am Beispiel eines hochfesten, duktilen bainitischen (HDB) Stahls“, HTM J. Heat Treatm. Mat. 69 (2014) 4, pp. 209-219
- Bucquet T., Fritsching U.; “Evaluating Heat Transfer Conditions in Gas Cooling for Complex Specimen Geometries“, HTM J. Heat Treatm. Mat. 69 (2014) 3, pp. 148-154, DOI: 10.3139/105.110222
- Bucquet T., Fritsching U.; “Flow Optimization of Gas Quenching Processes Using Perforated Plates“, ASTM International, Special Issue on Materials Performance and Characterization 3.4 (2014), DOI: 10.1520/MPC20130099

Other papers

- Fritsching U., Bucquet T.; “Forger dans la chaude : le projet Ecoforge“, La forge 59.1 (January 2015), pp. 34-38
- Bucquet T., Fritsching U., Fischer M., Dickert H. H., Bleck W., Huskic A., Kazhai, M.; Hadifi, T.; Bouguecha, A.; Behrens, B.-A.; Labanova, N.; Felde, A.; Liewald M., Egorov F., Garbrecht M., Brinksmeier E., Reimche W., Bruchwald O., Frackowiak W., Maier H. J., Hoja T., Hoffmann F., Zoch H.-W.; “Ecoforge: Energieeffiziente Prozesskette von Hochleistungs-Schmiedebauteilen“, Schmiede-Journal (September 2014), Deutsche Massivumformung, pp. 22-27

Conferences

- Bucquet T., Gulpak M., Wagner A., Fritsching U.; “High-Strength Steel Bainitizing using Controlled In-Situ Gas Quenching within Machining Processes“ (Heat Treat 2015, Detroit, MI) 28th ASM Heat Treating Conference and Exposition and Gear Expo, 20.10-22.10.2015, Cobo Center, Detroit, USA
- Bucquet T., Fritsching U.; “Flow Conditioning in Heat Treatment Gas Quenching“ (IDE2015, Bremen), 5th International Conference on Distortion Engineering, 23.09-25.09.2015, Bremen
- Bucquet T., Fritsching U.; “Gas Quenching for Complex Geometries“, 11. Internationale Fachmesse und Symposium für Thermoprozesstechnik (THERMPROCESS 2015 16.06-20.06.2015, Düsseldorf, DE)
- Bucquet T., Fritsching U.; “Heat Treatment Strategies in the Hot Forging Process Chain“ (NEMU2015, Fellbach), International Conference “New Developments in Forging Technology”, 04.05-06.05.2015, Fellbach
- Bucquet T., Fritsching U.; “Ultrasound Application for the Improvement of Gas Cooling Processes“, Jahrestreffen der Fachgruppen Trocknungstechnik und Wärme- und Stoffübertragung, 04.03-06.03.2015, Leipzig
- Bucquet T., Sander S., Fritsching U.; “Characterization of Spray Nozzles for Quenching of Metal Components“ (ILASS2014, Bremen), 26th European Conference on Liquid Atomization & Spray Systems, 08.09-10.09.2014, Bremen
- Bucquet T., Fritsching U.; “Spray-Quenching for Process-Integrated Heat Treatment of Construction Components“ (FEDSM2014, Chicago), 4th Joint US-European Fluids Engineering Summer Meeting, 03.08-07.08.2014, Chicago
- Fritsching U., Bucquet T.; “Resource-Efficient Process Chains for High-Performance Steel Components“ (IFC2014, 30.07.2014, Berlin)
- Bucquet T., Fritsching U.; “Kontrollierte Abkühlung von Bauteilen aus der Schmiedewärme“, 4th International Conference on Steel in Cars and Trucks (SCT2014, 15.06-19.06.2014, Braunschweig)
- Bucquet T., Fritsching U.; “Adaptive Spray-Quenching for Process Integrated Heat Treatment of High-Performance Forged Components“ (IFHTSE2014, 13.05.2014, München), Proceedings of the 21st IFHTSE Congress, 12.05-15.05.2014, Munich
- Fritsching U., Bucquet T., Fischer M., Dickert H. H., Bleck W., Huskic A., Kazhai M., Hadifi T., Bouguecha A., Behrens B.-A., Labanova N., Felde A., Liewald M., Egorov F., Garbrecht M., Brinksmeier E., Reimche W., Bruchwald O., Frackowiak W., Maier H. J., Hoja T., Hoffmann F., Zoch H.-W.; “EcoForge – Resource-efficient process chains for highperformance steel components“ (UKH2014, 27.02.2014, Hannover), Proceedings des 21. Umformtechnischen Kolloquium Hannover 2014, pp. 245-264
- Bucquet T., Fritsching U.; “Kontrollierte Abkühlung von Bauteilen aus der Schmiedewärme“, Umformtechnisches Kolloquium Hannover 2014 (UKH2014, 27.02.2014, Hannover)

- Bucquet T.; “Ultraschallunterstütze Gasabschrecken“, FA16 „Energieeffizienz“, 19.11.13, GTD Graphit Technologie GmbH, Langgöns
- Fischer M., Dickert H. H., Bleck W., Huskic A., Kazhai M., Hadifi T., Bouguecha A., Behrens B.-A., Labanova N., Felde A., Liewald M., Egorov F., Garbrecht M., Brinksmeier E., Reimche W., Bruchwald O., Frackowiak W., Maier H. J., Bucquet T., Hinrichs B., Fritsching U., Hoja T., Hoffmann F., Zoch H.-W.; “Ecoforge: Energieeffiziente Prozesskette von Hochleistungs-Schmiedebauteilen am Beispiel eines hochfesten, duktilen bainitischen (HDB) Stahls“ (HK 2013, 10.10.2013, Wiesbaden)
- Bucquet T.; “Steigerung der Energieeffizienz in der Gasabschreckung“, FA16 „Energieeffizienz“, 04.06.13, WS Wärmeprozesstechnik GmbH, Renningen
- Liewald M., Fritsching U., Hajyheydari E.; “EcoForge – Ressourceneffiziente Prozessketten für Hochleistungsbauteile; Ein Leittechnologieprojekt der AIF - Stand und Perspektiven“, Proc. Int. Conf. New Developments in Forging Technology, June 4-5, 2013, Stuttgart
- Fritsching U., Bucquet T., Beneke F.; “Energie- und Ressourceneffizienz in der Wärmebehandlung und Thermoprozesstechnik“, AWT-VDMA Seminar Energieeffizienz, 13+14-6-2012, Bremen, URN: nbn-resolving.de/urn:nbn:de:gbv:46-00102705-14

7.2 Supervised student works

The present thesis contains results from the following supervised student works:

Diplomarbeit/Master's Thesis

- Tell, J.; "Entwicklung eines Strömungsmesssystemes zur Qualifizierung von Gasabschreckprozessen", Diplomarbeit, Universität Bremen, 2011

Bachelor's Thesis

- Jabbour Monreal, B.; "Characterization of a Two-Fluid Flat-Spray Nozzle for Quenching Purpose", Universität Bremen/Escola Politécnica da USP, 2014
- Cimorelli Lima, A.; "Measurement of Local and Integral Heat Transfer for Cylinders in Transverse and Horizontal Flows", Universität Bremen/Escola Politécnica da USP, 2013
- Poulet, G.; "Development of an Automated System for Flow Qualification", Universität Bremen/Ecole des Mines de Douai, 2012

8 Bibliography

[Afa12] Afazov S. M., Becker A. A., Hyde T. H.; “Development of a finite element data exchange system for chain simulation of manufacturing processes”, Advances in Engineering Software, 2012, 47.1, pp. 104-113

[Alt91] Altena H.; “Wärmebehandlung von Schnellarbeitsstahl-Werkzeugen in Vakuumanlagen“, HTM Härtereitechnische Mitteilungen, 1991, 46.3, pp. 173-176

[Alt98] Altena H.; “Niederdruck-Aufkohlung mit Hochdruck-Gasabschreckung“, HTM Härtereitechnische Mitteilungen, 1998, 53.2, pp. 93-101

[Alt00] Altena H.; Stolar, P.; Jurci, P.; Klima, F.; Pavlu, J.; Schmidt, G.; Lübben, T.; Hock, S.; Reese, U.; Liedtke, D.; Dengel, D.; “Einfluss der Abschreckparameter auf die Mass- und Formänderung von Zahnrädern bei Gas- und Ölabschreckung. Diskussion.“, HTM Härtereitechnische Mitteilungen, 2000, 55.5, pp. 312-324

[Alt02] Altena, H., Schrank E.; “Niederdruck-Aufkohlung mit Hochdruck-Gasabschreckung: Grundlagen, Einsatzmöglichkeiten und Anlagentechnik“, HTM Härtereitechnische Mitteilungen, 2002, 57.4, pp. 247-256

[Alt04] Altena H., Schrank F.; “Low pressure carburizing with high pressure gas quenching”, Gear Technology, 2004, 21.2, pp. 27-32

[Alt05] Altena H., Schrank F., Jasienski W.; “Reduzierung der Formänderung von Getriebeteilen in Gasaufkohlungs-Durchstoßanlagen durch Hochdruck-Gasabschreckung“, HTM Härtereitechnische Mitteilungen, 2005, 60.1, pp. 43-51

[Alt06] Altena H., Schobesberger P., Schrank F.; “Advanced gas carburizing technology for the automotive industry”, Gaswärme International, 2006, 55.7

[Alt08] Altena H., Schobesberger P., Schrank F.; “Anlagen- und prozesstechnischer Vergleich von Ringherdofen und Durchstoßanlage“ HTM Härtereitechnische Mitteilungen, 2008, 63.2, pp. 65-74

[Ast12] Atraszkiewicz R., Januszewicz B., Stachurski W., Dybowski K., Rzepkowski A.; “High pressure gas quenching: Distortion analysis in gears after heat treatment”, Materials Science and Engineering: A, 2012, 558, pp. 550-557

[Bau85] Bauer R.; “Das Härten von hochwertigen Werkzeugen in modernen Vakuumanlagen mit Überdruck-Gasabkühlung“ HTM Härtereitechnische Mitteilungen, 1985, 40, pp. 25-34

[Bea04] Beauchesne D., Goldsteinas A.; “Quenching after vacuum carburizing”, Heat Treating Progress, Sept./Oct. 2004, pp. 41-46

[Beh12] Behrens B. A., Bach F. W., Bouguecha A., Nürnberger F., Schaper M., Yu Z., Klassen A.; “Numerische Berechnung einer integrierten Wärmebehandlung für präzisionsgeschmiedete Bauteile, HTM Journal of Heat Treatment and Materials, 2012, 67.5, pp. 337-343

[Beh14] Behrens B. A., Huskic A., Kazhai M.; “Experimentelle und numerische Untersuchungen zur kontrollierten Wärmebehandlung von hochbeanspruchten Stahlschmiedebauteilen“, Umformtechnisches Kolloquium Hannover, Germany, 27.02.2014

[Bel10] Belinato G., Canale L. C. F., Totten G. E.; “Chapter 13: Gas Quenching” in Quenching Theory and Technology, Taylor and Francis, 2010, pp. 445-483

[Bös07] Böswirth L.; “Technische Strömungslehre“, Vieweg-Verlag, Wiesbaden, 2007

[Bri11] Brinksmeier E., Lübben T., Fritsching U., Cui C., Rentsch R., Sölter J.; “Distortion minimization of disks for gear manufacture”, International Journal of Machine Tools and Manufacture, 2011, 51.4, pp. 331-338

[Buc14a] Bucquet T., Fritsching U.; “Evaluating Heat Transfer Conditions in Gas Cooling for Complex Specimen Geometries“, HTM J. Heat Treatm. Mat. 69 (2014) 3, pp. 148-154, DOI: 10.3139/105.110222

[Buc14b] Bucquet T., Fritsching U.; “Flow Optimization to Enhance Gas Quenching Efficiency for Helical Gears Specimen“, Modeling and Numerical Simulation of Material Science 4 (2014) 4, pp. 143-152

[Buc15] Bucquet T., Fritsching U.; “Heat Treatment Strategies in the Hot Forging Process Chain“ (NEMU2015, Fellbach), International Conference “New Developments in Forging Technology”, 04.05-06.05.2015, Fellbach

[Cal07a] Callister W. D.; “Chapter 11: Applications and Processing of Metal Alloys” in Materials Science and Engineering – An Introduction, John Wiley & Sons, 2007, pp. 358-413

[Cal07b] Callister W. D.; “Chapter 6: Mechanical Properties of Metals” in Materials Science and Engineering – An Introduction, John Wiley & Sons, 2007, pp. 131-173

[Cal07c] Callister W. D.; “Chapter 4: Imperfections in Solids” in Materials Science and Engineering – An Introduction, John Wiley & Sons, 2007, pp. 80-108

[Can10] Canale L. C. F., Totten, G. E.; “Chapter 1: Hardening of Steels” in Quenching Theory and Technology, Taylor and Francis, 2010, pp. 1-41

[Cha08] Chaffotte F., Bockel-Macal S.; “Trempe gazeuse : la réponse technique et environnementale aux exigences des opérations de trempe”, Traitement thermique, 2008, 387, pp. 29-34

[Cla09] Clausen B., Frerichs F., Kohlhoff T., Lübben T., Prinz C., Rentsch R., Sölter J., Surm H., Stöbener D., Klein D.; “Identification of process parameters affecting distortion of disks for gear manufacture-Part II: heating, carburizing, quenching“, Materialwissenschaft und Werkstofftechnik, 2009, 40.5-6, pp. 361-367

[Col96] Colucci D. W., Viskanta R.; ”Effect of nozzle geometry on local convective heat transfer to a confined impinging air jet”, Experimental Thermal and Fluid Science, 1996, 13.1, pp. 71-80

[Con93] Conybear J. G.; “High pressure gas quenching“, Advanced Materials and Processes, 1993, 143.2

[Cor13] Cordisco N.; “Maximizing Vacuum Furnace Gas Quenching Performance”, Industrial Heating, 2013, 81.3

[Cos12] Cosentino F., Gebelin J.C., Warnken N., Reed R.C.; “Multi-Scale Modelling of High-Pressure Gas Fan Quenching for Gas Turbine Applications”, 9th International Conference on CFD in the Minerals and Process Industries, Melbourne, Australia, 10-12.12.2012

[Dav05a] Davis J. R.; “Preface” in Gear Materials, Properties, and Manufacture, ASM International, 2005

[Dav05b] Davis J. R.; “Chapter 1: Basic Understanding of Gears” in Gear Materials, Properties, and Manufacture, ASM International, 2005

[Dav05c] Davis J. R.; “Chapter 3: Ferrous and Nonferrous Alloys” in Gear Materials, Properties, and Manufacture, ASM International, 2005

[DeB57] De Bray B. G.; ”Low Speed Wind Tunnel Tests on Perforated Square flat Plates Normal to the Airstream”, Technical Report of the Ministry of Supply, Aeronautical Research Council, UK, 1957

[Dei89] Deiters T. A.; Mudawar I.; “Optimization of spray quenching for aluminum extrusion, forging, or continuous casting” Journal of Heat Treating, 1989, 7.1, pp. 9-18

[Dou08] Douce J.F.; “Modélisation de la trempe gazeuse haute pression : application aux aciers de cémentation et de trempe”, Doctorat Université Nancy, 2008

[Ede97] Edenhofer B., Bouwman J. W., Peter W., Bless E., Bauer R., Heilmann P., Löser K., Kunst H.; "Erfahrungen und Ergebnisse beim Gasabschrecken in einer kalten Kammer mit und ohne Düsenfeld. Diskussion", HTM Härtereitechnische Mitteilungen, 1997, 52.3, pp. 138-144

[Ede98] Edenhofer B., Bouwman J. W.; “Ofen- und Chargeneinfluss auf die Wärmeübergangszahl bei der Gasabschreckung“ HTM Härtereitechnische Mitteilungen, 1998, 53.2, pp. 102-107

[Ego14] Egorov, F.; “Prozessintegrierte Heißzerspanung aus der Schmiedewärme“, Dissertation der Universität Bremen, Shaker-Verlag, 2014

[Ele14] Elek L., Fischer C., Melz T., Wagener R., Wirths V., Bleck W.; ”New generation of forging steels for cyclic loaded safety components with improved fatigue properties”, SAE Technical Paper No. 2014-28-0005, 2014

[Elk03] Elkatatny I., Morsi Y., Blicblau A. S., Das S., Doyle E. D.; “Numerical analysis and experimental validation of high pressure gas quenching”, International Journal of Thermal Sciences, 2003, 42.4, pp. 417-423

[Eve83] Everett K. N., Gerner A., Durston D. A.; ”Seven-hole cone probes for high angle flow measurement: Theory and calibration”, AIAA Journal, 1983, 21.7, pp. 992-998

[Fau98] Faura F., Campo A., Zamora B.; “A mixture of pure gases that produce maximum heat transfer characteristics for quenching”, Journal of Materials Engineering and Performance, 1998, 7.3, pp. 420-424

[Fer03] Ferrari J., Lior N., Slycke J.; “An evaluation of gas quenching of steel rings by multiple-jet impingement”, Journal of Materials Processing Technology, 2003, 136.1, pp. 190-201

[Fis14] Fischer M., Dickert H. H., Bleck W., Huskic A., Kazhai M., Hadifi T., Bouguecha A., Behrens B.-A., Labanova N., Felde A., Liewald M., Egorov F., Garbrecht M., Brinksmeier E., Reimche W., Bruchwald O., Frackowiak W., Maier H. J., Bucquet T., Hinrichs B., Fritsching U., Hoja T., Hoffmann F., Zoch H.-W.; “Ecoforge: Energieeffiziente Prozesskette von Hochleistungs-Schmiedebauteilen am Beispiel eines hochfesten, duktilen bainitischen (HDB) Stahls“, HTM Journal of Heat Treatment and Materials, 2014, 69.4, pp. 209-219

[Fod07] Fodemski T. R., Jasiński P.; ”Computer simulation study of high-pressure gas quenching of a steel element within vacuum furnace batch for different working conditions”, 5th International Conference on Heat Transfer, Fluid Mechanics and Thermodynamics (HEFAT), Sun City, South Africa, 1-4.07.2007

[Fre05] Frerichs F., Luebben T., Hoffmann F., Mayr P.; “Distortion of long cylinders with small diameters due to axial symmetric cooling”, International Journal of Materials and Product Technology, 2005, 24.1, pp. 244-258

[Fri08] Fritsching U., Schmidt R.; “Gas Flow Control in Batch Mode High Pressure Gas Quenching”, Innovation in Heat Treatment for Industrial Competitiveness, Verona, Italy, 7-9.05.2008

[Fri14] Fritsching U., Bucquet T.; “Resource-efficient process chains for high-performance steel components”, International Forging Conference, Berlin, Germany, 30.07.2014

[Gni10a] Gnielinski V.; “Chapter G6: Heat Transfer in Cross-flow Around Single Tubes, Wires and Profiled Cylinders“, in VDI Heat Atlas, Springer-Verlag, 2010, pp. 723-724

[Gni10b] Gnielinski V.; “Chapter G1: Heat Transfer in Pipe Flow“, in VDI Heat Atlas, Springer-Verlag, 2010, pp. 693-699

[Gni10c] Gnielinski V.; “Chapter G7: Heat Transfer in Cross-flow Around Single Rows of Tubes and Through Tube Bundles“, in VDI Heat Atlas, Springer-Verlag, 2010, pp. 725-729

[Grä01] Gräfen W., Edenhofer B.; “Acetylen-Unterdruckaufkohlung - eine neue und überlegene Aufkohlungstechnologie“, HTM Härtereitechnische Mitteilungen, 2001, 56.3, pp. 185-190

[Grj93] Grjotheim K., Kvande H.; “Introduction to Aluminium Electrolysis: Understanding the Hall-Heroult Process”, Aluminium-Verlag, 1993

[Guo13] Guo B. Y., Hou Q. F., Yu A. B., Li L. F., Guo J.; ”Numerical modelling of the gas flow through perforated plates”, Chemical Engineering Research and Design, 2013, 91.3, pp. 403-408

[Hal97] Hall D. D., Mudawar I., Morgan R. E., Ehlers S. L.; “Validation of a systematic approach to modeling spray quenching of aluminum alloy extrusions, composites, and continuous castings”, Journal of Materials Engineering and Performance, 1997, 6.1, pp. 77-92

[Haq07] Haque S., Rasul M., Rao S., Deev A., Khan M. M. K.; ”Numerical modeling for optimizing flow distribution inside an electrostatic precipitator”, International Journal of Mathematics and Computers in Simulation, 2007, 1, pp. 255-261

[Har13] Harrison C. S.; “A case study on automating a hot forge for manual and robotic operation”, Control and Automation 2013: Uniting Problems and Solutions, Birmingham, UK, 4-5 June 2013

[Hec01] Heck U., Fritsching U., Bauckhage K.; ”Fluid flow and heat transfer in gas jet quenching of a cylinder”, International Journal of Numerical Methods for Heat & Fluid Flow, 2001, 11.1, pp. 36-49

[Her04] Herring D. H., Lindell G. D.; “Reducing Distortion in Heat-Treated Gears”, Gear Solutions, 2004, pp. 27-35

[Her15] Herring D. H., Lindell G. D.; “Vacuum Equipment Innovations”, Industrial Heating, 11th November 2015

[Heu03] Heuer V., Löser K.; “Entwicklung des dynamischen Abschreckens in Hochdruck-Gasabschreckanlagen“, Materialwissenschaft und Werkstofftechnik, 2003, 34.1, pp. 56-63

[Heu04] Heuer V., Löser K.; “Experimentelles Verfahren zur Ermittlung von Wärmeübergangskoeffizienten bei der Hochdruck-Gasabschreckung“, HTM Härtereitechnische Mitteilungen, 2004, 59.6, pp. 432-438

[Heu09] Heuer V., Löser K., Ruppel J.; “Dry bainitizing – a new process for bainitic microstructures”, HTM Journal of Heat Treatment and Materials, 2009, 64.1, pp. 28-33

[Heu11a] Heuer V., Bolton D., Lifshits M., Löser K.; “Application of “Dynamic quenching” and “Reversing gas flow” technologies to minimize distortion-values after High Pressure Gas Quenching”, Technical report, ALD Inc., 2011

[Heu11b] Heuer V., Löser K., Schmitt G., Ritter K.; “Integration of Case Hardening Into the Manufacturing-Line: “One Piece Flow””, AGMA Technical Paper 11FTM23, 2011

[Heu13a] Heuer V., Faron D. R., Bolton D., Lifshits M., Löser K.; “Distortion Control of Transmission Components by Optimized High Pressure Gas Quenching”, Journal of Materials Engineering and Performance, 2013, 22.7, pp. 1833-1838

[Heu13b] Heuer V., Löser K., Schmitt G., Ritter K.; “Einsatzhärten im Fertigungstakt“, HTM Journal of Heat Treatment and Materials, 2013, 68.3, pp. 113-123

[Hin12] Hinrichs B., Reimche W., Bruchwald O., Frackowiak W., Fritsching U., Bach F. W.; “Sensorkontrolliertes Bainitisieren im Spraydüsenfeld“, GWI Gaswärme International, 2012, 03, pp. 77-85

[Hof92] Hoffmann R., Steinmann H., Uschkoreit D.; “Möglichkeiten und Grenzen der Gasabkühlung“, HTM Härtereitechnische Mitteilungen, 1992, 47.2, pp. 112-122

[Hof98] Hoffmann F., Gondesen B., Lohrmann M., Lübben T., Mayr P.; “Möglichkeiten und Grenzen des Gasabschreckens“, HTM Härtereitechnische Mitteilungen, 1998, 53.2, pp. 81-86

[Hol99] Holmberg D. G., Womeldorf C. A.; “Performance and modeling of heat flux sensors in different environments”, ASME Heat Transfer Division 364, 1999, pp. 71-78

[Hon07] Hong D., Kim C., Kim M. Y., Lee S. M., Ahn K. Y.; ”A numerical study on the flow characteristics in the mixing region of the catalytic combustor”, Journal of Mechanical Science and Technology, 2007, 21.11, pp. 1791-1798

[Hou09] Hou Q. F., Guo B. Y., Li L. F., Yu A. B.; ”Numerical simulation of gas flow in an electrostatic precipitator”, 7th International Conference on CFD in the Minerals and Process Industries, Melbourne, Australia, 9-11.12.2009

[Hu13] Hu F. Z., Hui W. J., Yong Q. L.; ”High-cycle fatigue fracture behavior of microalloyed bainitic steels for hot forging”, Advanced Materials Research, 2013, 634, pp. 1746-1751

[Hun04] Hunkel M., Schüttenberg S., Frerichs F., Fritsching U., Zoch H. W.; “Verzugskompensation mittels Gasabschreckung in flexiblen Düsenfeldern: Teil 2: Wärmebehandlung“, HTM Härtereitechnische Mitteilungen, 2004, 59.5, pp. 351-357

[IPA93] Industrial Perforators Association (IPA); “Designers, Specifiers And Buyers Handbook For Perforated Metals”, A publication of the Industrial Perforators Association, 1993, p. 27

[Irr04] Irretier A., Keßler O., Hoffmann F., Mayr P.; “Dry and clean age hardening of aluminum alloys by high-pressure gas quenching”, Journal of Materials Engineering and Performance, 2004, 13.5, pp. 530-536

[Jes10] Jeschar R., Specht E., Köhler C.; “Chapter 6: Heat Transfer during Cooling of Heated Metals with Vaporizable Liquids” in Quenching Theory and Technology, Taylor and Francis, 2010, pp. 159-178

[Jur07] Jurči P., Stolař P., Šťastný P., Podkovičák J., Altena H.; “Investigation of distortion behaviour of machine components due to carburizing and quenching”, HTM Härtereitechnische Mitteilungen, 2007, 63.1, pp. 27-32

[Kas10] Kast W. (revised by Nirschl, H.); “Chapter L1: Pressure Drop in Single Phase Flow“, in VDI Heat Atlas, Springer-Verlag, 2010, pp. 1055-1115

[Kat05] Katsumata K.; “Vacuum Quenching Furnace Using High Pressure Gas”, Engineering Review, 2005, 38.2, pp. 77-82

[Kad81] Kader B. A.; “Temperature and concentration profiles in fully turbulent boundary layers”, International Journal of Heat and Mass Transfer, 1981, 24.9, pp. 1541-1544

[Kay92] Kay A.; “Multiflow pressure quenching in vacuum furnaces”, Materials Science Forum, 1992, 102, pp. 885-896

[Kes06] Keßler O., Irretier A., Pieper O., Dolatta G., Hoffmann F., Zoch, H. W.; “Distortion Behaviour and Mechanical Properties of AlCu4Mg1 Sheet Components after High-Pressure Gas Quenching in Comparison to Liquid Quenching”, Materialwissenschaft und Werkstofftechnik, 2006, 37.1, pp. 110-115

[Keu12] Keul C., Wirths V., Bleck W.; “New bainitic steels for forgings”, Archives of Civil and Mechanical Engineering, 2012, 12.2, pp. 119-125

[Kha06] Khan W. A., Culham J. R., Yovanovich M. M.; “Fluid flow and heat transfer in power-law fluids across circular cylinders: analytical study”, Journal of Heat Transfer, 2006, 128.9, pp. 870-878

[Kle02] Kleff J., Kellermann I., Mallener H., Wirth M. S.; “Niederdruck-Aufkohlen und Hochdruck-Gasabschrecken - Leistungsversgleich mit konventionellen Einsatzhärten”, HTM Härtereitechnische Mitteilungen, 2002, 57.4, pp. 257-266

[Kor16] Korecki M., Wolowiec-Korecka E., Glenn D.; “Single-Piece, High-Volume, and Low-Distortion Case Hardening of Gears”, Thermal Processing, 16th September 2016

[Kow08] Kowalewski J., Korecki M., Olejnik J.; “Next-Generation HPQ Vacuum Furnace”, Heat Treating Progress, Sept. 2008, pp. 39-44

[Kul91] Kulmburg A.; “Beitrag zur Wärmebehandlung von Schnellarbeitsstählen in Vakuumöfen“, HTM Härtereitechnische Mitteilungen, 1991, 46.3, pp. 131-135

[Lau98] Laumen C., Holm T., Lübben T., Hoffmann F., Mayr P.; “Hochdruck-Gasabschrecken mit Wasserstoff“, HTM Härtereitechnische Mitteilungen, 1998, 53.2, pp. 72-80

[Lea13] Léal L., Miscevic M., Lavieille P., Amokrane M., Pigache F., Topin F., Nogarède B., Tadrist L.; “An overview of heat transfer enhancement methods and new perspectives: Focus on active methods using electroactive materials”, International Journal of Heat and Mass Transfer, 2013, 61, pp. 505-524

[Leg11] Legay M., Gondrexon N., Le Person S., Boldo P., Bontemps A.; “Enhancement of heat transfer by ultrasound: review and recent advances”, International Journal of Chemical Engineering, 2011

[Lho92] Lhote B., Delcourt O.; “Gas quenching with helium in vacuum furnaces“, Materials Science Forum, 1992, 102, pp. 867-884

[Lin07] Lin M.; “Gas Quenching With Air Products’ Rapid Gas Quenching Gas Mixture”, Report of Air Products and Chemicals, Inc., 2007

[Lio04] Lior N.; “The cooling process in gas quenching”, Journal of materials processing technology, 2004, 155, pp. 1881-1888

[Lio09] Lior N., Papadopoulos D.; “Gas-Cooling of Multiple Short Inline Disks in Flow Along Their Axis”, Journal of ASTM International, 2009, 6.2

[Liš07] Liščić B.; “Gas quenching with controllable heat extraction” Materials Science Forum, 2007, 539, pp. 4663-4668

[Loh96a] Lohrmann M.; “Experimentelle und theoretische Untersuchungen zur Vorausbestimmung des Wärmebehandlungsergebnisses beim Hochdruckgasabschrecken“, Dissertation Universität Bremen, 1996

[Loh96b] Lohrmann M., Hoffmann F., Mayr P.; “Abkühlintensität von Gasen in Wärmebehandlungsanlagen und deren Bestimmung“, HTM Härtereitechnische Mitteilungen, 1996, 51.3, pp. 183-187

[Lös95] Löser K., Heilmann P., Melber A.; “Hochdruck-Gasabschreckung mit Helium und Wasserstoff zum Härten niedriglegierter Stähle.“, HTM Härtereitechnische Mitteilungen, 1995, 50.5, pp. 314-321

[Lös03] Löser K., Heuer V.; “Neue Entwicklungen auf dem Gebiet der Hochdruck-Gasabschreckung“, HTM Härtereitechnische Mitteilungen, 2003, 58.2, pp. 74-82

[Lös05] Löser K., Heuer V., Schmitt G.; “Auswahl geeigneter Abschreckparameter für die Gasabschreckung von Bauteilen aus verschiedenen Einsatzstählen“, HTM Härtereitechnische Mitteilungen, 2005, 60.4, pp. 248-254

[Lös07] Löser K.; “Operating Experiences with the Flexible Vacuum Heat Treatment System ModulTherm® in Serial Production“, Thermprocess-Symposium 2007

[Lös08] Löser K., Heuer V., Faron D. R.; “Distortion Control by Innovative Heat Treating Technologies in the Automotive Industry”, HTM Härtereitechnische Mitteilungen, 2008, 61.6, pp. 326-329

[Lüb98] Lübben T., Hoffmann F., Mayr P., Laumen C.; “Scattering of Heat Transfer Coefficient in High Pressure Gas Quenching”, Proceedings of the 18th ASM Heat Treating Society Conference, 13-15.10.1998, Rosemont, USA

[Lut10] Luty W.; “Chapter 12: Cooling Media and Their Properties” in Quenching Theory and Technology, Taylor and Francis, 2010, pp. 359-443

[Mac05] Macchion O.; “CFD in the design of gas quenching furnace”, Technical Reports from Royal Institute of Technology, Department of Mechanics, S-100 44 Stockholm, Sweden, June 2005

[McG08] McGuinn A., Persoons T., Valiorgue P., O'Donovan T. S., Murray D. B.; "Heat transfer measurements of an impinging synthetic air jet with constant stroke length", 5th European thermal sciences conference, Eindhoven, The Netherlands, 18-22.05.2008

[Men03a] Menter F. R., Kuntz M., Langtry R.; "Ten years of industrial experience with the SST turbulence model", Turbulence, Heat and Mass Transfer, 2003, 4.1

[Men03b] Menter F. R., Ferreira J. C., Esch T., Konno B., Germany A. C.; "The SST turbulence model with improved wall treatment for heat transfer predictions in gas turbines", Proceedings of the International Gas Turbine Congress, Tokyo, Japan, 2003

[Men09] Menter F. R.; "Review of the shear-stress transport turbulence model experience from an industrial perspective", International Journal of Computational Fluid Dynamics, 2009, 234, pp. 305-316

[Mid96] Midea S. J., Holm T., Segerberg S., Bodin J.; "High pressure gas quenching - technical and economical considerations", Report No. CONF-961140-. ASM International

[Nar09] Narazaki M., Kogawara M., Ming Q., Watanabe Y.; "Measurement and database construction of heat transfer coefficients of gas quenching", Strojniški vestnik, 2009, 55.3, pp. 167-173

[Nav06] Navarro M. A., Santos A. A. D.; "Numerical simulation of water flow through the bottom end piece of a nuclear fuel assembly", Journal of Power and Energy Systems, 2008, 2.2, pp. 744-755

[Nit06] Nitsche W, Brunn A.; "Strömungsmesstechnik", Springer-Verlag, 2006

[Pav06] Pavlova A., Amitay M.; "Electronic cooling using synthetic jet impingement", Journal of heat transfer, 2006, 128.9, pp. 897-907

[Pel05] Pellegrino G., Chaffotte F., Douce J. F., Denis S., Bellot J. P., Lamesle, P; "Efficient numerical simulation techniques for high pressure gas quenching", Proceedings of the 23rd Heat Treating Society Conference, Pittsburgh, Pennsylvania, USA, 25-28.09.2005, Herring, D. (Ed.); ASM int., Ohio, USA, 2006, pp. 320-328

[Pet92] Peter W., Bless F., Edenhofer B.; "Lösung von Umweltproblemen mit Hilfe von Ein-und Mehrkammer-Vakuumhärteöfen" HTM Härtereitechnische Mitteilungen, 1992, 47.2, pp. 100-106

[Pol13] Pola A., Gelfi M., La Vecchia G. M.; "Simulation and validation of spray quenching applied to heavy forgings", Journal of Materials Processing Technology, 2013, 213.12, pp. 2247-2253

[Pus00] Puschmann F., Specht E., Schmidt J.; “Evaporation quenching with atomized sprays”, 3rd European Thermal Sciences Conference, Heidelberg, Germany, 10-13.09.2000, pp. 1071-1074

[Pus03] Puschmann F.; “Experimentelle Untersuchung der Spraykühlung zur Qualitätsverbesserung durch definierte Einstellung des Wärmeübergangs“, Dissertation Otto-von-Guericke Universität Magdeburg, 2003

[Qin08] Qin M.; “Vacuum carburising and high pressure gas quenching technology in automotive industry”, International Heat Treatment and Surface Engineering, 2008, 2.3-4, pp. 116-120

[Rak00] Rakhit A. K.; “Chapter 1” in Heat treatment of gears: a practical guide for engineers, ASM International

[Rat92] Rath, H. J.; “Mechanik IV – Grundlagen der technischen Strömungslehre“, Universität Bremen, Fachbereich Produktionstechnik, 1992

[Red11] Redmann R., Keßler O.; “Charakterisierung der Abschreckwirkung einer ultraschallunterstützten Wasserabschreckung von Aluminiumzylindern”, HTM Journal of Heat Treatment and Materials, 2011, 66.5, pp. 281-289

[Rei09] Reich M., Schöne S., Keßler O., Nowak M., Grydin O., Nürnberger F., Schaper M.; “Simulation of gas and spray quenching during extrusion of aluminium alloys”, Key Engineering Materials, 2009, 424, pp. 57-64

[Rei14] Reimche W., Bruchwald O., Frackowiak W., Bach F. W., Maier H. J.; “Hochleistungsbauteile für den Leichtbau mit sensorkontrollierter Bainitumwandlung aus der Schmiedewärme“, Tagung Massiver Leichtbau im Automobilbau, Stuttgart, Germany, 18-19.11.2014

[Rit03] Ritter K.; “Flexible Anlagenkonzepte für die Vakuumwärmebehandlung mit Hochdruck-Gasabschreckung“, HTM Härtereitechnische Mitteilungen, 2003, 58.2, pp. 98-103

[Ros06] Rose A., Keßler O., Hoffmann F., Zoch H. W., Krug P.; “Age Hardening of Forged Aluminium Components–Mechanical Properties and Distortion Behaviour after Gas Quenching”, Materials Science Forum, 2006, 519, pp. 383-388

[Sah87] Sahin B., Ward-Smith A. J.; “The use of perforated plates to control the flow emerging from a wide-angle diffuser with application to electrostatic precipitator design”, International Journal of Heat and Fluid Flow, 1987, 8.2

[Sch01] Schaub B., Heuer V.; “Die Simulation des Einflusses der Bauteianordnunhg auf die Abschreckung in Hochdruck Gasabschreckungsanlagen”, 19th CAD-FEM Users‘ Meeting, International Congress on FEM Technology, Berlin, Germany, 17-19.10.2001

[Sch04] Schüttenberg S., Frerichs F., Hunkel M., Fritsching U., Mayr P.; “Verzugskompensation mittels Gasabschreckung in flexiblen Düsenfeldern: Teil 1“, HTM Härtereitechnische Mitteilungen, 2004, 59.3, pp. 185-192

[Sch05] Schüttenberg S., Hunkel M., Fritsching U., Zoch H. W.; “Controlling of distortion by means of quenching in adapted jet fields”, Materialwissenschaft und Werkstofftechnik, 2005, 37.1, pp. 92-96

[Sch07] Schmidt R. R.; “Strömungsführung zur Homogenisierung des Härteergebnisses in Wärmebehandlungsanlagen bei der Hochdruck-Gasabschreckung“, Technical Report, AiF Nr. 13840, 2007

[Sch09] Schmidt R. R., Fritsching U.; “Quenching Homogeneity and Intensity Improvement in Batch Mode High Pressure Gas Quenching”, Journal of ASTM International, 2009, 6.4

[Sch10a] Schmidt R. R., Fritsching U.; “High pressure gas quenching intensity of cylinder loads”, Gaswärme International, 2010, 59.6, pp. 467-471

[Sch10b] Schabel W., Martin H.; “Chapter G10: Impinging Jet Flow Heat Transfer“, in VDI Heat Atlas, Springer-Verlag, 2010, pp. 746-751

[Sch12] Schöne S.; “ Integration des Düsenfeld-Gasabschreckens in den Strangpressprozess von Aluminiumlegierungen“, Dissertation Universität Rostock, 2012

[Sch13] Schmidt R. R.; “Zur Thermo-Fluid-Dynamik beim Hochdruckgasabschrecken“, Dissertation Universität Bremen, 2013

[Sha01] Shao Z.; “Numerical and experimental evaluation of flow through perforated plates”, PhD at the Rand Afrikaans University, 2001

[Sha12] Shakouchi T., Suzuki T., Kugimoto M., Tsujimoto K., Ando T.; “Effects of Pressure Fluctuation on Flow-Accelerated Corrosion in the Downstream of Orifice Nozzle”, Journal of Fluid Science and Technology, 2012, 7.1, pp. 129-139

[Shu10] Shuey R. T., Tiryakioglu M.; “Chapter 2: Quenching of Aluminum Alloys” in Quenching Theory and Technology, Taylor and Francis, 2010, pp. 43-83

[Sig08] Sigloch H.; “Technische Fluidmechanik“, Springer-Verlag, Berlin, 2008

[Şim09] Şimşir C., Lübben T., Hoffmann F., Zoch H. W., Wolff M.; “Prediction of distortions in through hardening of cylindrical steel workpieces by dimensional analysis”, Proceedings of the New Challenges in Heat Treatment and Surface Engineering (CHTSE), Dubrovnik, Croatia, pp. 351-358

[Sin10] Since J. J., Irretier O.; “Vacuum heat treatment and high pressure gas quenching – Aspects in Distortion Control”, Heat Processing, 2010, 8.2

[Sin89] Sinha A. K.; “Chapter 10 – Basic Heat Treatment” in Ferrous physical metallurgy, Butterworths, Boston, MA, 1989, pp. 403-440

[Sta14] Stark P.; “Prozesssimulation der Bauteil Abschreckung in flüssigen Medien: Zur Analyse des mehrphasigen Strömungs- und Wärmetransports in Siedeprozessen“, Dissertation Universität Bremen, 2014

[Sto01] Stolar P., Altena H., Jurci P., Klima F., Honzik O.; ”Distortion of gear wheels after quenching in gas and oil”, Proceedings of the 8th Seminar of the International Federation for Heat Treatment and Surface Engineering, IFHTSE, 2001, pp. 95-102

[Stra06] Stratton P. F., Bruce S., Cheetham V.; “Low-pressure carburizing systems: A review of current technology”, BHM Berg- und Hüttenmännische Monatshefte, 2006, 151.11, pp. 451-456

[Stra07] Stratton P.; “Validating the modelling of a gas-jet quenched carburised gear”, International Journal of Microstructure and Materials Properties, 2007, 4.2, pp. 156-167

[Sug06] Sugimoto T., Qin M., Watanabe Y.; “Computational study of gas quenching on carburizing hypoid ring gear”, BHM Berg- und Hüttenmännische Monatshefte, 2006, 151.11, pp. 456-461

[Swa10] Swaminathan M. R., Mahalakshmi N. V.; “Numerical modeling of flow through perforated plates applied to electrostatic precipitator”, Journal of Applied Sciences, 2010, 10.20, pp. 2426-2432

[Thu99] Thuvander A., Melander A., Lind M., Lior N., Bark F.; “Prediction of convective heat transfer coefficients and examination of their effects on distortion of cylindrical tubes quenched by gas cooling”, Metallurgia Italiana, 1999, 91.4, pp.25-32

[Tot12] Totten G. E., Albano L. L. M.; “IFHTSE Global 21: Heat treatment and surface engineering in the 21st century. Part 18: Quenching: current status and future developments”, International Heat Treatment and Surface Engineering, 2012, 6.1, pp. 4-14

[Tro98] Troell E., Segerberg S., Holm T.; “Cold chamber gas cooling for low-pollution hardening”, proceedings of the 18th ASM Heat Treating Society Conference, 1998, pp. 13-15

[Tyr86] Tyrkiel E. F.; “Multilingual Glossary of Heat Treatment Terminology: Theory and processes of heat treatment”, The Institute of Metals, London, 1986

[Vil11] Vilums R.; “Implementation of Transient Robin Boundary Conditions in OpenFOAM”, Technical Report, 2011

[Vol01] Volkmuth J., Hengerer F., Wünning J.; “Erfahrungen mit Einzel-Gasabschreckung von Ringen aus durchhartendem Walzlagerstahl“, HTM Hartereitechnische Mitteilungen, 2001, 56.3, pp. 179-184

[Wan12] Wang Z., Zhao Y.; “Numerical Simulation of the Effects of Pressure, Velocity and Types of Quenching gas on the Cooling Performance of Workpieces in Vacuum High-Pressure Gas Quenching Furnace”, International Journal of Digital Content Technology and its Applications, 2012, 6.18, pp. 192-202

[War91] Ward-Smith A. J., Lane D. L., Reynolds A. J., Sahin B., Shawe D. J.; “Flow regimes in wide-angle screened diffusers”, International Journal of Mechanical Sciences, 1991, 33.1

[Wen08] Wendelstorf J., Spitzer K. H., Wendelstorf R.; “Spray water cooling heat transfer at high temperatures and liquid mass fluxes”, International Journal of Heat and Mass Transfer, 2008, 51.19, pp. 4902-4910

[Wib03] Wiberg R., Lior N.; “Convection heat transfer coefficients for axial flow gas quenching of a cylinder”, Proceedings of the 4th International Conference on Quenching and the Control of Distortion, 2003, 20

[Wib05] Wiberg R., Lior N.; “Heat transfer from a cylinder in axial turbulent flows”, International Journal of Heat and Mass Transfer, 2005, 48.8, pp. 1505-1517

[Win05] Wingens T., Edenhofer B., Wingens U.; “Bauweise und Funktion eines neuartigen Großkammer-Vakuumofens zum Härten von schweren Formen und Gesenken“ HTM Härtereitechnische Mitteilungen, 2005, 60.3, pp. 173-177

[Wir14] Wirths V., Wagener R., Bleck W., Melz T.; “Bainitic forging steels for cyclic loading”, Advanced Materials Research, 2014, 922, pp. 813-818

[Wün93] Wünning J.; “Einzelhärtung von Serienteilen in Gasdüsenformen“, HTM Härtereitechnische Mitteilungen, 1993, 48.3, pp. 199-203

[Xia11] Xiao B., Wang G., Rong Y.; “Hardenability and distortion control of steel parts in High Pressure Hydrogen Quenching”, International Journal of Manufacturing Research, 2011, 6.1

[Zie13] Zieger B.; “Purpose-directed hot zone and cooling-gas stream design of vacuum furnaces”, The Heat Treatment Market, 2013, 20.2, pp. 5-11

[Zie14] Zieger, B.; “Advanced hot-zone and cooling-gas stream design in vacuum furnaces for automotive applications”, European Conference on Heat Treatment and 21st IFHTSE Congress, Munich, Germany, 12-15.05.2014

[Zoc09] Zoch H. W.; “Distortion engineering: vision or ready to application?“, Materialwissenschaft und Werkstofftechnik, 2009, 40.5-6, pp. 342-348

[Zuc06] Zuckerman N., Lior N.; “Jet impingement heat transfer: physics, correlations, and numerical modeling”, Advances in Heat Transfer, 2006, 39, pp. 565-631

[Zuc08] Zuckerman N., Lior N.; “The relationship between the distributions of slot-jet-impingement convective heat transfer and the temperature in the cooled solid cylinder”, Numerical Heat Transfer, Part A: Applications, 2008, 53.12, pp. 1271-1293